A and F stars with circumstellar dust

A thesis
Submitted For The Degree of

Doctor of Philosophy

In
Faculty of Science

Bangalore University

By

T. Sivarani

Indian Institute of Astrophysics
Bangalore 560 034, India

2000

Declaration

I hereby declare that this thesis, submitted to Bangalore University, Bangalore, for the award of a Ph.D. degree, is a result of the investigations carried out by me at Indian Institute of Astrophysics, Bangalore, under the supervision of Professor M. Parthasarathy. The results presented herein have not been subject to scrutiny, by any university or institute, for the award of a degree, diploma, associateship or fellowship whatsoever.

T. Sivarani
(PhD. Candidate)

Indian Institute of Astrophysics
Bangalore 560 034, India
March 23, 2000

To my parents

A and F stars with circumstellar dust

Abstract:

Circumstellar dust plays an important role in stellar evolution. From the analysis of IRAS (Infra Red Astronomical Satellite) data of several A and F stars which are young (pre-mainsequence) and evolved (Asymptotic Giant Branch (AGB) and post-AGB), showed the presence of circumstellar dust shells.

the circumstellar dust around stars changes the spectral energy distribution as well as the spectral line features of the photosphere. Some stars show shell lines. In some cases the circumstellar dust plays a major role in understanding the peculiar chemical composition of the photosphere. Studying the circumstellar environment of these stars and the influence of circumstellar matter on the photospheric spectrum helps us to understand the pre-mainsequence and post-mainsequence evolution.

Pre-mainsequence stars have circumstellar envelopes as a natural process of star formation. But as it reaches the mainsequence stage only some stars retain their circumstellar disk. These stars could probably be having a planetary system. In connection to the planetary formation, it is interesting to study these stars which have circumstellar dust. Recently even the evolved stars which is a proto-planetary nebula (Red Rectangle Nebula (Jura and Turner, 1998)) seem to show evidence of planetary formation. After the discovery of planets around pulsars, this is the first evidence of planets around a post-mainsequence star. A-F stars have the most simple atmosphere compared to any other spectral type. Still there are only a few normal A stars Bidelman says that "He has never seen any normal A-star". λ boo stars are one of the chemically peculiar stars seen in the mainsequence in the spectral range A-F. These stars seem to have got the peculiar composition as a result of the influence of circumstellar dust. They show depletion in metals and show normal C,N,O,S and Zn abundances. Many of the λ boo stars show IR (Infra Red) excess due to dust.

Some of the metal poor post-AGB stars also show similar characteristics like the λ boo stars. And these post-AGB stars are associated with circumstellar dust shells. So it is very essential to know that the metal poor character is due to the population II nature of the object or due to fractionation or both.

The pre-mainsequence stars and post-AGB stars have detached dust shells. Some of the pre-mainsequence stars have similar IRAS colors like that of Proto Planetary Nebulae (PPN). In order to distinguish the evolutionary stage of the various type of stars with circumstellar dust shells and to understand the physical processes (mass-loss, shocks, mixing, and fractionation), we need to carry out high resolution spectroscopic study.

Acknowlegements

It is a pleasure to thank my supervisor Prof. M. Parthasarathy for his valuable help and guidance through out the work. It is a great source of encouragement discussing with him.

I thank Dr. P. Garcia-Lario for obtaining some of the spectra. I am thankful to Prof. S.R. Pottasch for encouraging discussions.

I thank Prof. Anadaram, the Chairman, Physics department, Bangalore university and also the earlier Chairmen, for the cordial and smooth manner in which the formalities related to the University were conducted.

I thank the Director, Indian Institute of Astrophysics, for all facilities provided to me. I thank the Board of Graduate studies for all their help during the stay at IIA.

The Faculty and scientific staff of IIA are thanked for their support. The help of the Library staff: Ms. A. Vagiswari and Co. and the Computer Centre (CC) Staff: Mr. A.V. Ananth and Mr. J.S. Nathan, is acknowledged with gratitude. I also thank Mr. K.T. Rajan, Mrs. Pramila, Mr. Ramesh, Mr. Mohan Kumar, Mr. Nagaraj, Mr. K. Sankar and Shri. Md. Khan for their good services right from my first days at IIA.

I thank Mr. P.N. Prabhakara, Mr. D. Kanagaraj and Thiyagaraj who took care of the photocopying and binding of this thesis. I thank all of them profusely for their help.

I thank all the observing staff of the Vainu Bappu Observatory, for their efficient assistance and also for providing a very friendly atmosphere. It was always been enjoyable to work with them. I thank all the electronics staff for providing all their help. I also thank Mr. Gabriel and Mr. Mani for their help.

I thank Eswar Reddy for the encouragement and help in the beginning of my work. I thank Rajesh for his help in teaching me about computers I thank Raji, Preeti and Geethanjali for a nice company.

I thank all my friends who were very understanding and helpful which made the stay at IIA very enjoyable.

I thank Arun for his support and encourgement through out the work. I thank my uncles, sisters and brothers for being very understanding. Last but not least I thank my parents, who motivated and encourged me from my school days.

Contents

Chapter 1

Introduction

1.1 General Introduction

The infrared sky survey by the IRAS (Infra Red Astronomical Satellite) in 1983 , led to a breakthrough in the observational study of stars with circumstellar dust. Many stars with cold dust, which emit in the far-infrared were detected. Most of them were identified as post-AGB stars from their optical charteristics (Parthasarathy and Pottasch 1986, Lamers et al. 1986, Trams et al. 1991). Even the well known standard star Vega, whose colours are used as zeropoint for the theoretical photometric grids was found to have circumstellar dust (Aumann et al. 1984). These class of main-sequence stars which exhibit profuse emission at far-IR wavelengths, are called the Vega-excess or Vega-like systems. They have fluxes at $\lambda \geq 60\mu$m, more than an order of magnitude that is expected from the photosphere corresponding to their spectral type. (Walker and Wolstencroft 1988) (e.g β Pic, α PsA, ϵ Eri).

Most of the stars possess circumstellar dust during its formation and subsequent evolution to RGB (Red Giant Branch) and AGB (Asymptotic Giant Branch) phases. The circumstellar dust around stars changes the spectral energy distribution as well

as the spectral line features of the photosphere. Some stars show shell lines. Stars with circumstellar dust show a characteristic double peak in their spectral energy distribution, one peak corresponds to the stellar radiation from the photoshere and the other one is due to the reradiation from the dust. In some cases the circumstellar dust plays an important role in explaining the peculiar chemical composition of the photosphere.

A-F stars, have the most simple atmosphere compared to any other spectral type. However there are only a few normal A stars found. Bidelman says that "He has never seen any normal A-star". It is interesting to study the chemical peculiarity of these objects in connection to the presence of circumstellar dust.

Morgan (1943) introduced a group of PopI A-F mainsequence stars with low metallic abundance. These stars are called the λ Boo stars, named after the prototype (Burbidge and Burbidge 1956). They are charaterized by a CaII K line which is too weak for its spectral type. Vega was also found to be a mild λ Boo star (Baschek and slettebak 1988).

Many group members were identified based on weak CaII K and MgII 4481Å line and peculiar hydrogen line profiles (Andersen and Nordström 1977, Graham and Slettebak 1973, Slettebak 1952,1954,1975). λ Boo stars have average rotational velocity of 100 kms^{-1} (Hauck and Slettebak 1983). Slettebak et al. (1968) used the space velocity and rotational velocity to distinguish λ Boo stars from Population II stars. Baschek et al. (1984) found some strong absorption features at 1600Å and 3040Å in IUE spectra. These features are observed only in λ Boo stars. Holweger et al (1994) identified the 1600Å feature as a satellite in the Lyman α profile due to perturbation by neutral hydrogen. The observations in the infrared and optical gave evidence for gas and dust shells around λ Boo stars (Gerbaldi and Faraggiana 1993: Bohlender and Walker 1994; Andrillat et al. 1995). Reliable measurements of magnetic fields in λ Boo stars have not been done (Bohlender and Landstreet 1990). Very few stars satisfy all these criteria, and the connection between the subset which

satisfy only few of the criteria is not known. Gray (1988), Gray and Corbally (1993) and Renson et al (1990) compiled a homogeneous group of λBoo stars. Recently (1997) Paunzen et al. compiled a catalogue with 45 λ Boo stars.

These star show depletion of refractory elements (Mg, Si, Ca, Sc, Fe etc.) and show normal abundances of volatile elements (C,N,O,S and Zn). The abundances of different elements show a correlation with the condensation temperatures (Venn and Lambert 1990) and it is similar to that seen in the interstellar medium (ISM), (Fig. 1) where the metals are locked up in the dust grains and the volatile elements in the gaseous phase. In many extreme metal poor post-AGB stars the metal poor characteristics is explained partially due to refractory elements condensing into dust grains (Waters etal. 1992). The formation of dust close to the star during the pre-mainsequence stage of λ boo star and the mass-loss phase in the AGB and post-AGB stars, with a subsequent gas and dust separation due to dust driven mass-loss (Yorke 1979) can explain the photospheric abundances of λBoo stars and post-AGB A-F stars. According to the theory of accretion of metal depleted gas, λ Boo stars are young, which are in the Zero Age Mainsequence (ZAM). The theory of diffusion and mass-loss (Michuad and Charland 1986) giving rise to metal poor composition, place the λ boo stars at the end of the mainsequence. In the catalogue by Paunzen et al. (1997) 2/3 of the samples show variability (Wiess et al 1994). λ Boo stars challenge our understanding of diffusion and accretion processs related to stars and their circumstellar environment. The statistical study of these objects are limited due to the small number of unambiguously identified λ Boo stars.

The transition phase from AGB to PN is one of the least understood phase in the HR diagram, due to mixing, pulsation and mass-loss playing a major role in the structure and evolution of these stars, which is not been derived observationally because of few numbers of trasition objects. When an AGB star becomes optically visible it is found in the spectral range F-A. Post-AGB stars show variety of elemental abundance pattern. Many of it cannot be explained due to nucleosynthesis processes.

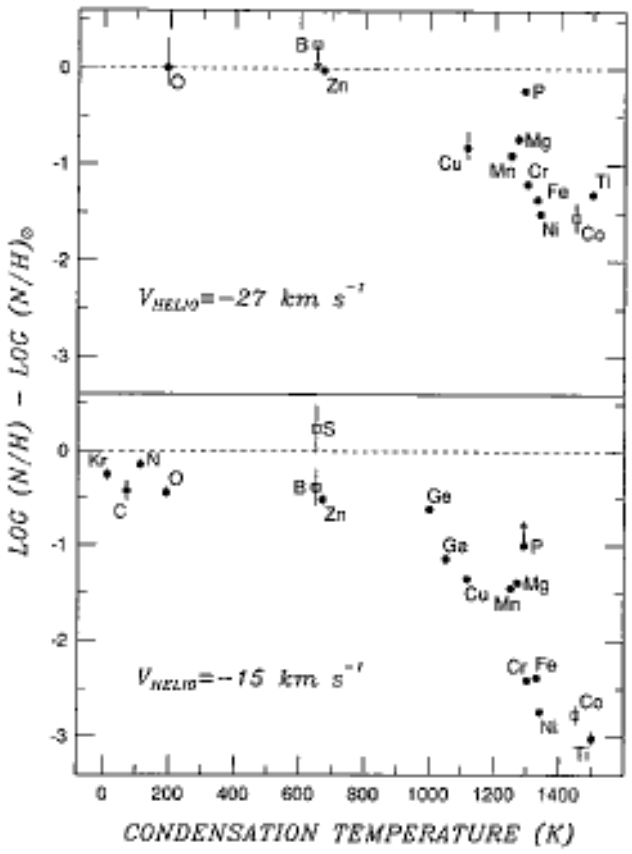

Figure 1: Interstellar elemental abundances for two clouds towards ξ Oph. (From Federman et al 1993)

The nuclear synthesis processes which happen in the AGB stage is still unclear. The AGB stars have a rich unidentified emission line features in the infrared. There are correlations seen between these emission lines features and the carbon or oxygen rich photospheric spectrum. A detailed study of the circumstellar environment along with the photosphere of the central star is essential for a clear understanding of these stars in the late stages of stellar evolution.

Recently there were evidences for planetary system around many vega-like systems. Even the evolved star which is a proto-planetary nebula (Red Rectangle Nebula (Jura and Turner, 1998)) seem to show evidence of planetary formation. After the discovery of planets around pulsars, this is the first evidence of planets around a post-mainsequence star. Though these stars are at different stages of evolution, they seem to share many things in common, like the chemical peculiarity, IR fluxes, proto planetary disks. Bipolar and disk geometry is quite common in both post-AGB and pre-mainsequence stars. Pulsations are also common to both λ boo and post-AGB A-F stars. In the HR diagram the extention of the instability strip to the mainsequence intersects at A-F spectral type. Pulsations seem to play an important role in the mass-loss, mixing and chemical peculiarity in these stars.

1.2 Evolution of low and intermediate mass stars

Both the low and intermediate mass stars go through the AGB phase of evolution and end up as white dwarfs.

Low and intermediate mass (LIM) stars are defined as those who end their life without proceeding through the carbon and heavier elements burning phases. Stars with masses in the range of 0.8 to 2.3 $M_{\odot}$ are defined as low-mass stars. They develop an electron-degenerate helium core immediately following the mainsequence phase. Stars with masses 2.3 to 8 $M_{\odot}$ are the intermediate mass stars, which burns helium non-degenerately, but develope an electron-degenerate carbon-oxygen (C-O)

core, after the core helium burning (Fig. 2). After the core helium burning the subsequent phase is same for both low and intermediate mass stars. This phase of evolution is called the Asymptotic Giant Branch (AGB) phase of evolution (it is called AGB since, for low mass stars the evolutionary track in the H-R diagram approaches that of first the giant branch (Fig.3)). During AGB phase the star has a double shell source. It has degenerate C-O core in the center and a He burning shell around that. There is also a thin Hydrogen burning shell (which is the main contributor to the lumminosity) around the He-shell. Surrounding the Hydrogen shell there is a thick Hydrogen envelope. At this phase the star goes through a heavy mass loss. Most of the envelope is thrown away into the interstellar medium (ISM) and enriches the ISM with the synthesis products. The subsequent evolution from AGB to PN depends on various factors, the mass-loss rate, core and envelop mass, pulsation and chemical composition. Both the low and intermediate mass stars, which are of intial mass 0.8 - 8.0 $M_{\odot}$ finally end up as a whitedwarf. The amount of time a star spends on the AGB and Post-AGB stage depends on the adapted mass-loss rates. The mechanism for the mass-loss in AGB stage is still an open problem.

1.2.1 Chemical evolution

The overall contraction phase prior to H-ignition in the core corresponds to the pre-mainsequence phase (PMS). This is characterised by the central star and an accretion disk. The far Infrared (IR) colours at this phase in most cases are similar to the Post-AGB star with a detached dust shell. In the PMS phase some of the light nuclides (D to C) which is already burnt at temperatures 10^6 K. Deutrium burns via D(p,γ) ^{3}He . ^{6}Li and ^{7}Li burn in the deep layers. Due to mixing the Li abundance in the surface is altered, and this depends on the initial stellar mass, rotation, etc.

Mainsequence phase is characterized by the major hygrogen burning in the core. From mainsequence upto AGB phase hydrogen burning is the only nucleosynthesis

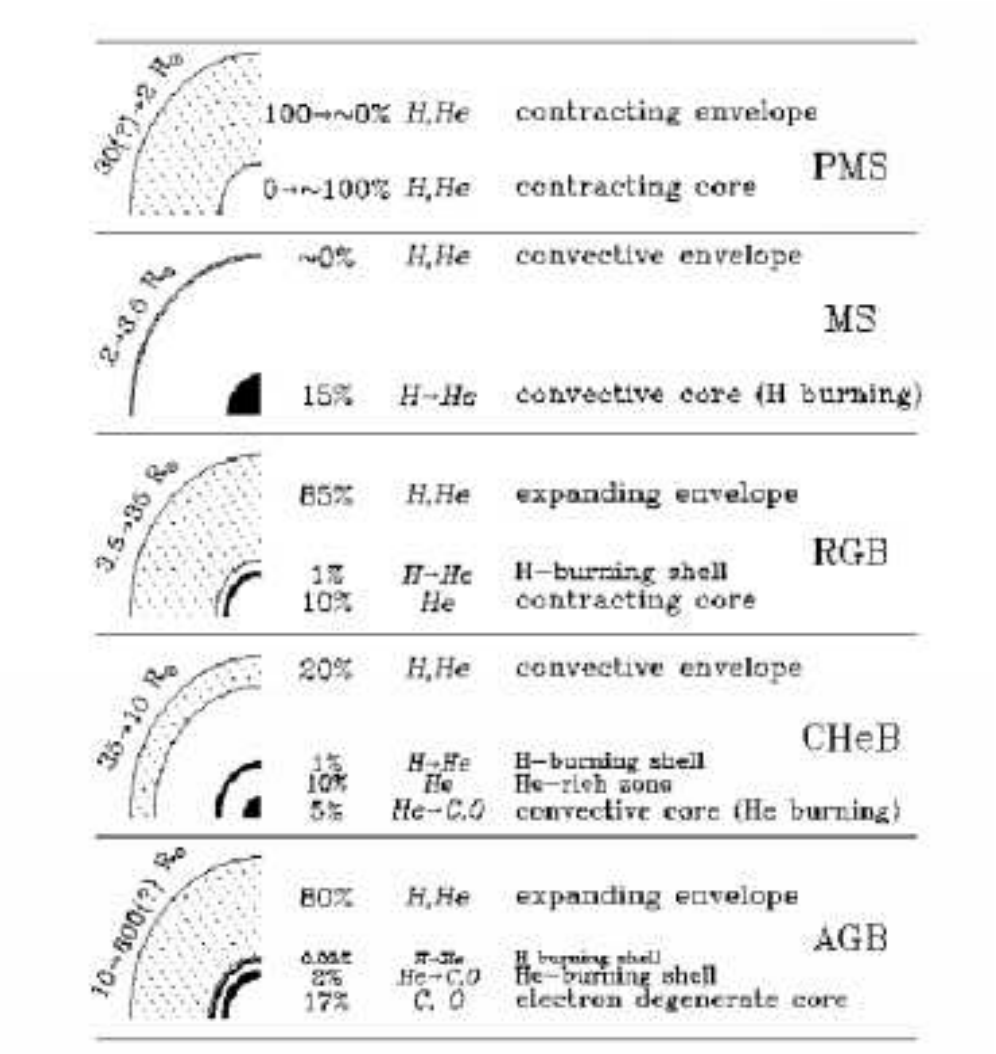

Figure 2: Schematic representations of the structure of a star star at different phases of evolution. The column on the right of each diagram indicate, the percent of total mass of the star contained in the given region. The hatched areas in the diagrams indicate convective regions, while filled areas denote regions where nuclear energy is produced. The quantities refer to a $3M_{\odot}$ Z=0.02 star. Taken from (Mowalvi 1997).

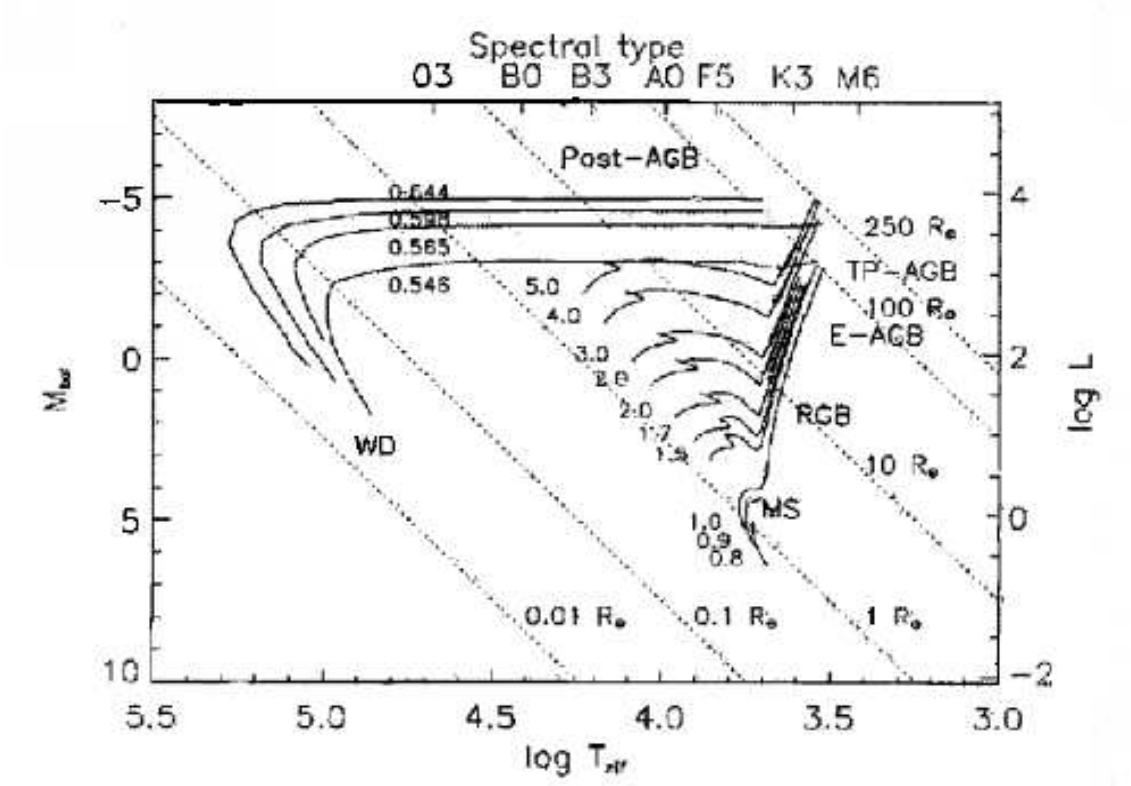

Figure 3: Theoretical evolutionary tracks for intermediate mass drawn in the HR diagram. The post-AGB tracks are taken from Schönberner 1983, the evolution from the Mainsequence to the AGB is taken from Schaller et al. 1992 (Figure is taken from Bakker 1995

process in LIM stars which is of interest. The core He burning products will be trapped into the whitedwarfs. There are four non-explosive H-burning modes identified todate (Rolfs and Rodney, 1988): the PP-chains, the CNO cycles, and the NeNa and MgAl chains. The major energy production comes from the PP-chains and CNO cycles. But all the four modes are of importance from a nucleosynthesis point of view.

Low mass stars are major contributors to the Galactic ^{3}He enrichment, through P(p,e$^+\nu$) D(p,γ) ^{3}He. It comes to the surface by the first dredge-up. In the intermediate mass stars ^{3}He is essentially destroyed in the deep layers (by ^{3}He (^{3}He , 2p) ^{4}He or ^{3}He$(\alpha,\gamma)^7$Be) . The core of intermediate mass stars and in the H-burning shells CNO cycle is the dominate nuclear process. During the first dredge-up episode which occurs in all the stars that become red giant for the first time, these hydrogen burning product is brought to the surface. As a result the surface abundances of C,N,Li,Be and C^{12}/C^{13} undergo changes. The nitrogen (N^{14}) abundance on the surface is doubled and the carbon (C^{12}) abundance is reduced by 30% and the C^{12}/C^{13} ratio becomes about 20 to 30. The surface abundances of Li and Be are reduced by several orders of magnitude. However there is no change in the oxygen as a result of first dredge-up.

Once helium is ignited in the core the star has two sources: the hydrogen shell and helium core. In the helium core it is primarily the triple α process providing ^{12}C and then further α capture giving ^{16}O. The large amount of ^{14}N left over from the CNO cycle, captures α particle and produce ^{18}O through $^{14}(\alpha,\gamma)^{18}F(\beta^+\nu)^{18}O$. The ^{18}O produces ^{22}Ne through a α capture process.

Moving to the hydrogen shell burning through CNO cycle, we have carbon depleted at the expense of nitrogen. ^{18}O is vitually destroyed by (p,α) and produces ^{15}N and further proton capture produces back again the ^{12}C, thus keeping the ^{15}N low. These nucleosynthesis products are brought to the surface by the second dredge up process. The dredge up matter can be as high as $1M_\odot$ in the massive intermediate mass stars, hydrogen has been completely converted into he-

lium and both carbon (C^{12}) and oxygen (O^{16}) have been converted almost completely into nitrogen (N^{14}). Thus only the most massive intermediate star experience a change in the surface composition as they reach onto the AGB. This contrasts with the first dredge-up phase when every star that becomes a giant experience a change in the surface composition after hydrogen exhaustion in the center. Thus the magnitude of the surface composition changes as a consequence of first and second dredge-up episodes in a single star are: if the initial composition of CNO elements is in the ratio (C:N:O)(initial)=1/2:1/6:1 in the units of initial oxygen abundance(C+N+O=5/3). During the first dredge-up phase the CNO abundances become(C:N:O=1/3:1/3:1) nearly independent of stellar mass. For the most massive intermediate masss stars which experience second dredge-up, the final abundances of CNO elements are C:N:O=0.29:0.52:0.86.

For stars of sufficiently large core mass(0.7 $M_{\odot}$ or more) and sufficiently large total mass (initial mass more than $2M_{\odot}$) the thermal pulse or helium shell flash approches limiting strength, the base of convective envelope extends into the region containing highly processed matter. The resulting mixing of freshly synthesized ^{12}C and neutron rich isotopes to the surface is called the third dredge-up. When third dredge-up and envelope burning process are simultaneously active, enormous variations in the surface are generated in the course of the AGB evolution. The over abundance of carbon and s-process elements in the carbon stars and related carbon-rich AGB stars is an observational evidence of third dredge-up.

As the star ascends the AGB the temperature at the base of the convective envelope increases dramatically, up to 82 million K, which can trigger hydrogen burning nuclear reactions(Hot Bottom Burning HBB). This reduces the abundances of ^{12}C and ^{13}C and increases ^{14}N. There is production of ^{25}Mg, ^{26}Al and ^{27}Al due to Mg-Al cycle. There is an order of magnitude increase in the ^{17}O abundance during the AGB phase. ^{7}Li increases rapidly once HBB begins and ^{3}He is depleted. The luminosity range and duration of the super-Li-rich phase has been shown by Boothroyd

and Sachmann (1992). As the envelope mass decreases due to massloss the HBB is shutdown (Vassilliads and Wood 1993). Though HBB stops, the third dredge-up still continues, and it is strong as the envelope mass reduces. The details of the surface composition depends critically on the competition between these effects (Groenewegen and deJong 1993). It may be possible for HBB to prevent a star from becoming a carbon star.

1.3 Properties of AGB stars

AGB stars have luminosities in the range of 3000 to 10000L$\odot$. Post-AGB stars are among the brightest and hottest in intermediate and old stellar populations, with a charateristic emission peaking in the middle and far ultraviolet (UV). The UV light from the population of P-AGB stars has been recently suggested as one of the major contributor of the rising branch in the early-type galaxies, and its dependence upon the age of the parent galaxy has been considered a powerful tool to constrain the cosmological model of the universe. However the properties of P-AGB stars, in particular the lifetime during their brightest phase, are very much dependent on their mass, in turn, on the mass-loss suffered during the previous phases. The mechanism of AGB mass-loss is still unknown. To understand one needs to know the mass-loss rate, flux from the star, outflow velocity. The dust distribution and the dust composition, that is whether it is carbon or oxygen rich also plays an important role in the mass-loss (Zuckerman and Dyck 1986, Jura 1983).

AGB stars are most of the time completely abscured by circumstellar dust. When the mass loss in the AGB stage is completed then the star has reached the post-AGB stage of evloution. At this phase the dust envelope expands and the central core starts contracting and increases the temperature. When the star reaches the post-AGB phase most of the time it is a F-type star. The envelope has expanded and starts cooling. So the post-AGB have a spectral type from F-B and have detached dust shell.

The IRAS Point Source Catalog (1985, IRAS (PSC) has proven to be a successful tool to identify the presence of circumstellar material. Infra Red Astronomical Satellite (IRAS) has surveyed objects in 12μ, 25μ, 60μ and 100μ wavelength bands. Some stars show excess of emission in these wavelengths above the blackbody continuum of the photosphere. This indicates the presence of dust, which is re-emitting the stellar continuum. We have chosen the objects (Table.1) on the basis of the far-IR colors, which have detached dust shells.

The presence of emission at these bands indicates the presence of circumstellar dust. In many cases IRAS fluxes are explained as emission from a combination of cold and warm dust. The presence of warm dust (1000K) indicates that the emission is from the material due to the recent mass-loss or it is coming from regions close to the star. The presence of cold dust (100K) indicates that the emission is from the material which is ejected due to mass-loss and has expanded and cooled down. The IRAS colour-colour diagram(Fig. 4) has proven a useful tool to discriminate between various types of objects with circumstellar dust. The oxygen rich and carbon rich AGB stars occupy different regions in the two colour diagram, due to their different dust properties. The oxygen rich circumstellar shell stars seem to form a sequence which represents increasing mass-loss and pulsations (van der Veen and Habing (1988) and Pottasch (1984). Interestingly, these searches yield large fractions of G type post-AGB stars. From the number counts one can derive the timescale of the sequence. There is gap seen observationally between regions I and II , which shows rapid increase in mass loss rate.

Many of the IRAS stars in the high galactic latitude are first thought to be massive supergiants which have escaped from the Galactic plane. Parthasarathy and Pottasch (1986) first pointed out that, indeed these stars are post-AGB stars which are having detached dust shells. We have selected stars which are in the high Galactic latitude. We have also looked into the OH and CO survey (Likkel 1986 and Morris ; Zuckerman and Dyck 1986) which indicates the presence of circumstellar gas. In the case of

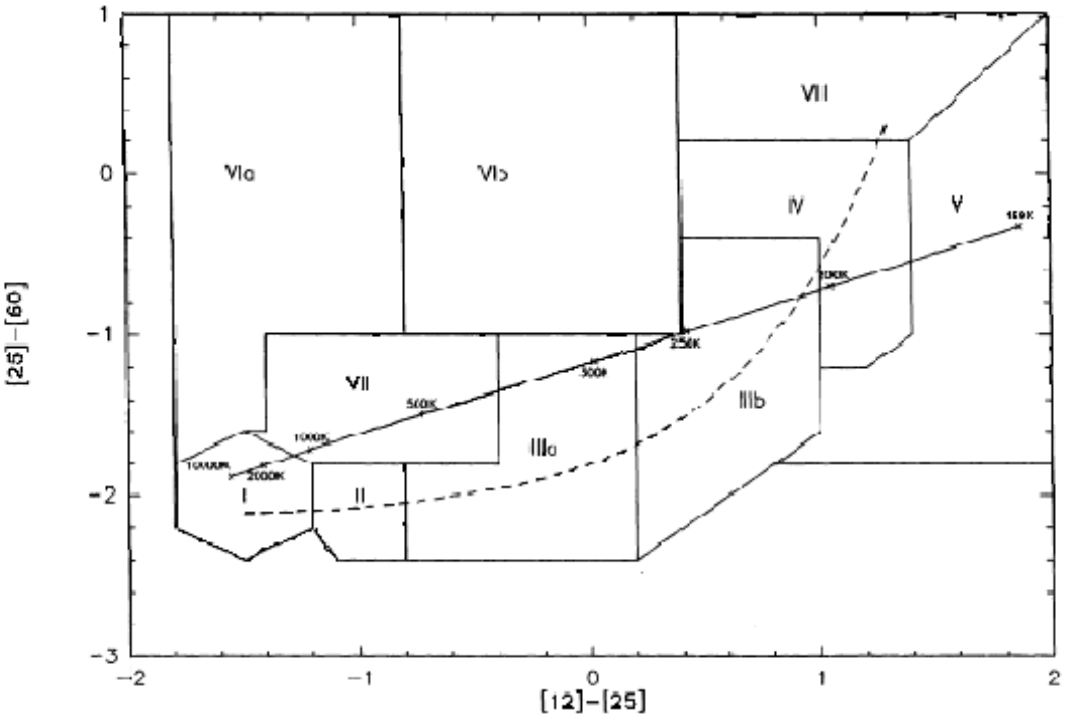

Figure 4: IRAS two-color diagram that separate different sort of DGE-stars. The evolutionary track is given as dashed lines and the black body curve by the full line. Figure is from van der Veen and Habbing (1988)

some of these stars the evolutionary status is not yet clear. We have also used high strömgren c_1 index and high galactic latitude as a criteria for luminous stars at high latitudes, which are post-AGB (Reddy et al. 1996). Many UV bright stars in clusters seem to be post-AGB stars.

Apart from the samples from the IRAS catalogue, we have also looked at A-F stars which have weak MgII 4481Å line. Many of these stars seem to have peculiar Hα line profile (Fig. 5). There are blue and red shifted lines within the photospheric absorption. Many of them show broad absorption wing and narrow absorption core, indicating the presence of extended shell like structure. Some of them show double peak emission indicating a disk like structure in circumstellar Many of them show broad absorption wing and narrow absorption core, indicating the presence of extended shell like structure. Some of them show double peak emission indicating a disk like structure in circumstellar disk.

The objects which are in the transition from AGB to planetary nebula (PN) are very less understood. The evolution in this stage is very fast. The theoretical calculations (Schönberner 1988) gives a value of 1000yr for the transition period, however there were two objects (Hen 3−1357 = Stingray Nebula, SAO85766) which were seen to evolve more rapidly (Parthasarathy et al. 1993, 1995; Bobrowsky et al. 1998, Parthasarathy et al 2000). The uncertainty in the determination of the mass-loss rates makes it difficult to do a theoretical modeling of these stars. Most of the time the star is obscured by the dust. When the star is going through the AGB to PN it goes through severe mass loss which will be surrounded as a dust envelope around the star. The circumstellar dust and the envelope modifies the spectrum emitted by the photosphere. Along the transition from AGB to PN also the star changes its color due to the contraction star. We have studied few individual objects from the selected sample.

Table 1.1: A and F stars selected from the analysis of IRAS data

Object	Sp.Type	V	b	Flux in Jy			
				12μ	25μ	60μ	100μ
IRAS 04101+3103	AIabe	10.14	-14.39	2.98	6.80	5.27	3.44
IRAS 02143+5852			-1.93	5.90	18.06	5.39	8.97
IRAS 15126-3658	F4Ve	8.70	17.3	1.59	6.71	25.60	25.10
IRAS 15373-4220	A7V	8.2	+10.20	4.11	18.14	19.30	13.94
IRAS 13110-5425	F5Ib/Iab	8.39	8.03	.31	2.11	7.60	5.33
IRAS 05273+2517	A3	8.1	-4.78	5.59	12.59	27.98	18.95
IRAS 04555+2949	A2eSh	7.66	7.9	10.30	10.30	11.10	12.50
HD 100412	B9IV	9.3	1.35				
HD 100453	A9V	7.9	+6.81	7.23	33.59	39.36	23.86
IRAS 05355-0117	A5III	9.88	-16.85	.68	3.89	10.38	9.00
HD 101584	F0Iape	7.01	+5.94	92.60	138	193.00	104.00
SAO 19283	A	8.8	+13.68	3.68	10.76	4.26	3.58
-31 5049	A0	8.60	-3.7	117.40	93.74	21.74	8.12
-49 3441	B8	10.0	-8.53	5.35	4.66	1.18	3.29
HD 44179	B8V	8.83	-11.76	421.60	456.10	173.10	66.19
HD 98922	B9Ve	6.7	+7.22	40.16	27.24	6.19	7.96
SAO 157401	F5	9.20	45.48	7.14	1.83	.82	1.00
V718 Sco	A8III/IV	9.00	+20.45	5.68	5.89	5.01	3.14
HEN 847	F	10.0	+13.95	36.07	48.75	13.04	3.31
HD 163506	F2Ibe	5.46	23.19	97.52	54.59	13.42	6.04
AB Aur	A0pe	7.08	-7.98	27.16	48.10	105.60	114.10
HD 87737	A0Ib	3.49	50.75	1.93	0.51	0.40	1.00
HD 58647	B9IV	6.81	1.0	4.95	2.87	0.47	7.36
β Pic	A5V	3.85	30.6	3.46	9.05	19.90	11.30
51 Oph	A0V	4.81	5.34	15.67	10.19	1.06	5.97
α PsA	A3V	1.16	-65.90				

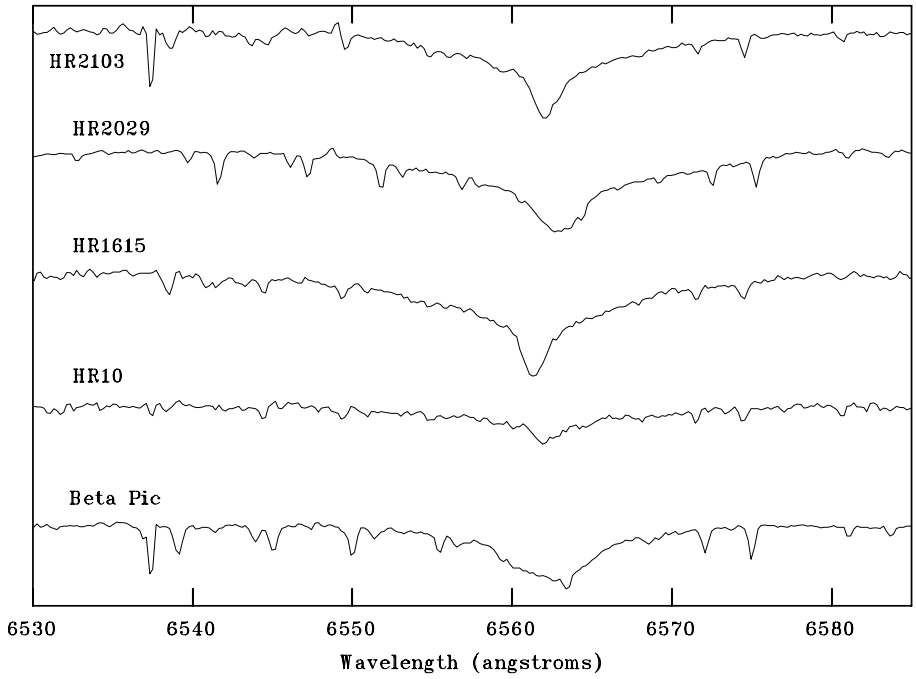

Figure 5: The high resolution spectra obtained from 1.2m Coude Echelle spectrograph at Kavalur, showing the peculiar Hα profiles

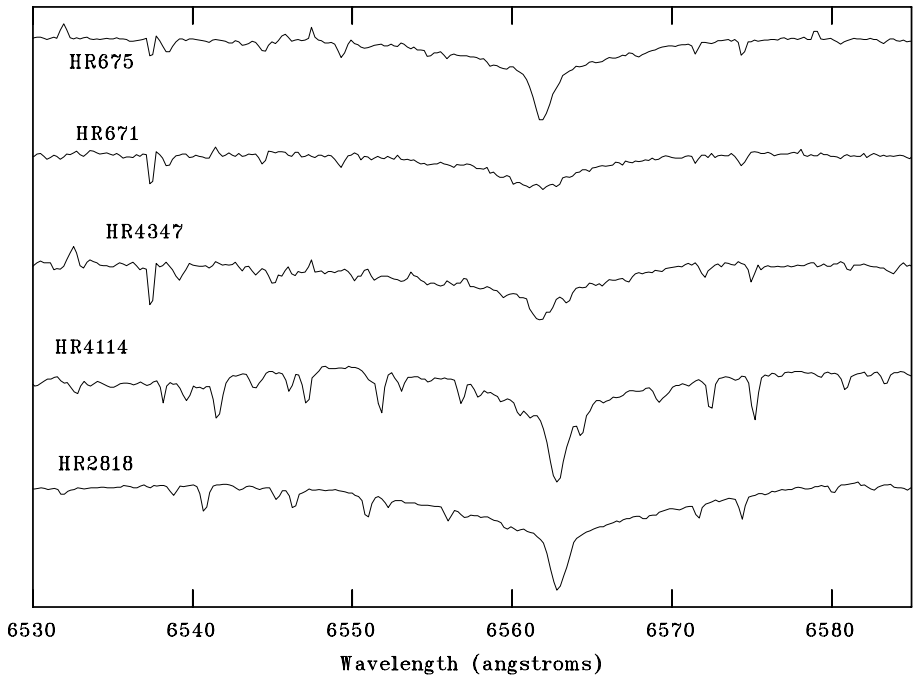

Figure 5(continued): Peculiar lineprofiles of Hα line indicating structures in the circumstellar environment.

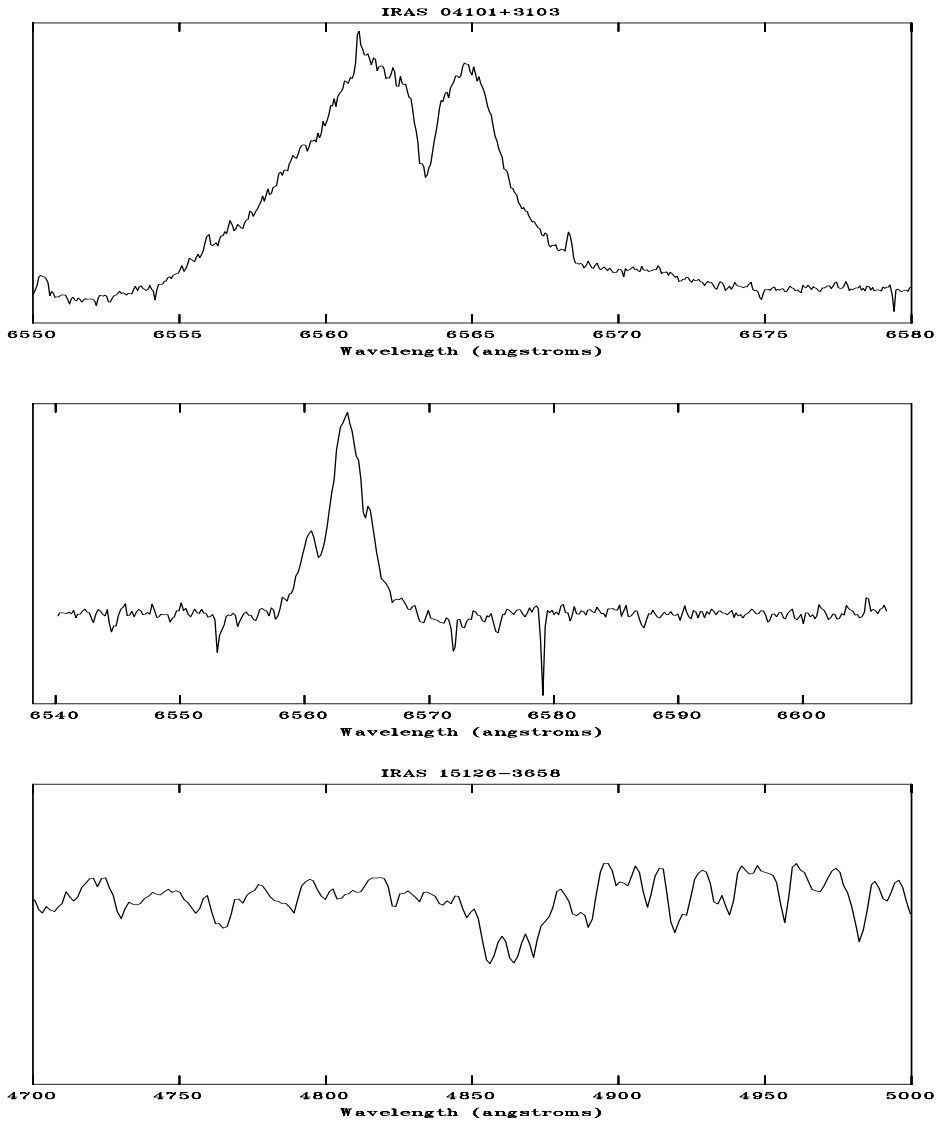

Figure 5(continued): The double peak emission in the top panel and the double peak emission inside the photospheric absorption in the lower panel indicating a disk geometry in the circumstellar region

1.4 Description of few individual objects

We have obtained low resolution spectra of the samples using the 2.3m and 1m telescope at Vainu Bappu Observatory (VBO), Kavalur. We will give a brief description of few of them here.

1.4.1 Redrectangle

This is a carbon rich post-AGB star which in the transition towards formation of a PN. It is a binary star. The central star of the Red Rectangle nebula, HD 44179 belongs to the small class of extremely metal deficient binary post-AGB stars. The object is famous for its remarkable optical reflection nebulosity with a pronounced X shape. The imaging at high angular resolution has shown that the central star is obscured from view in the optical, and that only scattered light from above and below what appears to be a disk reaches the observer (Roddier et al. 1995). The nebular material is carbon-rich, as evidenced by the prominent UIR bands, which are attibuted to C-rich dust. The gas around the star shows metal poor composition, because of metals locked up in the dust grains. Redrectangle nebula is a very interesting object to study the dust formation, gas-dust seperation and selective gas accretion to provide metal depletion. Recently there were some evidence of a planetary system around this star(Jura et al 1997). From our low resolution spectrum we looked for photmetric and spectroscopic variations and the correlation with the orbital motion.

1.4.2 V718 Sco (IRAS 16102-2221)

This star is known as a eclipsing binary. The IRAS colors of the star shows that it could be a pre-mainsequence star or a post-AGB. The evolutionary status of this star is not very clear. The Hα profiles of this star is varying. Some times it looks like a shell line. The variations in the line profiles could be due to the mass loss and shocks

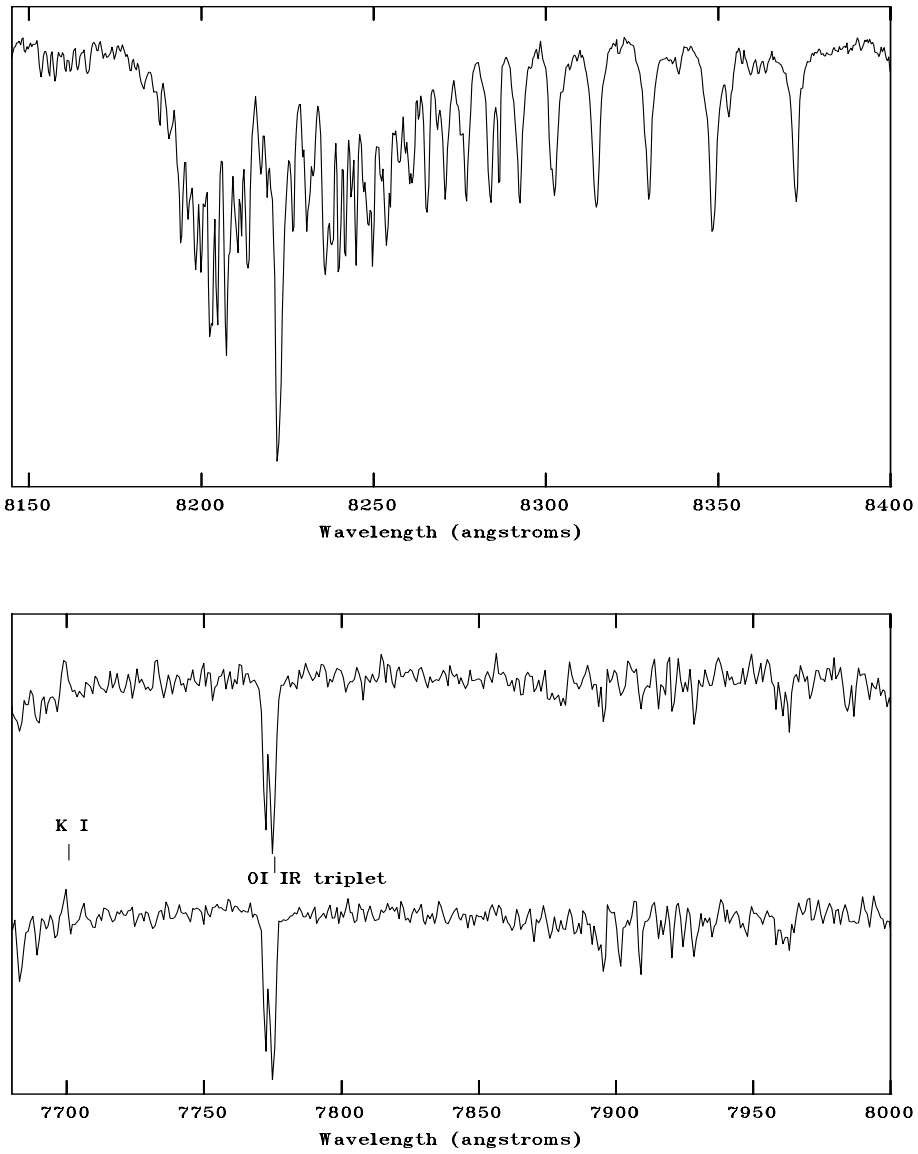

Figure 6: The spectra of the central star of the redrectangle nebula

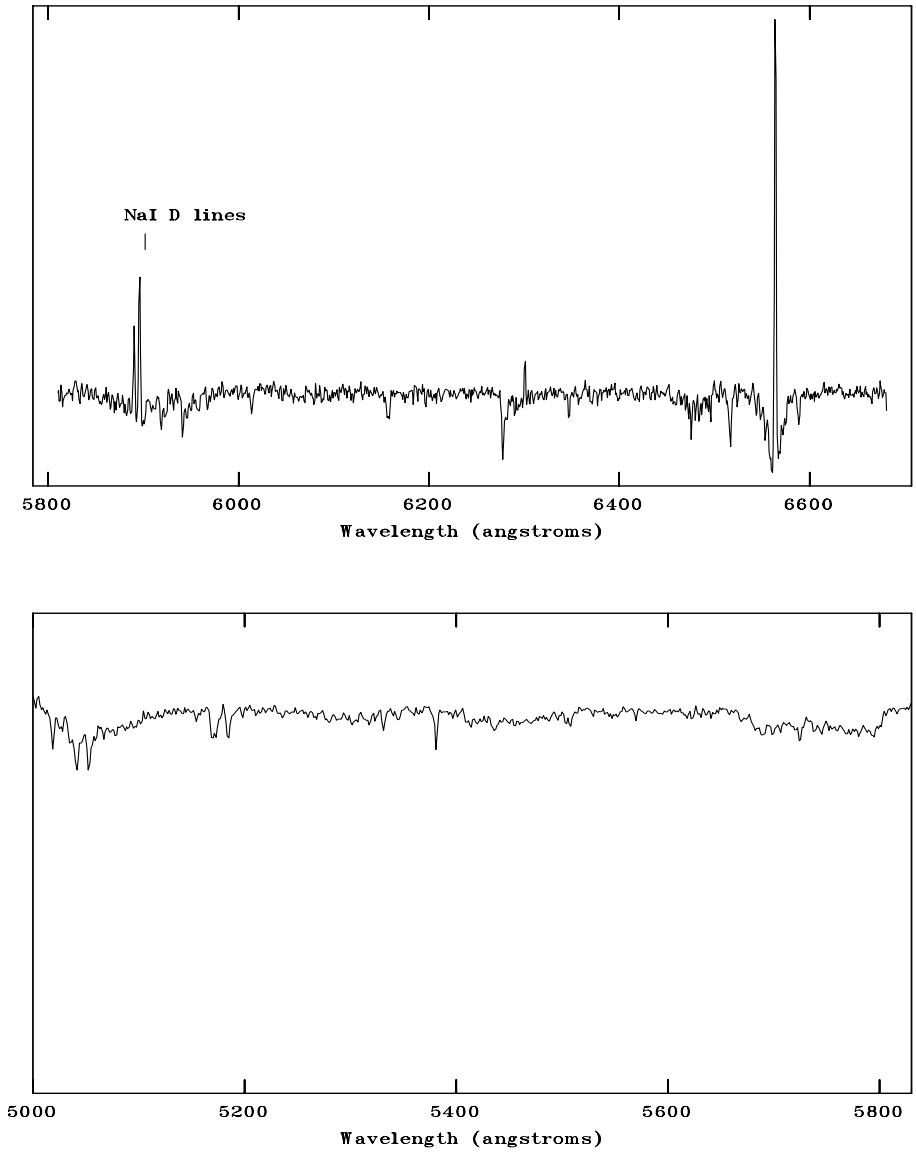

Figure 6(continued): The spectra of the central star of the redrectangle nebula. The absence of metallic lines shows significant underabundance of iron as result of condensation into dust grains

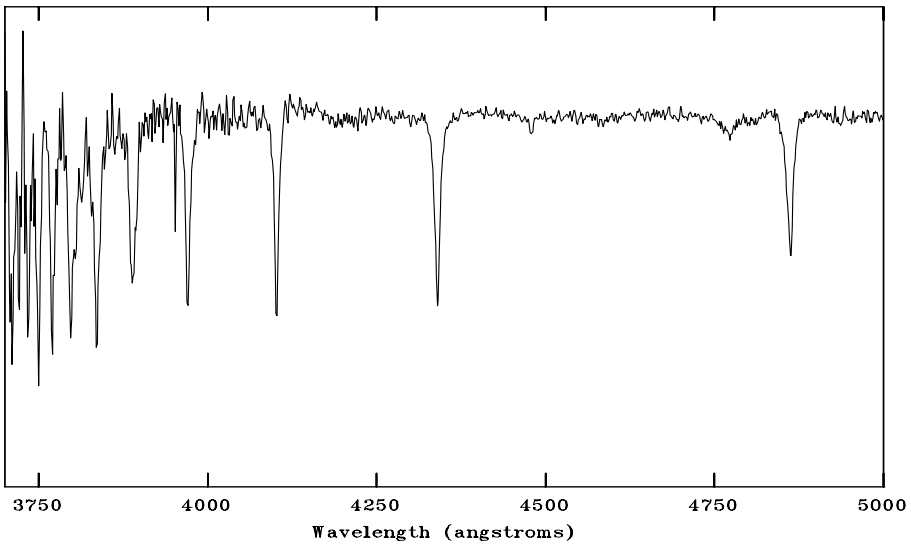

Figure 6(continued): The spectra of the central star of the redrectangle nebula in the post-AGB stage.

1.4.3 HD 100412

It is a B9IV star. We have obtained the optical spectrum of HD 100412 with a resolution of 1.2Å and with 2.5Å. We found Hα in emission and Hβ has filled in emission. These emissions seem to show slight variations in the intensity. The Balmer lines indicate a surface gravity of 4.0. So this object could be a pre-mainsequence Herbig A_e/B_e star. We have done theoretical spectrum synthesis of HD 100412 and found that the star is of A spectral type and we see that the star is slightly metal poor. In that case HD 100412 could be a progenitor of a λ boo star. We also see the carbon and nitrogen and oxygen abundance to be solar.

1.4.4 HD 100453

This star was found to have cold circumstellar dust. It CO emission in the sub-mm wavelength. It shows a shell like emission in the Hα.

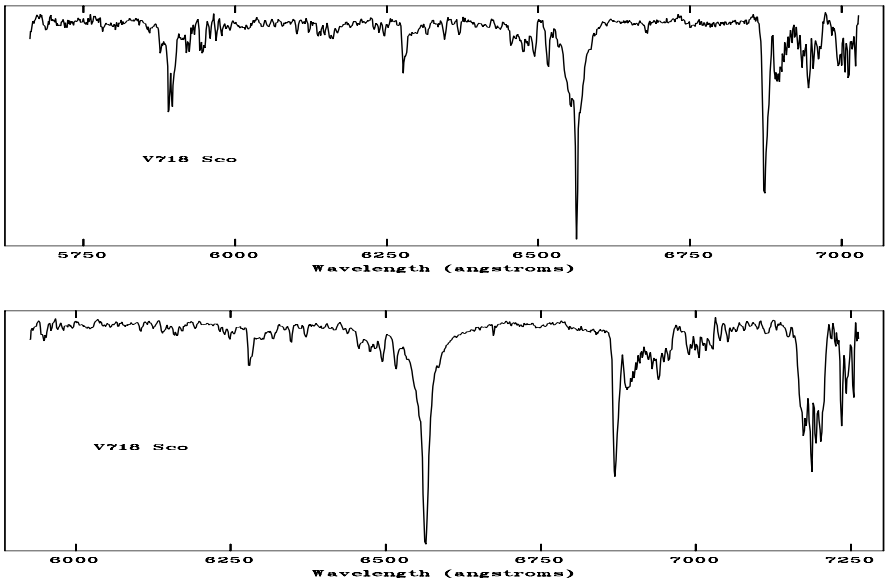

Figure 7: Inside the photospheric absorption line profile of Hα, in the V718 Sco spectrum there is a narrow absorption in the core and a double peak emission in the either side. The Hα line profile also shows variation

1.4.5 HD 98922

This is included as a new member of Herbig Ae/Be star list. We see P-Cygni profile of the Hα line. The Hβ line also shows a asymmetry in the line profile due to the filled in emission. The OI 7777Å IR triplet lines are in emission. This indicates a warm gas.

1.4.6 Hen 416

This object is also included as a new member of the Herbig Ae/Be star. We find strong Hα emission. Even all the other balmer lines are in emission. The Hβ line shows a P-cygni profile indicating a mass loss. There are lots of forbidden emission lines. This should be coming from a thin nebula.

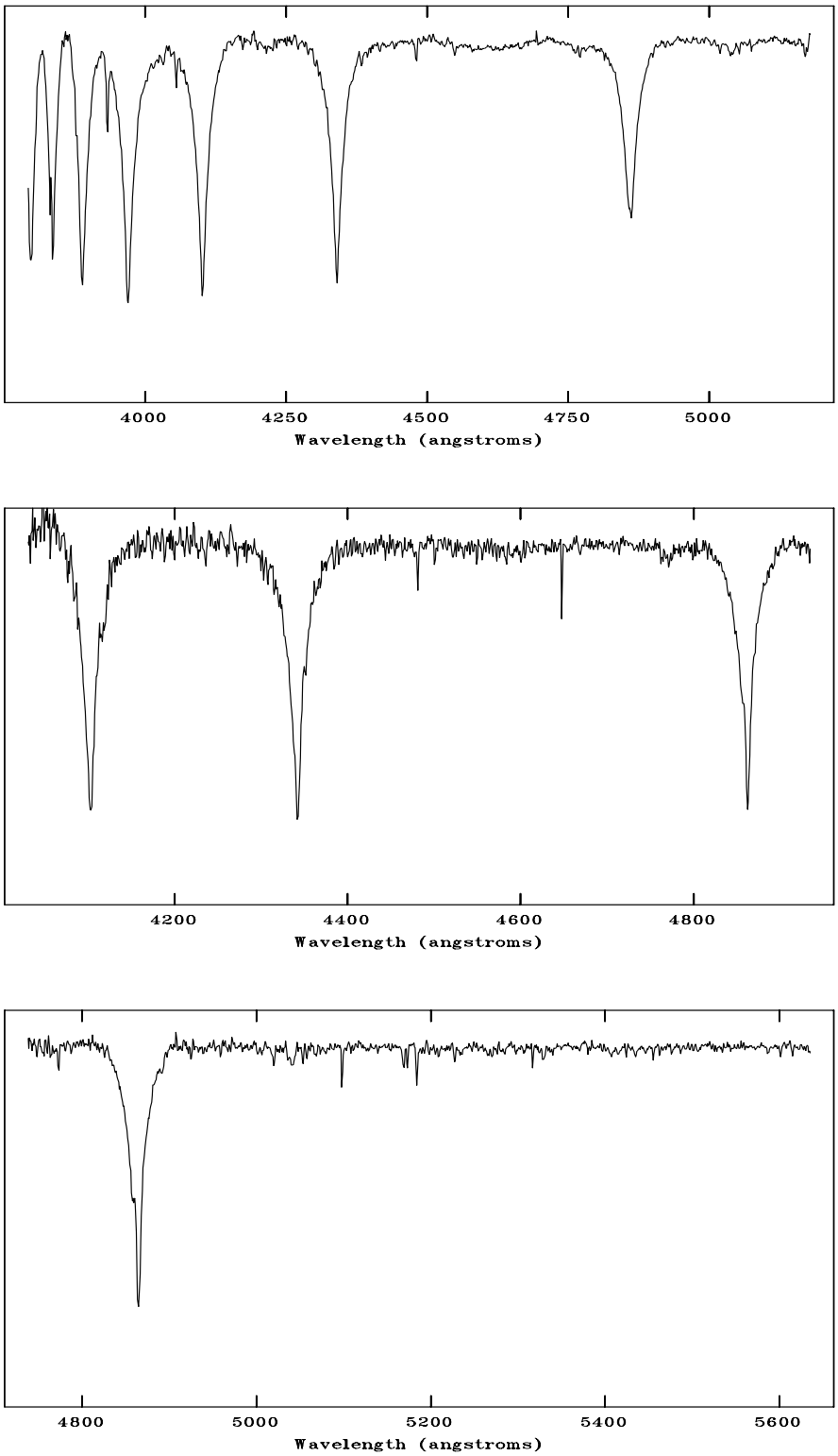

Figure 8: Spectra of HD100412 which shows Hα in emission and the Hβ line shows filled emission.

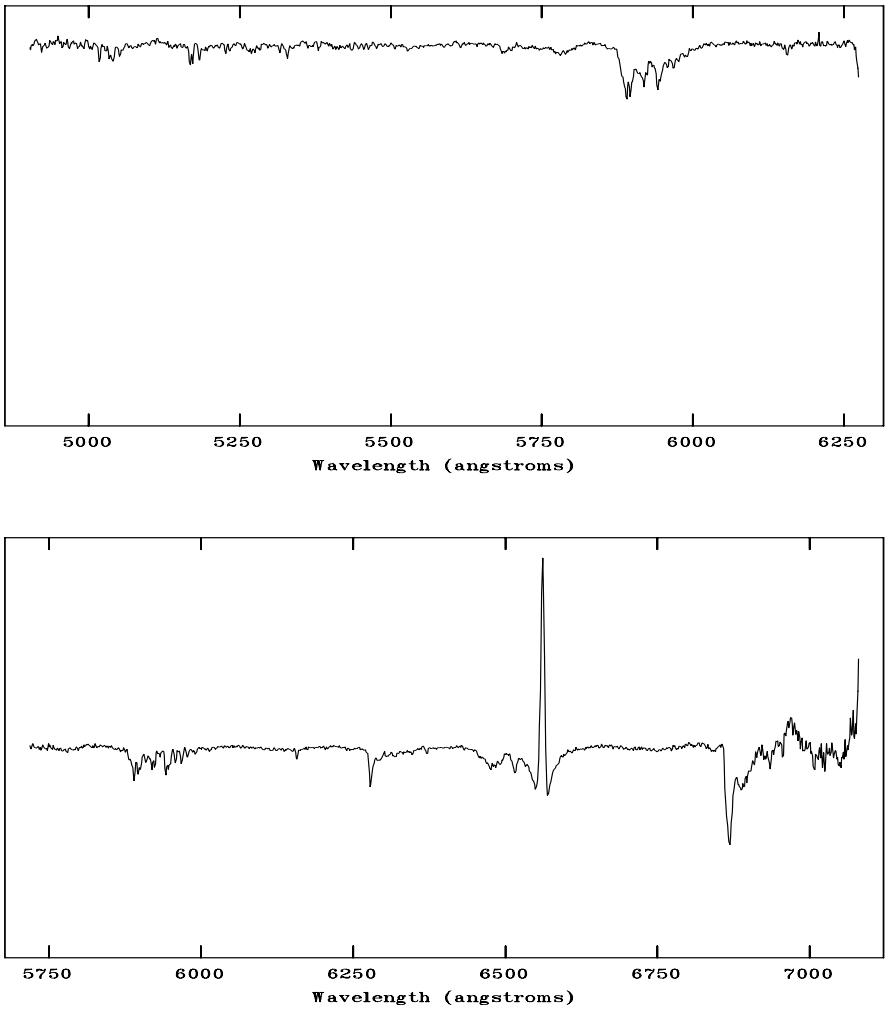

Figure 8(continued): Spectra of HD100412 which shows Hα in emission and the Hβ line shows filled emission.

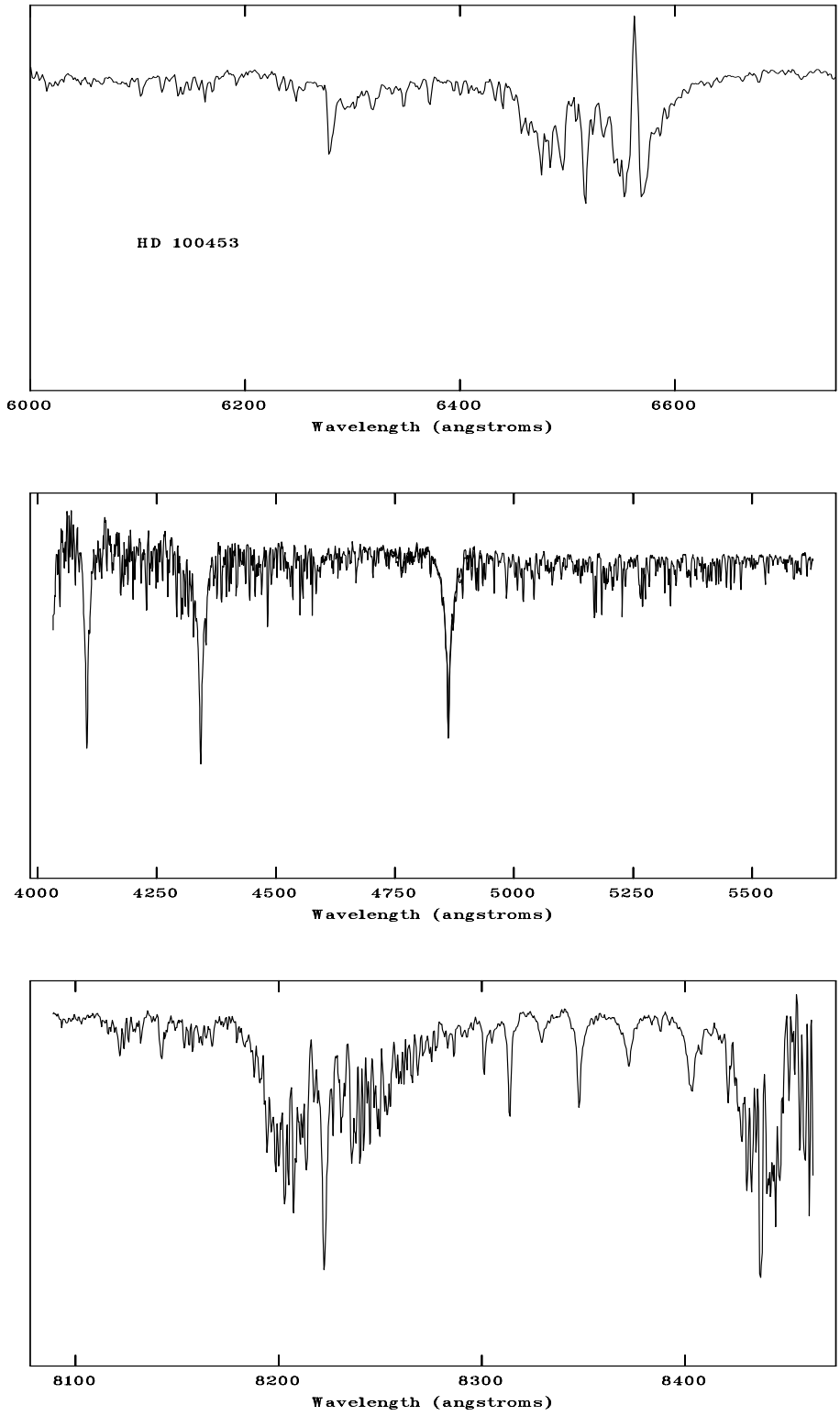

Figure 9: Spectra of HD 100453 showing shell emission in Hα

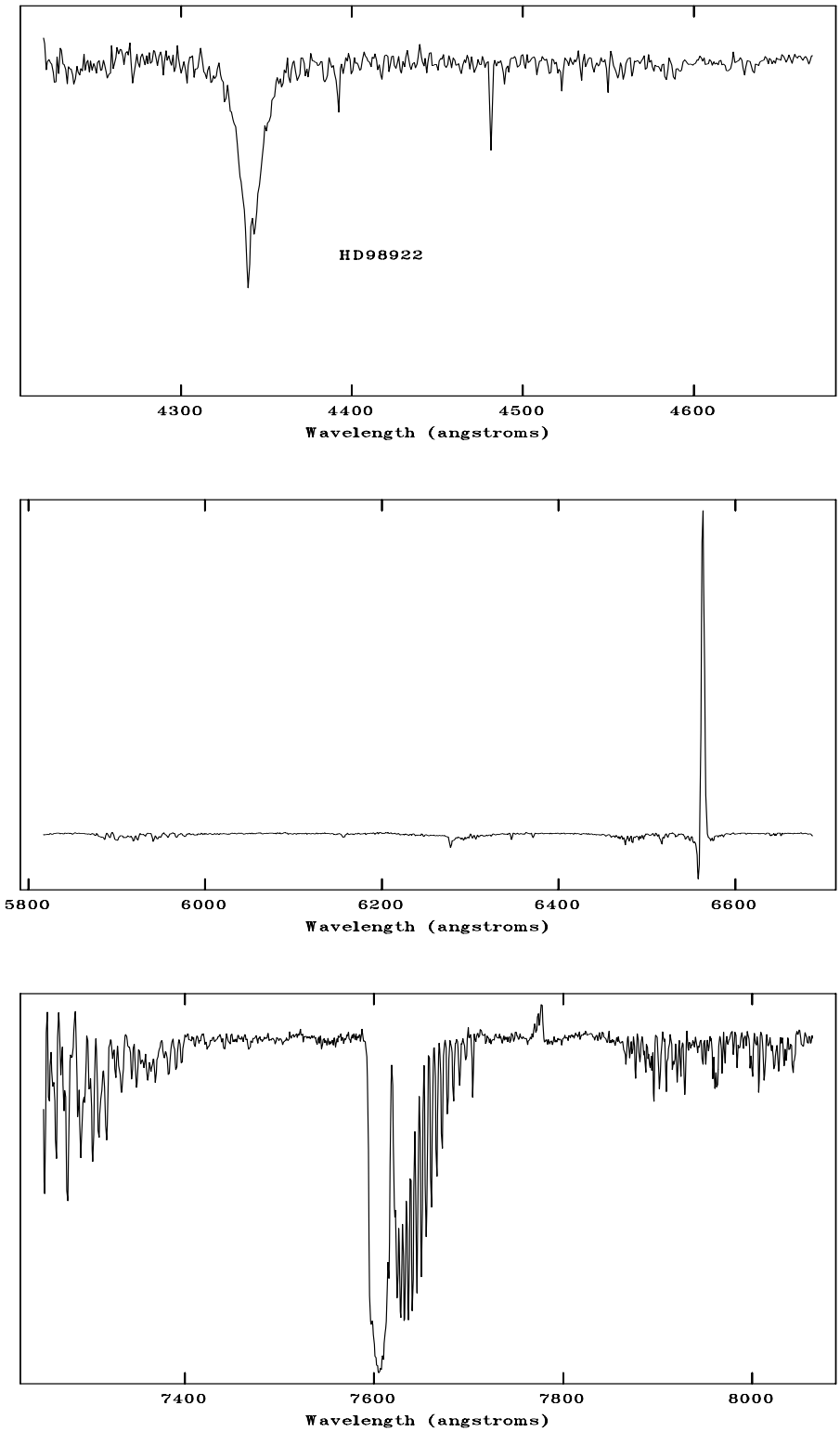

Figure 10: Spectra of HD 98922 showing a strong P-Cygni emission in Hα. The OI IR triplet lines also show emission

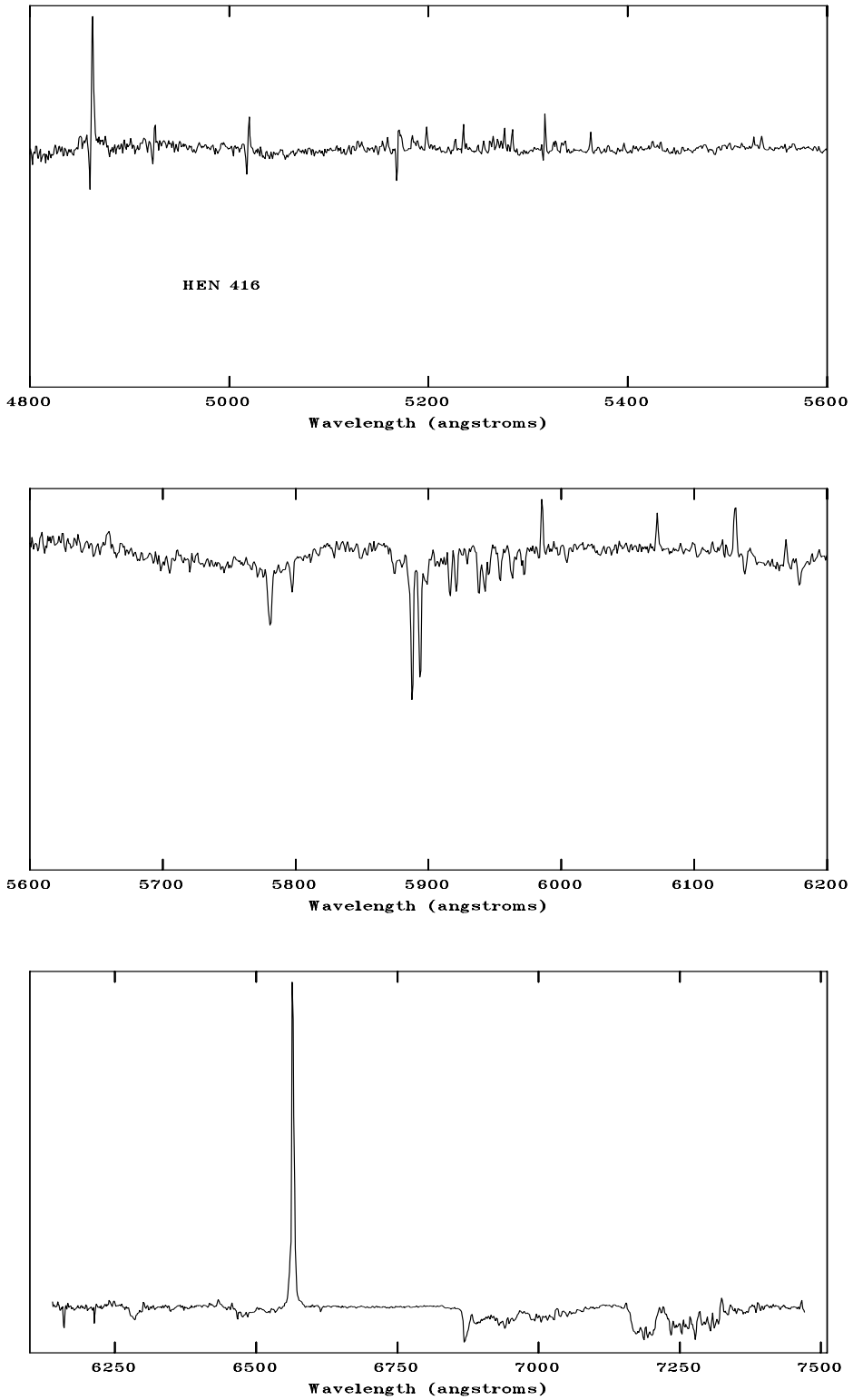

Figure 11: Spectra of HEN 416 showing sharp Balmer lines emission. The Hβ shows P-Cygni profile.

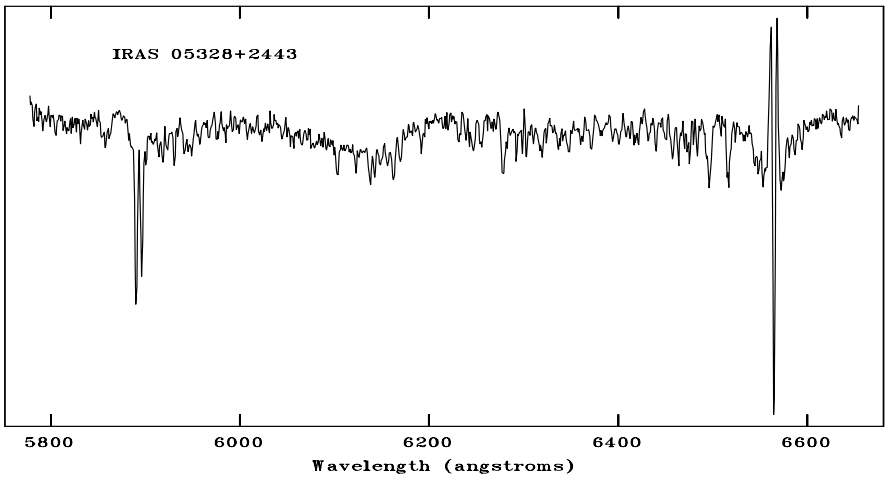

Figure 12: Spectra of IRAS 05328+2443 with a double peak shell like Hα emission

1.4.7 IRAS 05328+2443

It is known as a Herbig Ae/Be star. We find a very sharp double peak emission. This could be due to a shell around the star.

1.4.8 IRAS 05355-0117

It is known as a δ scuti type variable star. We find a strong emission line feature of Hα. The Hα line shows P-Cygni profile. At some epochs the P-Cygni profile becomes a normal symmetric emission. This idicates episodic mass loss in this star. This could be the probable cause for the photometric variabilities observed.

1.4.9 IRAS 15126-3658

It is classified as a A0 mainsequence star with circumstellar dust. It shows strong Hα emission. The CaIIK and the CaI IR triplet lines suggest that the object is cooler than A type. Probably a F type and also the lines are more sharp for a mainsequence star. So it could be pre-mainsequence or a post-AGB star. The Paschen lines are

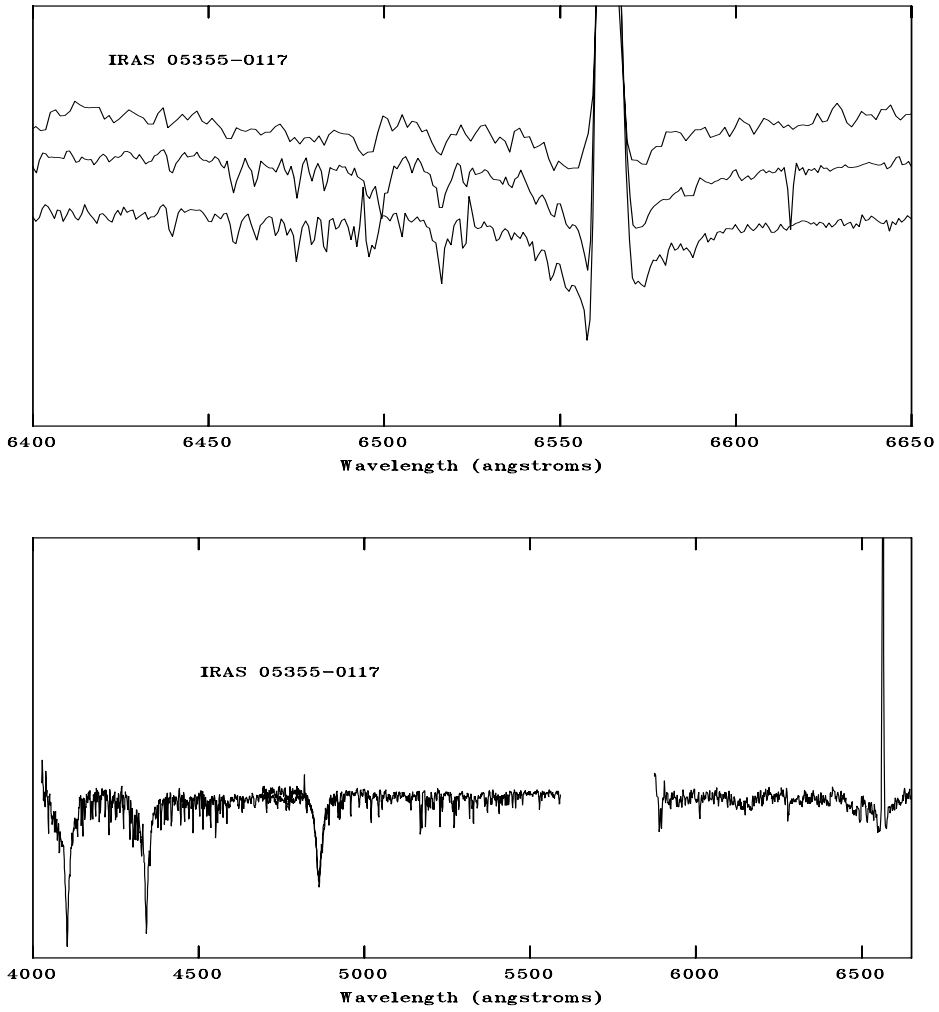

Figure 13: Spectra of IRAS 05355-0117, shows variations in the Hα line profile (P-Cygni to single peak). It is showed in the top panel.

almost not there indicating a spectral type later than A.

1.4.10 IRAS 15373-4220

IRAS 15373-4220 has 12μm excess amd 100μm fluxes like β pic disks. From the 10μm spectroscopy and sub-mm observations, silicate dust and optically thick dust at 1300μm (Walker and Butner 1995). Van der veen et al. (1989) classified it as a transition object between AGB and PN stages. Walker and Wolstencroft (1988) proposed it as a vega type star with a protoplanetary disk, but the optical emission lines suggests that the IR excess could be due to mass loss processes.

1.5 Description of selected samples for a detailed study

1.5.0.1 HD 101584 (IRAS 11385-5517)

HD 101584 is a peculiar F supergiant. From the IRAS colors and energy distribution Parthasarathy and Pottasch (1986) suggested that it is a low mass star in the post-AGB stage of evolution. The spectrum of the star is quite peculiar it has lot of emission lines,P-Cygni line profiles and asymmetric line profiles. This makes it difficult to estimate the stellar parameters and chemical composition. We derived T_{eff} = 8500K and log g = 1.5 from the blue opical spectra. We found that carbon and nitrogen are overabundant and oxygen is solar. The metallicity of the star is also solar. Oloffson and Nyman (1999) also see evidence of enhancement in $^{13}C/^{12}$C. This clearly shows that HD 101584 is post-AGB supergiant and not a luminous blue variable.

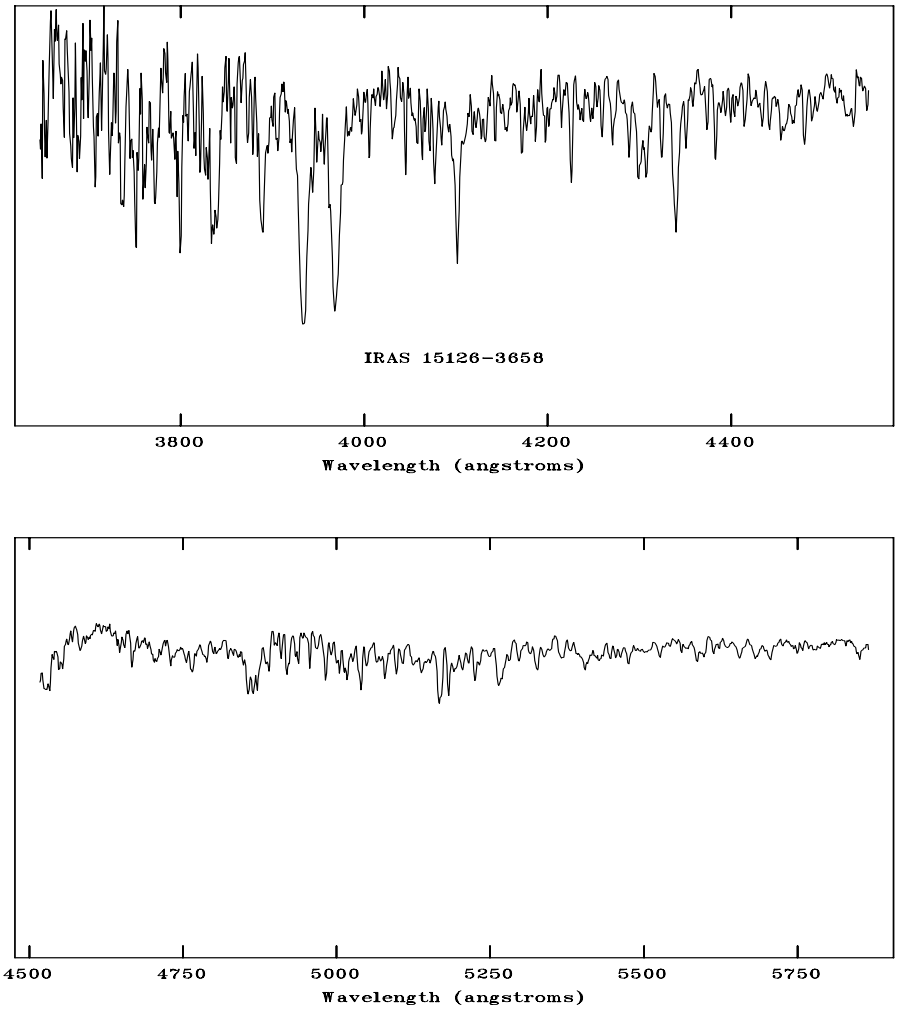

Figure 14: The spectra of IRAS 15126-3658 in the top panel shows a strong CaII K line.

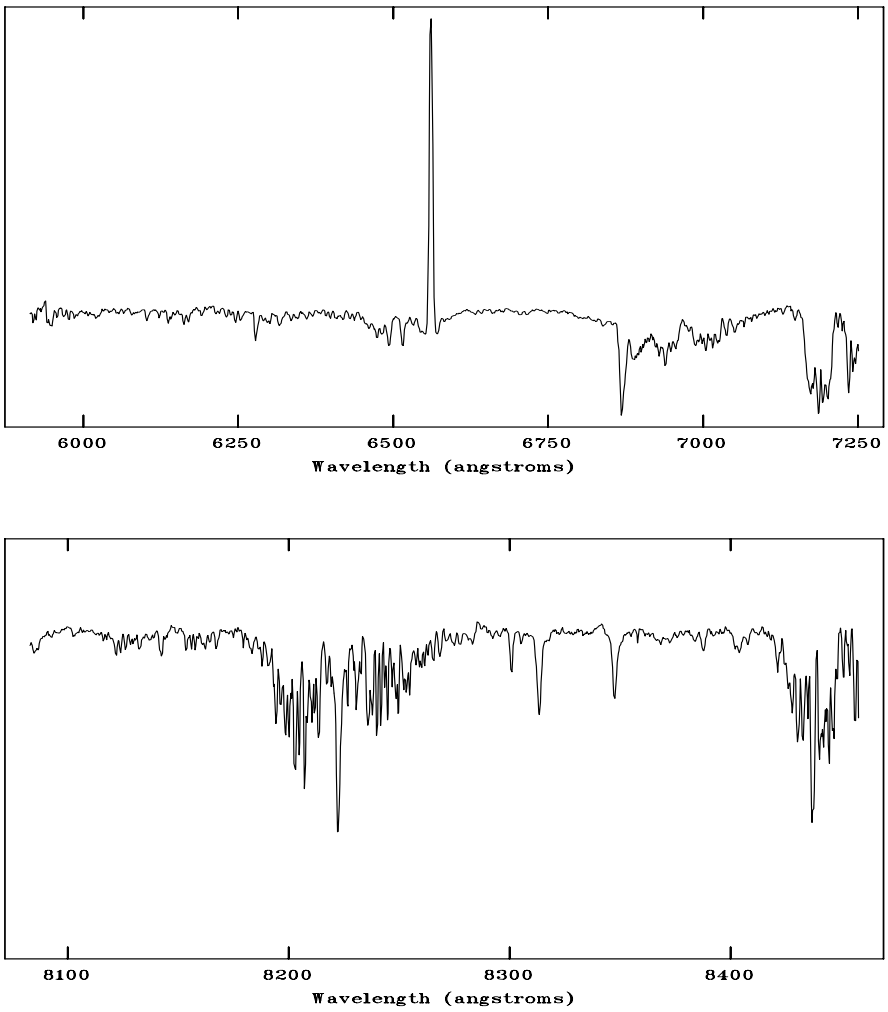

Figure 14(continued): The spectra of IRAS 15126-3658 shows a strong emission in Hα and it shows strong CaII IR triplet lines. There are no Paschen lines visible.

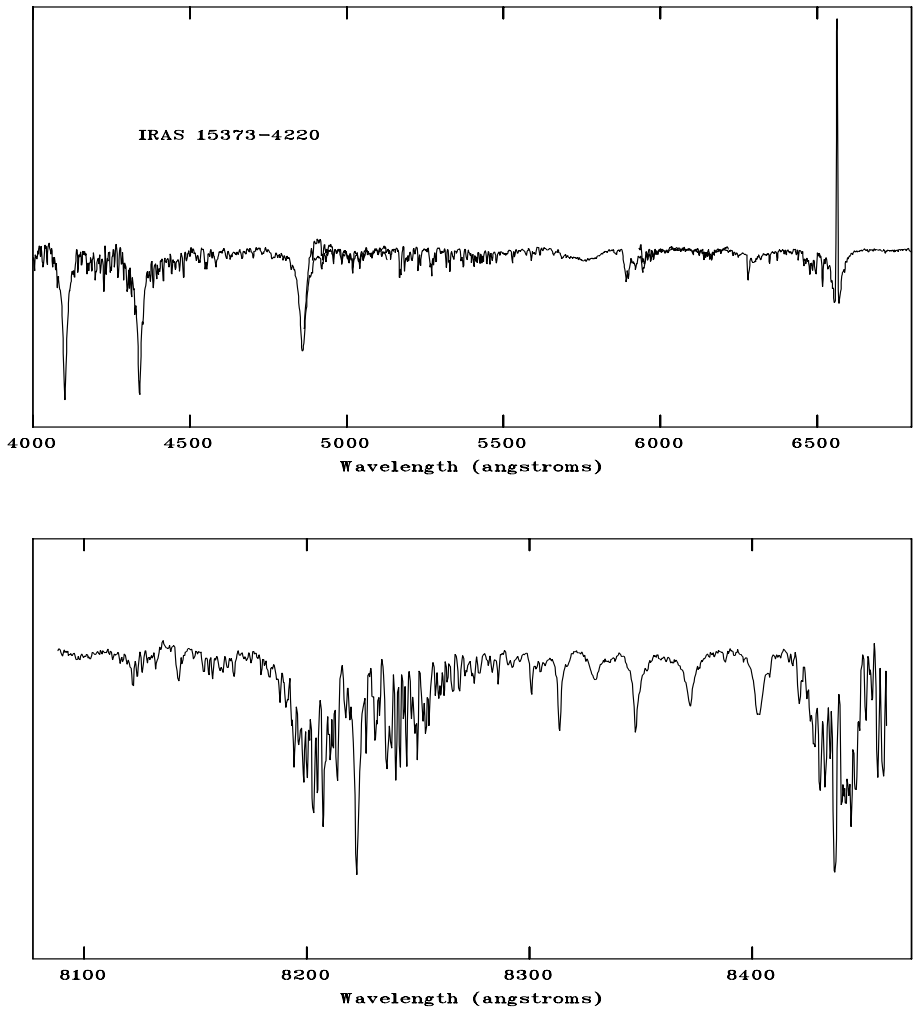

Figure 15: Spectra of IRAS 15373-4220 showing strong emission in Hα. In the bottom panel both Paschen and CaII IR triplet lines are seen.

1.5.0.2 HD 331319 (IRAS 19475+3119)

HD 331319 is a high Galactic latitude Post-AGB F3 supergiant. It has IRAS colors and CO emission like the other post-AGB stars. We have got the high resolution spectrum of this object, from the Issac Newton Telescope, at La Palma. The object shows strong absorption lines of metals similar to a F star. From the theoretical spectrum synthesis of Hβ line region we derived T_{eff} = 7500K and log $g = 0.5$. We found that the ionized lines of Fe, Ti etc. are very strong. This indicates that the atmosphere of the star is very extended. There are many spectral lines of r and s process elements seen in the spectrum. We have done detailed chemical composition analysis of this star.

1.5.1 HD 187885

We have analysed high resolution spectrum of the post-AGB F-supergiant HD 187885. We have derived T_{eff} from different methods. We discuss here the chemical composition of HD 187885 and the atmospheric parameters. We find that HD 187885 is a metal poor [Fe/H] $\sim$ -1.0, and overabundant in carbon and s-process elements. It appears to have experienced third dredge up and has gone through the carbon star phase on the AGB.

1.5.2 IRAS 10215-5916

IRAS 10215-5916 is a double-lined spectroscopic binary. In our high resolution spectra we found molecular features from a cool companion of T_{eff}=3750K. We also see the spectral signature of a relatively hotter star of T_{eff}=7250K. We found that both the components of the binary system are metal poor. We have derived the carbon and oxygen abundances. They are also depleted compared to the solar value. The α process elements are also depleted with respect to the solar value. Since we see the

volatile elements also depleted, the binary system correspond to a older population.

1.5.2.1 HD 168265 (IRAS 18184-1623)

This is a emission line star with a B9 spectral type. The evolutionary status is unclear, whether it is massive luminous blue variable or a post-AGB star. We have got the high resolution spectra of this object from the Issac Newton Telescope (INT), at La Palma. We have found nebular lines of NII and SII indicating that the object has a low excitation nebula. There are neutral helium lines, OII lines, CII and NII lines seen in the spectrum. We have done detailed chemical composition of this object.

1.5.2.2 HD 31648 (IRAS 04555+2946) and HD 36112 (IRAS 05273+2517)

Gaseous disks, which are seen in many of the pre-mainsequence stars are potential sites for studying planets in their formation. Observing the variations of emission lines originating from these gaseous disks will give information on the structure of the disk. Any structural changes in the disk will give rise to variations in the optical depth and this in turn gives variations in the intensity as well as in the profiles of the emission lines.

We have obtained optical spectrum of HD 31648 and HD 36112 in the region 5800Å to 6690Å. About 30 frames have been taken over a period of two years. We see hourly and day to day variations in the spectrum. The variations seem to be periodic. The variations are seen in HeI 5876Å and HeI 6678Å emission lines. We also see variation in Hα and NaI D lines and OI triplet lines. The Hα emission line changes from P-Cygni to single peak emission. The equivalent width of SiII 6347Å and 6372Å also show variations. From the double peak emission from Hα we derived the period assuming that the emission is coming from a gaseous Keplerian disk. From the spatial direction of the spectra, we found that the emission at Hα is extended. We found the spatial extension of the emission to be 1AU. Assuming a Keplerian

disk we get same period as we got from the Hα double peak. The variation in the line profile of the He 5876Å also show similar periods. So the variations in the line profiles could be due to rotation. In the case of HD 36112 we see sharp decline in the intensity of HeI 6678Å line in one of the epoch. Here we show that these variations can due to planetesimals moving in the disk crossing the line of sight. Imaging in CO millimeter wavelengths (Mannings et al. 1997) it has been found th the HD 31648 is having a rotating disk.

1.6 Conclusions

We have selected around 25 stars on the basis of the IRAS colors and the Galactic latitude. We have obtained high and low resolution spectra for these stars. From the analysis of the spectrum we found that some these stars are post-AGB having low surface gravity. HD 101584 shows many emission lines in the optical spectrum. The presence of forbidden lines indicates the presence of a low excitation nebula. It is likely that it is having a dusty disk and a bipolar nebula.

HD 168265 shows [NII] and [SII] lines in emission indicating the presence of a nebula. It is classified as a Luminous Blue Variable (LBV). Few others stars which have been selected turned out to be pre-mainsequence stars, having broad Balmer lines profiles indicating a higher gravity. Both these post-AGB and the pre-mainsequence stars have similar IRAS colors and have dust shells. Many of these objects show Hα in emission and also show variability in the line profiles. This indicates that the circumstellar environment in these objects which are in two different stages of evolution is to some extent similar. Both these systems undergo similar physical processes like outflow, shocks, mixing and fractionation. Even the planetary formation also seem to occur in the post-AGB stage (Jura and Turner 1998). Still there are many faint IRAS sources for which the optical spectra have not yet been obtained. Only from the high resolution optical spectroscopy of these stars we can understand the evolu-

tionary status of these stars. High angular resolution and multiwavelength imaging will reveal the presence of nebula, bi-polar flows and disks around these objects.

Chapter 2

Observations and analysis

The main results of this work are based on ground based low and high resolution optical spectra.

2.1 Observations

The low resolution optical spectra were obtained from 2.3m and 1.2m telescopes at Vainu Bappu Observatory, Kavalur. The 2.3m telescope is equipped with a medium resolution Boller and Chivens (B&C) spectrograph [1] and a medium resolution Optometrics Research Spectrograph (OMRS), at the Cassegrain focus (f/13 with a scale of 6.8″/mm). These spectrographs use 150l/mm, 300l/mm, 600l/mm, 650l/mm and 1200l/mm gratings. For a optimum slit width, the spectrographs gives a maximum resolution of 2.5Å at 5000Å. The 1.2m telescope is equipped with a Universal Astronomical Grating Spectrograph (UAGS) at the Cassegrain focus. This gives a maximum resolution of 0.8Å with 1800l/mm grating. At the Coude focus there is Echelle spectrograph which gives a resolution of 0.4Å at 5000Å. For some of the bright

[1] Recently modified into a medium resolution spectropolarimeter

sources we have used this spectrograph. A 1024x1024 pixel TEK CCD, with a pixel size of 24μ is used in all these instruments.

The high resolution spectroscopic data for the detailed chemical composition analysis were obtained with the European Southern Observatory (ESO) Coude Auxiliary Telescope (CAT) equipped with a Coude Echelle Spectrograph (CES). The Coude Auxiliary Telescope (CAT) was designed to feed the Coude Echelle Spectrometer (CES). The telescope has a clear aperture of 1.4m. We have also obtained data from the 2.5m Issac Newton Telescope (INT) located at La Palma, which is equipped with a Intermediate Dispersion Spectrograph (IDS), mounted in cassegrain.

All our program stars are IRAS sources with circumstellar dust shells. For some of our program stars we have analysed the IUE low resolution spectra, which are available in the IUE archieve.

2.2 Data reduction

The data is reduced using Image Reduction and Analysis Facility (IRAF) software developed by National Optical Astronomy Observatories (NOAO). Combining the frames, bias substraction, flatfielding is done by the CCDRED package in IRAF (Philip Massey). The spectroscopic reduction, that is converting into a one dimension image, wavelength calibration, flux calibration and normalization are done using the SPECRED and ECHELLE packages in IRAF. Measuring the equivalent widths and deblending the lines were done by the SPLOT package in IRAF. This uses a Guassian, Lorenzian or a Voigt profile to get the equivalent widths. Multiple gaussians are fit for blended lines. The SPECRED and ECHELLE packages have routines for air mass corrections and removal of telluric lines.

The IUE data were reduced using the IUERDAF software which uses the (Interactive Data Language) IDL routines.

For the emission line analysis, especially for the nebular lines we have used the NEBULAR package of STSDAS in IRAF environment. They use the statistical equilbrium of five levels. The electron density, electron temperature and ionic abundances are derived using various line ratios. A three zone model is used which separates out the low, medium and high ionization zones from different lines and derives the N_e, T_e and other parameters seperately for each region.

2.3 Analysis

The analysis involves following steps.

1. Preliminary estimates of the stellar parameters.

2. Choosing a realistic stellar atmospheric model.

3. Calculation of the theoritical spectrum, using the spectrum synthesis techniques and model atmospheres.

4. Comparing the theoritical spectra with the observed spectrum and deriving the atmospheric parameter and chemical composition of the program stars.

2.3.1 Initial estimates of stellar parameters

The most commonly used methods for determining the stellar parameters are the photometry, spectrophotometry and hydrogen line profiles.

2.3.1.1 Photometry

The intensity of stellar flux varies as a function of wavelength and these variations are linked to temperature, surface gravity and chemical composition. A measurement of stellar flux at several wavelengths can be used to determine such parameters.

Wide and intermediate band photometric systems have been developed to describe the shape of stellar flux distributions via magnitude (colour) differences. Since they

use wide bandpasses, the observations can be obtained in a fraction of the time required by spectrophotometry and can be extended to much fainter magnitudes. The use of standardized filter sets allows for the quantitative analysis of stars over a wide magnitude range.

By carefully designing the filter bandpasses that define a photometric system, colour indices can be obtained that are particularly sensitive to one or more of the stellar parameters. Indeed, photometric surveys of faint stars are used to identify anomalous stars which warrant much closer spectroscopic investigation. Photometric colour indices, once calibrated with model atmospheres, can be used to determine atmospheric parameters. Three photometric systems are in general use:

The most widely used photometric system is the UBV system, developed by Johnson & Morgan (1953). The calibrations by Buser & Kurucz (1978, 1992) are worth noting. However, while UBV colours do agree well with spectral type for stars of similar composition, they do not provided for the separation of luminosity classes and are strongly affected by reddening (Johnson, 1958). The uvbyβ system, developed by Strömgren (1963, 1966) and Crawford & Mander (1966), overcomes some of the limitations of the UBV system. Several model calibrations have been produced, including Relyea & Kurucz (1978), Moon & Dworetsky (1985), Lester, Gray & Kurucz (1986), Kurucz (1991), Castelli (1991) and Smalley & Dworetsky (1994). Moon (1985) produced two very useful programs for dereddening observed uvbyβ colours (UVBYBETA) and obtaining T_{eff} and log g (TEFFLOGG). Geneva seven-colour system has been used since around 1960 at the Geneva Observatory. Calibrations include North & Hauck (1979), Kobi & North (1990) and North & Nicolet (1990).

2.3.1.2 Spectrophotometry

In contrast to the wide bandpasses used by photometric systems, spectrophotometry is the measurement of stellar flux through (generally) narrow bandpasses, usually over

wider wavelength ranges. Only a restricted wavelength range can be observed from the ground; optical spectrophotometry generally covers 3300- 10000Å. However, a lot can be determined from such spectrophotometry, since it contains the Balmer Jump and the Paschen continuum, as well as representing a large fraction of the total energy output of A and F stars (Malagnini et al., 1986). Since the emergent flux distribution of a star is shaped by the atmospheric parameters, we can use spectrophotometry to determine values for these parameters, by fitting model atmosphere fluxes to the observations.

2.3.1.3 Hydrogen line profiles

The Balmer lines provide an excellent Teff diagnostic for stars cooler than about 8000 K due to their virtually nil gravity dependence (Gray, 1992). For stars hotter than 8000 K, however, the profiles are sensitive to both temperature and gravity. For these stars, the Balmer lines can be used to obtain values of log g, provided that the Teff can be determined from a different method. While the hydrogen lines are relatively free from other absorption lines in most B-type stars, the same cannot be said of stars later than mid A-type. Fitting is hampered by the numerous metal lines in the spectra of these stars, ironically just as the hydrogen lines become insensitive to log g! Nevertheless, by careful reductions and analysis, observations of Balmer lines can still be used to determine Teff. Normalization of the observations is critical. Naturally, the shape of the Balmer line must be preserved (Smith& van't Veer, 1988). A useful check is to observe Vega or Sirius and compare the reduced spectrum with those given by Peterson (1969). While it is very difficult – if not impossible – to use Echelle spectra, medium-resolution spectra can be used. We have to allow for the effects of blending of metal lines and the effects of rotation. Rotation is potentially a more difficult problem, since by increasing resolution we can reduce the effects of blending, but not that caused by rotational smearing. The continuum changes due to metallicity also. Overall, hydrogen lines give very good values of Teff for A and

F stars, with internal errors of the order of 100 K or less. But, naturally, the actual value of Teff is model dependant.

All the stars in our selected sample have IR excess, which indicates the presence of dust. So getting the extinctions due circumstellar dust and correcting the fluxes obtained from the photometry is difficult. And hence deriving the stellar parameters from photmetry is not very accurate. The Balmer line profiles in the spectral region A-F depends both on the T_{eff} and log g values. So one has to have a estimate of one of the parameter to obtain the other. The balmer lines Hα and Hβ, in some of the objects are affected by the emission due to wind and circumstellar gas. However the higher members of the Balmer series the effect due to circumstellar may not be significant. So we have used Hγ and Hδ lines. Objects for which we had obtained high resolution spectra, we had derived more accurate values of the stellar parameters from the line analysis and spectrum synthesis.

2.3.2 Choice of the stellar stmospheric model

The stellar atmospheric models are generally defined by the effective temperature T_{eff}, surface gravity log g, the metallicity [M/H] and the microturbulaence velocity ξ_t. To decide upon the correct models generally one uses, the excitation equibrium for the correct temperature of the model. and ionization equilibrium is used to decide the correct surface gravity of the model. Microturbulence velocity is a parameter that is generally not considered physically except in the sun. Usually it is treated as the parameter that minimizes scatter among the lines of same ion in the abundance analysis. Microturbulence varies with temperature, gravity and chemical composition.

The trignometric parallaxes measured by the Hipparcos mission provide accurate appraisals of the stellar surface gravity for nearby stars, which are used (C.A. Prieto et al. 1999) to check the gravities found from the photospheric iron ionization balance. They find an approximate agreement for stars in the metallicity range -1.0

$\leq [Fe/H] \leq 0.0$, but the comparision shows that the differences between the spectroscopic and trignometric gravities decrease towards lower metallicities. This casts a shadow upon the abundance analysis for extreme metal-poor stars that make use of the ionization equilibrium to constrain the gravity. The strong-line gravities (by matching the profile) derived by Edvardsson (1988) and Fuhrmann (1998) confirms that this method provides systematically larger gravities than the ionization balance. Even there are inconsitency in the obtained temperature of the models using the excitation equilibrium.

2.3.3 Stellar atmospheric models

After obtaining equivalent widths and line profile from a high resolution and high signal to noise ratio data, it is analysed using a classical model atmosphere, which has following assumptions:
local thermodynamical equilibrium (LTE), hydrostatic equilibrium, conservation of flux, and plane-parallel stratification. Also, the mixing-length theory is used to take convection into account.

Plane parallel models are usually hotter the than corresponding spherical models in the region of line formation. So calculated neutral lines will often be weaker and ionized lines stronger for plane parallel models than for spherical ones.

In low metallicity stars there is much weaker metal-absorption in the ultraviolet, so more amount of non-local UV flux is able to penerate from the deeper layers. This flux is vital in determining the ionization equilibrium of the atoms. As a consequence the role of radiation on the thermodynamical state of matter becomes more important, resulting in stronger deviations from LTE. These are even more critical in the low gravity stars due to low densities.

We have used the Kurucz (1993) stellar atmospheric models, which are LTE line blanketed models, which assumes plane parallel geometry. The Kurucz model grids

are seperated by 250K in T_{eff} and 0.25 in log g values around temperatures, 10000K. For lesser temperature the separations are more closer. The models are available for four different values of microturbulence velocities (2,4,6,8kms^{-1}).

2.3.4 Atomic data for spectroscopy

In many cases lack of accurate atomic data is still the major obstacle for extracting the finer details embedded in the observations. The primary parameters for making the line identifications in stellar spectra are wavelengths, energy levels and oscillator strengths. Most serious problems appear in the short wavelength end of the satellite region. The accuracy of 5 to 10 percent obtained from OP and OPAL databases, is at present sufficient for the "visible" opacities. i.e. the structure of interiors and atmospheres of stars, accretion disks etc. can be calculated reliably. However, when visible layers are modelled, e.g. by spectrum synthesis techniques, certainly better line opacity data than presently available are required. These needs include accurate line positions and oscillator strengths, in particular for the ions of iron group. Seaton (1995) lists the basic atomic data required for astronomers. For light elements having few valence electrons the theoritical gf values are better. In the case of iron group elements the experimental data is more accurate.

The atomic data which we have used for the theoritical spectrum synthesis is taken from the Vienna atomic line database (VALD) where all the new atomic lines data is been compiled. The major source of the archieve is by Piskunov et al. (1995) and reference therein. We have also used the linelist complied by Kurucz (1994). It is a huge linelist, but in cases where there are no reliable atomic data available in the literature, semi-empirical values are used in the Kurucz linelist.

2.3.5 Line analysis and Spectrum synthesis

We have used the MOOG (Sneden 1973, 1998) LTE stellar line analysis program for radiative transfer calculations through cooler stars and for calculations of theoritical spectrum synthesis. The code was originally written for cool stars and later modified to include other stars also. The molecular dissociation equilibrium is included in deriving the abundances. The program has many driver routines:

synth -spectrum synthesis, varying abundances
isotop -spectrum synthesis, varying isotopic abundances
abfind - force-fitting abundances to match single-line equivalent widths
cog - curve of growth creation for individual lines
cogsyn - curve of growth creation for blended lines
ewfind - calculation of equivalent widths of individual lines
MOOG uses super-MONGO plotting package. It uses KURUCZ (1993) models and also MARCS models. The various smoothing mechanisms are included, rotation, instrumental broadening, and macroturbulence.

The SYNSPEC (Hubeny 1985) spectrum synthesis code is used for slightly hotter stars. It does not use molecular dissociation equilibrium in the abundance determinations. SYNSPEC reads the input model atmospheres from Kurucz (1979, 1993) and TLUSTY (Hubeny 1988) and solves the radiative transfer equation, wavelength by wavelength, in a specified wavelength range and in a specified resolution.

In principle, the line and continuum opacity sources used in calculating a model stellar atmosphere and in calculating the detailed spectrum should be identical. However, it is a common practice that model atmospheres, particularly those allowing for some departures from LTE, are calculated with fewer opacity sources than a subsequent calculation of a synthetic spectrum. The rationale for this approach is that the atmospheric structure is predominantly influenced by the strongest opacity sources,

while the emergent spectrum has to be computed in detail.

SYNSPEC also offers broadening by rotation and instrumental resolution. It uses the IDL plotting routines for graphics.

Our program stars belong to A-F spectral type which do not have too many crowded lines compared to the cooler spectral types. So the line analysis is easy. And also compared to the hotter spectral types A-F stars are less affected by NLTE effects. So the above model atmospheres and the spectrum synthesis, line analysis gives a reliable results. The error in our estimations are T_{eff}= 500K, log g=0.5 and 0.2 dex in the chemical composition.

Chapter 3

Spectroscopy of the post-AGB F supergiant HD 101584 (IRAS 11385-5517)

3.1 Abstract

HD 101584 belong to a class of peculiar stars at a relatively high galactic latitude with F0 Ia supergiant-like spectrum. It is an IRAS source with hot and cold circumstellar dust shell. From an analysis of the spectrum (4000Å to 8800Å) of HD 101584 we found that most of the neutral and singly ionized metallic lines are in emission. The forbidden emission lines of [OI] 6300Å and 6363Å and [CI] 8727Å are detected, which indicate the presence of a very low excitation nebula. The Hα, FeII 6383Å, NaI D_1, D_2 lines and the CaII IR triplet lines show P-Cygni profiles indicating a mass outflow. The Hα line shows many velocity components in the profile. The FeII 6383Å also has almost the same line profile as the Hα line indicating that they are formed in the same region. It is likely that HD 101584 is a bi-polar proto-planetary nebula

with a dusty disk. From the spectrum synthesis analysis of absorption lines, we find the atmospheric parameters to be T_{eff}=8500K, log g=1.5, V_{turb}=13km s^{-1} and [Fe/H]=0.0. From an analysis of the absorption lines the photospheric abundances of some of the elements are derived. Carbon and nitrogen are found to be overabundant, indicating the mixing due to the third dredge-up. From the analysis of Fe emission lines we derived T_{exi} = 6100K±200 for the emission line region.

3.2 Introduction

Humphreys and Ney (1974) found near-infrared excess in HD 101584 and suggested that it is a massive F-supergiant with an M-type binary companion star (Humphreys 1976). However, HD 101584 (V=7.01, F0 Iape (Hoffleit et al. 1983)) was found to be an IRAS source (IRAS 11385−5517) (Parthasarathy and Pottasch 1986). On the basis of its far-infrared colors, flux distribution and detached cold circumstellar dust shell, Parthasarathy and Pottasch (1986) suggested that it is a low mass star in the post-Asymptotic Giant Branch (post-AGB) stage of evolution.

CO molecular emission lines at millimeter wavelengths were detected by Trams et al. (1990). The complex structure of the CO emission shows large Doppler velocities of 130 km s^{-1} with respect to the central velocity of the feature, indicating a very high outflow velocity. Te Lintel Hekkert et al. (1992) reported the discovery of OH 1667 MHz maser emission from the circumstellar envelope of HD 101584. The OH spectrum has a velocity range of 84 km s^{-1} and shows two unusually broad emission features. Te Lintel Hekkert et al. (1992) found from the images obtained from the Australian Telescope, that the OH masers are located along the bipolar outflow. The post-AGB nature of HD 101584 is also suggested by the space velocity of the star derived from the central velocity of the CO and OH line emission. This velocity of V_{rad} = 50.3 ± 2.0 km s^{-1} does not agree with the galactic rotation curve assuming it to be a luminous massive population I F supergiant.

Bakker et al. (1996a) studied the low and high resolution ultraviolet spectra and the high resolution optical spectra of HD 101584. Based on the strength of HeI (see also Morrison and Zimba 1989) N II, C II lines and Geneva photometry, Bakker et al. (1996a) suggest that HD 101584 is a B9 II star of T_{eff} = 12000K ± 1000K and log g = 3.0. Bakker et al. (1996b) also found small amplitude light and velocity variations and suggested that HD 101584 is a binary with an orbital period of 218 days. According to the authors, the most likely explanation is the presence of a low-mass companion in a close, eccentric orbit (separation 10 R_*), but this is regarded as tentative. Optical emission and low excitation absorption lines suggest the presence of a circumsystem disk (size 100R_*) that is seen nearly edge-on (Bakker et al. 1996a). The presence of OH emission and a 10μm feature (Bakker et al. 1996a) suggests that the circumstellar material is O-rich (i.e., C/O< 1)

The CO radio line observations (Olofsson and Nyman 1999) reveal a molecular gas envelope of 0.1 $M_\odot$, with very similar characteristics to those of well-known young post-AGB objects viewed edge-on.

The optical spectrum of HD 101584 is very complex and shows many lines in emission. Here we report an analysis of the high resolution optical spectrum of HD 101584.

3.3 Observations and analysis

High resolution and high signal to noise ratio spectra of HD 101584 were obtained with the European Southern Observatory (ESO) Coude Auxiliary Telescope (CAT) equipped with the Coude Echelle Spectrograph (CES) and a CCD as detector. The spectra cover the wavelength regions 5360-5400Å, 6135-6185Å, 6280-6320Å, 6340-6385Å, 6540-6590Å, 7090-7140Å, 7420-7480Å, 8305-8365Å and 8680-8740Å. The spectral resolution ranged from 0.165Å at 6150Å to 0.210Å at 8700Å. We have also obtained 2.5Å resolution spectra of HD 101584 from 3900Å to 8600Å with the 1.2 m telescope and UAGS spectrograph and a CCD as detector at the Vainu Bappu Obser-

vatory (VBO), Kavalur, India. In addition we obtained CCD spectra with the same telescope and Coude Echelle spectrograph, covering the wavelength region 4600Å to 6600Å with a resolution of 0.4Å. All spectra mentioned above were used in this analysis.

All the spectra were analyzed using IRAF software. We carried out spectrum synthesis calculations using KURUCZ stellar models (1994). SYNSPEC code (Hubeny et al. 1985) was used for calculating the theoretical line profiles. The gf values were taken from Wiese et al. (1966), Wiese and Martin (1980), Hibbert et al.(1991), Parthasarathy et al. (1992) and Reddy et al. (1997 and references therein). For the analysis of forbidden lines we have used the IRAF software package NEBULAR under STSDAS.

3.4 Description of the spectrum

The remarkable characteristic of the optical spectrum of HD 101584 is the fact that different spectral regions resemble different spectral types. The spectrum in the UV region is similar to that of α Lep which is an F-supergiant (Bakker 1994). The optical spectrum in the range 3600Å-5400Å is dominated by absorption lines. Most of them are due to neutral and single ionized lines of Ti, Cr and Fe. The CaII H and K absorption lines are strong. The strength of the absorption lines are similar to that observed in an A2 supergiant. In the yellow and red spectral regions, most of the lines are in emission (Fig. 1).

The emission lines show complex line profiles. The absorption lines of NI, OI, CII and SiII are broad. The Paschen lines are in absorption. Some of these absorption lines are blended with emission lines and many have asymmetric profiles. The OI lines at 6156Å are blended with emission lines of FeI. The NI lines are strong and asymmetric. The blue wing is shallow compared to the red wing. The CII lines at 6578Å and 6582Å are weak. The Na D lines, KI 7700 Å (Fig. 2), the CaII IR triplet

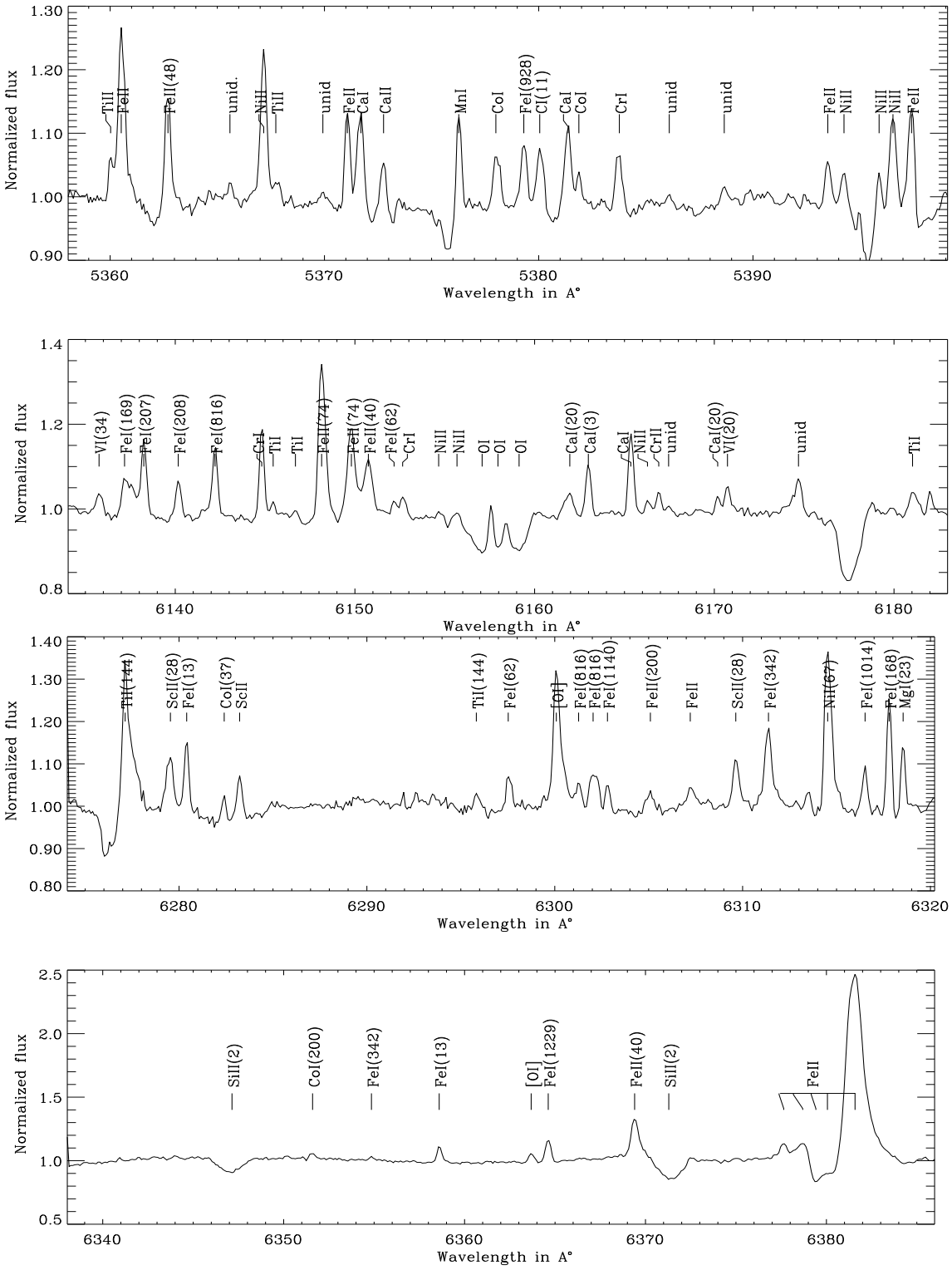

Figure 1: High resolution spectra of HD 101584 obtained with the ESO CAT-CES

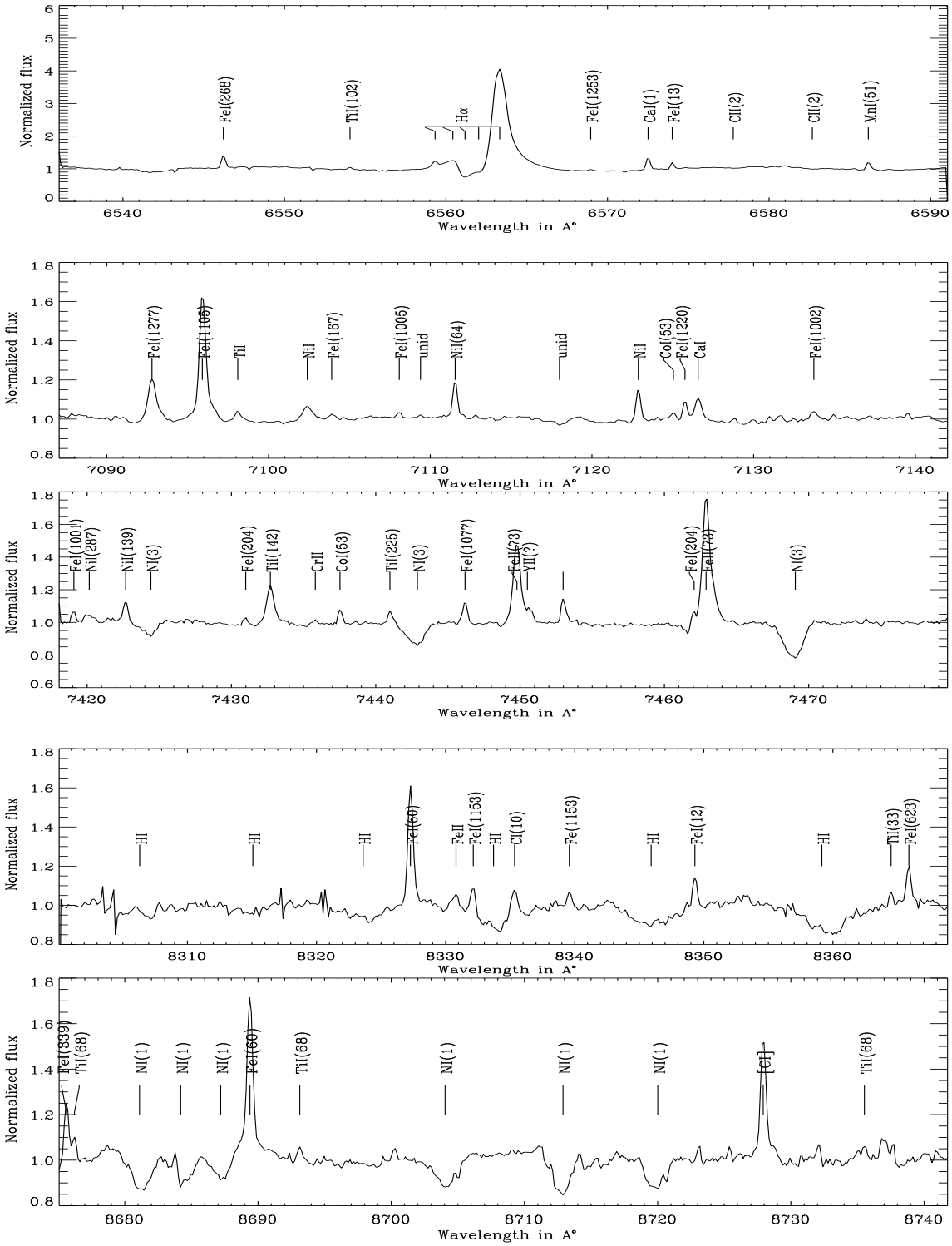

Figure 1 (continued): High resolution spectra of HD 101584 obtained with the ESO CAT-CES

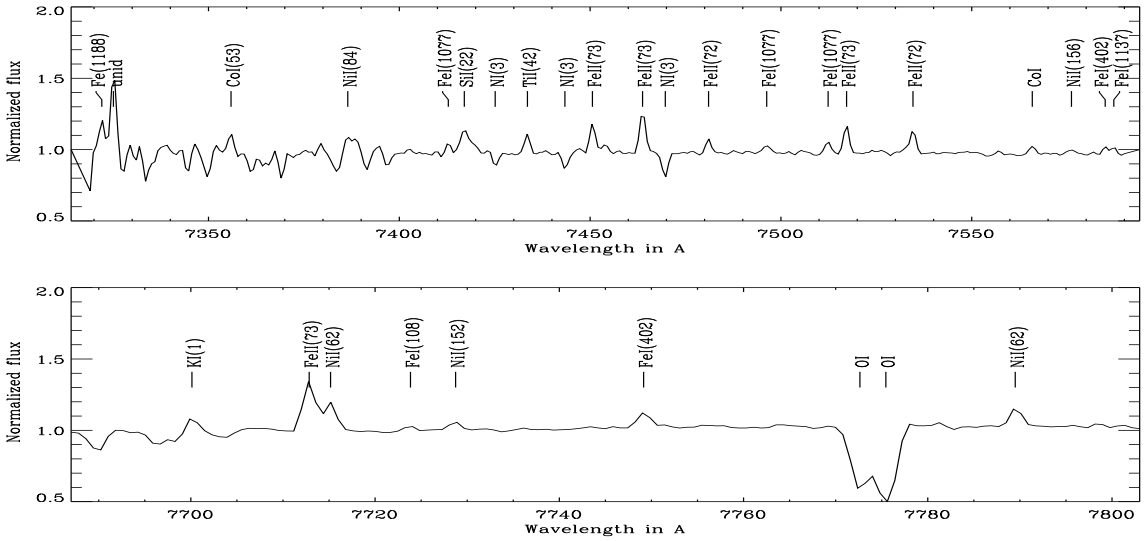

Figure 2: The spectrum in the upper panel shows several nitrogen lines and emission lines of Fe. The lower panel shows the KI 7699Å in emission and the strong absorption due to OI triplet at 7777Å.

lines (Fig. 3), [OI], [CI] and MgI 6318.7Å lines are found in emission. The OI triplet lines (Fig. 2) are very strong indicating an extended atmosphere and NLTE effects.

3.4.1 P-Cygni profiles

The Hα line has a very strong P-Cygni profile indicating an outflow. The profile looks very complex. It shows at least 6 velocity components. The FeII line at 6383Å is in emission and the profile is very similar to that of Hα (Fig. 4). Similar behaviour of the 6383Å FeII line and Hα line is also noticed in the post-AGB F supergiant IRAS 10215-5916 (García-Lario et al. 1994). The Hα and the FeII 6383Å line show an outflow velocity of 100$\pm$10 km s^{-1}. The P-Cygni profile component of the Balmer lines show that the star is losing mass with a outflow velocity 100 kms^{-1}. The Hβ line also shows a P-Cygni profile. It has a broad emission wing at the red end. This indicates that the line forming region is extended. The Hβ, NaI D1, D2 and the CaII IR triplet lines (Fig. 3) show an outflow velocity of 75$\pm$20 km s^{-1}. The velocity structure seen in these P-Cygni profiles could be due to emission from different shells

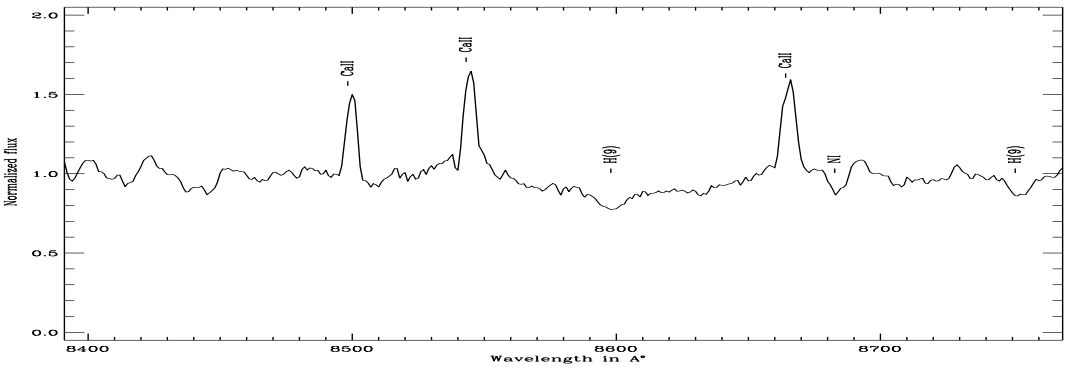

Figure 3: CaII IR triplet lines showing P-Cygni emission.This spectrum is of 2.5Å resolution, obtained from VBO, Kavalur.

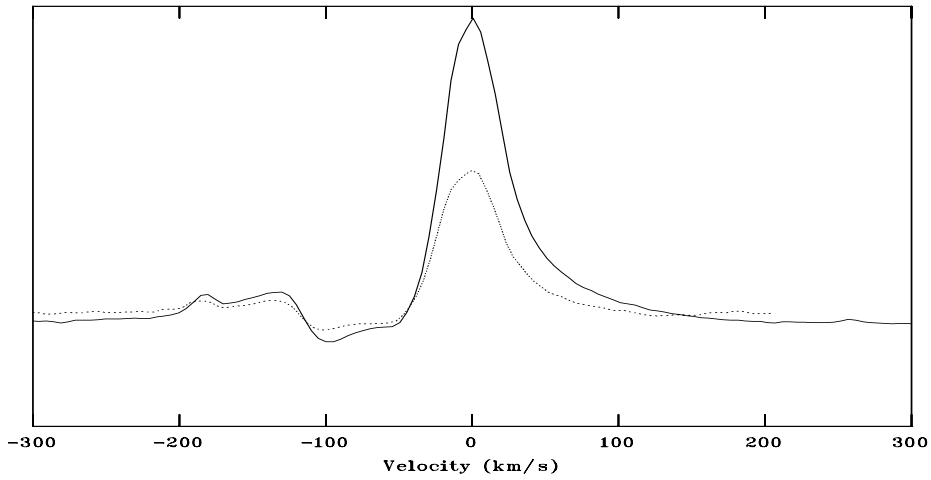

Figure 4: P-Cygni profile of Hα and FeII(6383Å) lines showing similar velocity structures

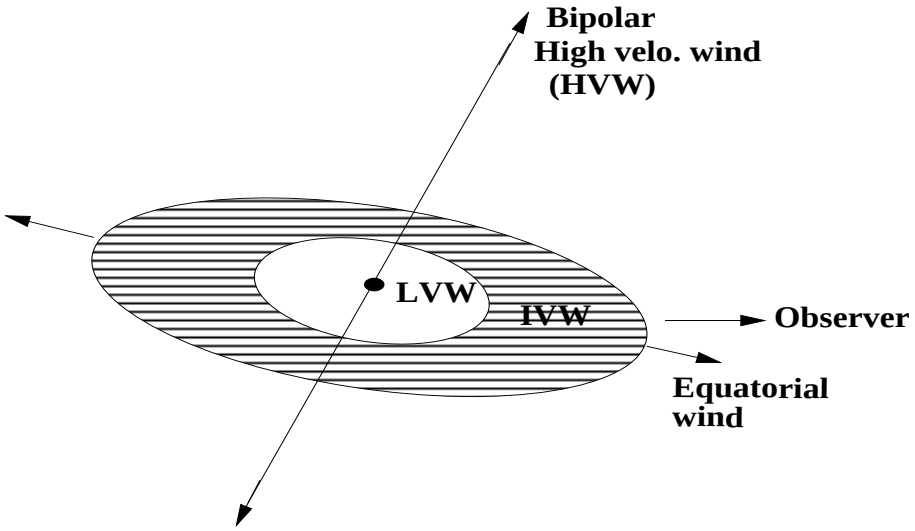

Figure 5: Schematic representation of a possible model for the molecular envelope of HD 101584 (based on Olofsson and Nyman, 1999)

formed during the episodic mass-loss events.

Olofsson and Nyman (1999) see evidence for an expanding disk-like structure seen close to edge-on, and high velocity bipolar outflow, from the CO radio line observations. The expansion velocity increases linearly with distance from the star, suggesting either a brief period of ejection or a fast wind interacting with a slower wind. From the CO observation they have proposed a simple model (Fig. 5) which explains different velocity components of CO emission. There is central star and an equatorial disk which is viewed edge-on. Very close to the star where it is optically thick, there is a low velocity wind (LVW). Further out there is intermediate velocity wind (IVW) which could be due to the former envelope of the AGB. Then there is a bipolar outflow which is perpendicular to the disk. The P-Cygni profiles which is seen in (Fig. 4) also seem to agree with this model. The profile can be explained by a superposing a double peak emission from a bipolar flow and two different P-Cygni profiles corresponding to low and intermediate velocities.

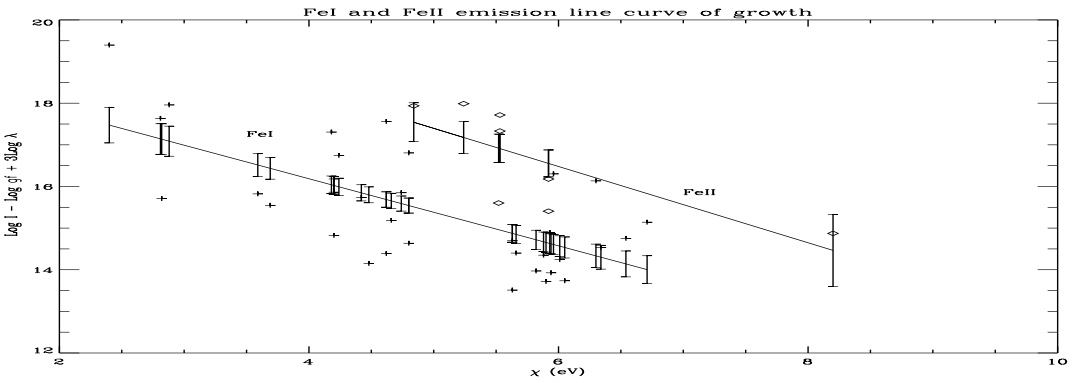

Figure 6: Curve of growth analysis of Fe emission lines. + represents the FeI lines and ♢ represents FeII lines. The slope gives T_{exi}=6300±1000K for FeI lines and T_{exi}=5550±1700K for the FeII lines. The large dispersion is because the lines are optically thick. The errors bar show the error in the least square fit.

3.4.2 FeI and FeII emission lines

The presence of numerous emission lines of FeI and FeII makes it possible to derive the physical conditions of the line forming region. From the curve of growth analysis of the FeI and FeII emission lines (Viotti 1969), we have derived T_{exi}=6300±1000K and 5550±1700K respectively (Fig. 6).

The scatter found could be due to the fact that the lines are not optically thin. On the other hand, there are only few emission lines of FeII present in the spectra and thus the estimate from FeII might not be accurate. In order to determine whether the large scatter observed in Fig. 6 is reflecting optical thickness effects we have done self-absorption curve (SAC) analysis (Friedjung and Muratorio 1987) for the FeI emission lines.

SAC is a kind of curve of growth applied to emission lines, but it has certain advantages as compared to the classical emission line curve of growth analysis. This method of analysis is also valid for optically thick lines. It deals with each transition separately, so that it is possible to get the population of different levels without assuming a Boltzmann distribution. In this curve, a function of the line flux emitted

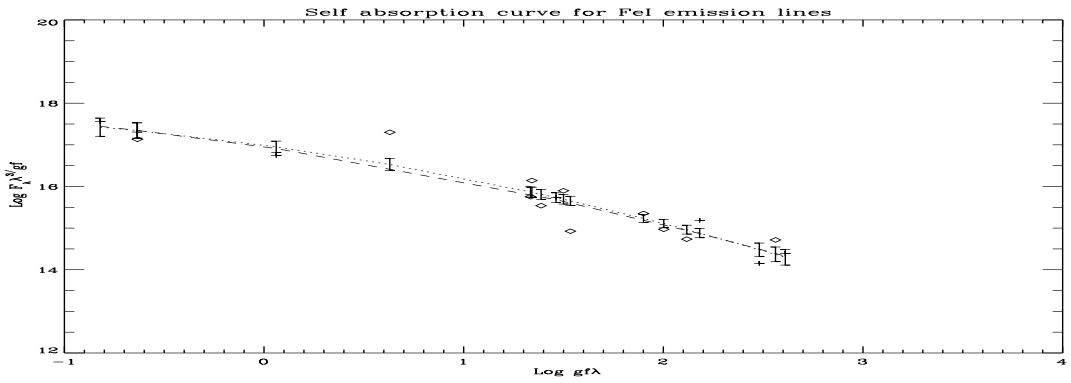

Figure 7(a): The plot shows the shape of the SAC. The + sign indicates multiplets 167,168,169,204,207,208 of Fe I having similar excitation potential. ♢ indicates multiplets 1002,1005,1014,1077,1105,1140,1153,1220,1229,1277 of FeI. The fit was obtained after shifting higher multiplets 1002,1005,1014,1077,1105,1140,1153,1220,1229,1277 w.r.to the lower multiplets 167,168,169,204,207,208.

in the different transition of a given multiplet is taken in such a way that it is constant for a optically thin uniform medium. As the optical thickness increases the curve will move towards a straight line inclined at -45^o. The shape of the SAC in Fig. 7(a) shows the lines are optically thick. The shape of the SAC is obtained by shifting all the multiplets with respect to a reference multiplet. Here we have taken multiplet 207 as reference. The X and Y shifts of each multiplet gives the relative population of the lower and upper level with respect to the reference multiplet. Fig. 7(b) and Fig.7(c) shows the Y and X shifts versus the upper and lower excitation potential from which we derive the T$_{exi}$=6100±200K.

3.4.3 Forbidden lines

The forbidden emission lines at 5577Å, 6300Å and 6363Å of neutral oxygen are present in the spectra. The forbidden line of neutral carbon at 8727Å is also seen. The 6300Å line is blended with ScII line and the 5577Å line is very weak. We have calculated the I(6300)+I(6363)/I(5577) to be 13.3. From the flux ratio we can calculate T$_e$

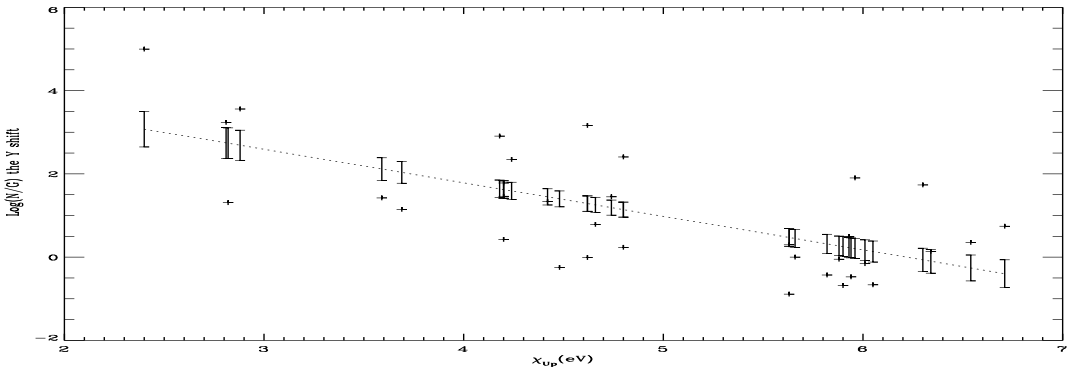

Figure 7 (b): The fit shows the distribution of upper level population of different multiplets of FeI with respect to the multiplet 207, versus the upper excitation potential.

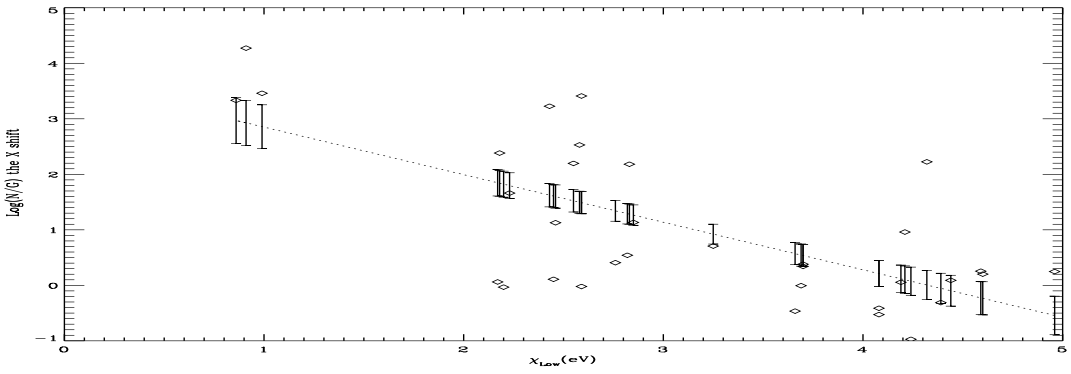

Figure 7 (c): The fit shows the distribution of lower level population of different multiplets of FeI with respect to the multiplet 207, versus the lower excitation potential.

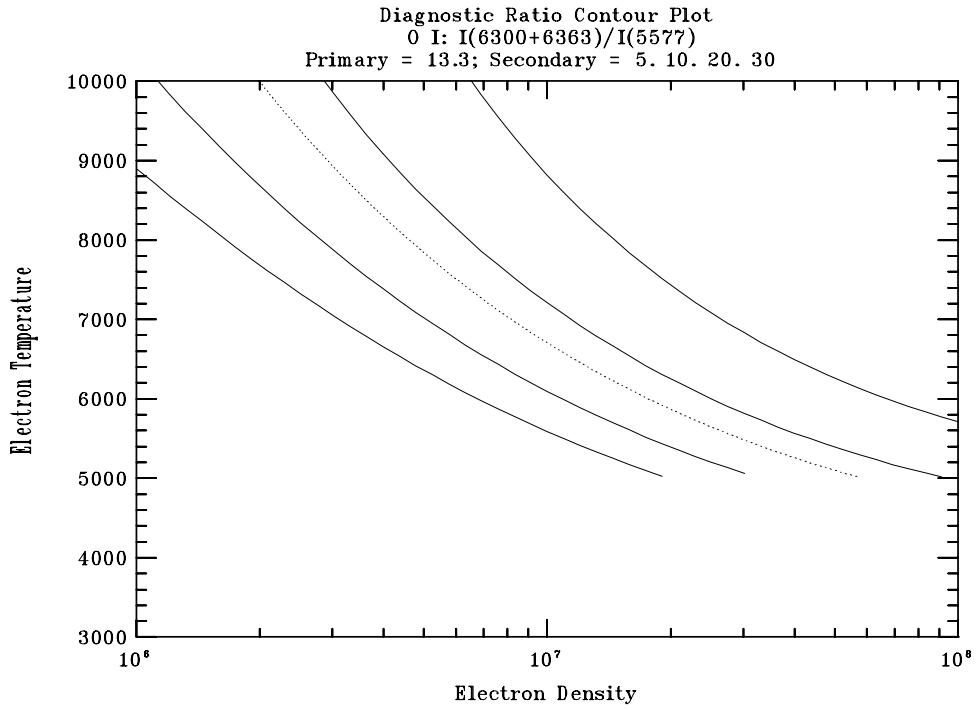

Figure 8: Plot of electron density N_e and electron temperature T_e. The dotted line is the contour for the observed ratio (13.3) of [O]I lines 5577Å, 6300Å and 6363Å. The flux ratio for the secondary contours are mentioned on the top of the plot.

(Osterbrock 1989). This flux ratio is not very accurate because of very the weak 5577Å line and poor signal to noise spectrum. For the flux ratio of 13.3 we derived a contour with possible electron density N_e and temperature T_e. Fig. 8 shows the N_e and T_e contours for different values of flux ratio around 13.3. Since we do not see any other forbidden lines which are sensitive to the electron density, we could not fix both N_e and T_e uniquely. But assuming a temperature derived from the Fe emission lines, an electron density of 1 x 10^7 is obtained. For this value of electron density and temperature the C/O = 0.5$\pm$ 0.2 has been obtained.

3.5 Radial velocities

There are very few absorption lines and most of these are affected by emission and or a shell component, therefore we derived the average radial velocity from the well defined emission lines. The average radial velocity from the emission lines is found to be 50 $\pm$ 2km s^{-1}. Morrison and Zimba (1989) using 14 best absorption lines found the radial velocity to be 69$\pm$ 1 km s^{-1}. From the equivalent widths of FeI absorption lines given by Rosenzweig et al. (1997) we find no correlation between log gf - $\chi\Theta$ and heliocentric radial velocity (Fig. 9). However, Bakker et al. (1996a) found a correlations between log gf - $\chi\Theta$ and heliocentric radial velocities of HD101584 in the UV. The discrepancy could be due to the poor resolution of Rosenzweig et al. (1997) data compared to that of Bakker et al. (1996a). It could also be that these lines are forming in the photosphere rather than in the wind. The large scatter seen in the radial velocities could be due to pulsation. Similar velocity variations were noticed in other post-AGB supergiants (García-Lario et al. 1997, Hrivnak 1997).

3.6 Atmospheric parameters and chemical composition

The UV (IUE) low resolution spectrum of HD 101584 matches well with that of an A6Ia star (HD 97534) (Fig. 10) indicating a T$_{eff}$ of 8400K (Lang 1992). The presence of CII lines at 6578Å and 6582Å indicates a T$_{eff}$ $>$ 8000K. For T$_{eff}$ $\leq$ 8000K the CII lines would be very weak or absent. The Paschen lines also indicates a low gravity (Fig. 11).

The luminosity class Ia also indicates a very low gravity. From the analysis of several nitrogen lines around 7440Å and 8710Å we derived the microturbulence velocity V$_{turb}$=13km s^{-1}. We synthesised the spectral region from 4000Å to 4700Å (Fig. 12) with low gravity (log g =1.5) models of Kurucz (1993) with temperatures

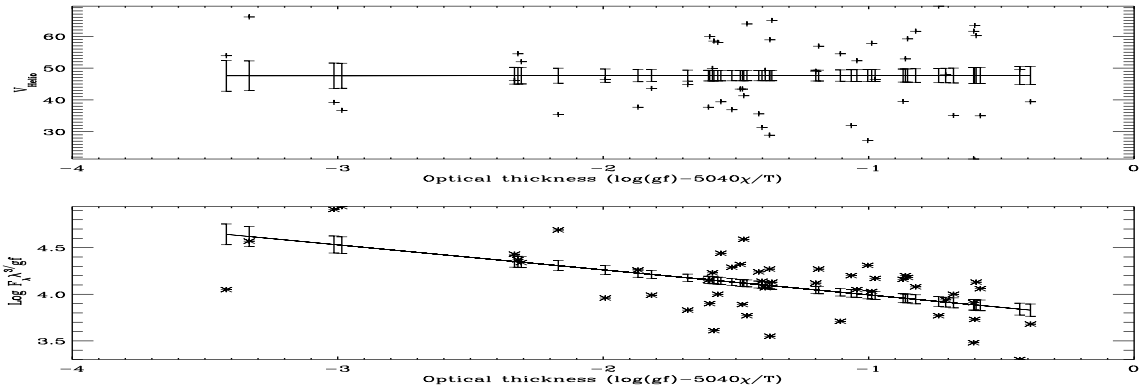

Figure 9: The plot in the upper panel does not show any correlation between the optical depth and the helio centric radial velocity for the FeI absorption lines of HD 101584 in the wavelength region 3600Å-4500Å. The plot in the lower panel shows the normalized strength of FeI absorption lines in the wavelength region 3600Å to 4500Å versus the optical depth. It shows clearly that the lines are forming at different optical depths. The equivalent widths are taken from the paper by Rosenzweig et al.(1997)

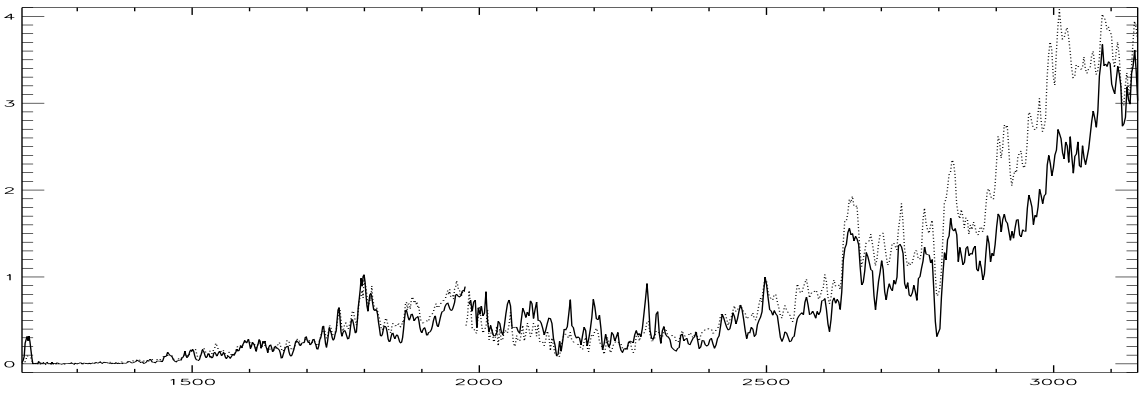

Figure 10: IUE low resolution spectrum of HD 101584 is compared with that the A6Ia star HD 97534. The dotted line corresponds to the spectrum of HD 97534 while the solid line is HD 101584.

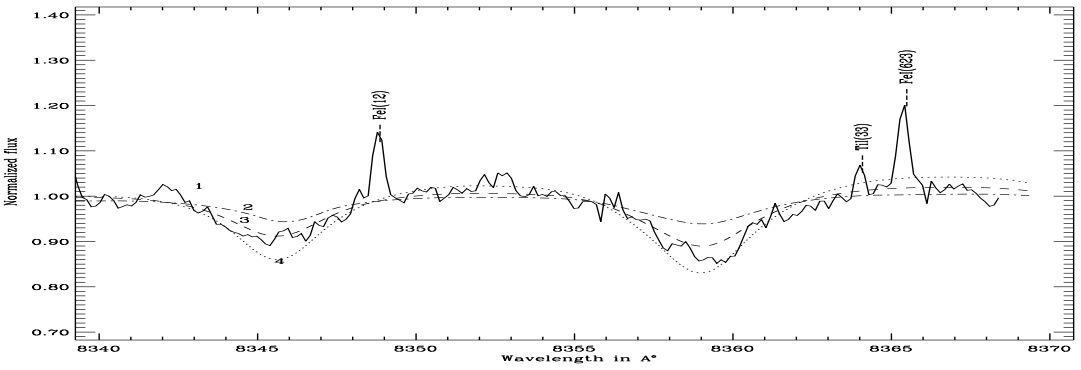

Figure 11: *Observed and synthetic spectra in the Paschen line region. 1-observed, 2-T_{eff}=8000K,log g=1.0, 3-T_{eff}=8000K,log g=2.0, 4-T_{eff}=8500K, log g=1.5. The peaks are FeI emission lines*

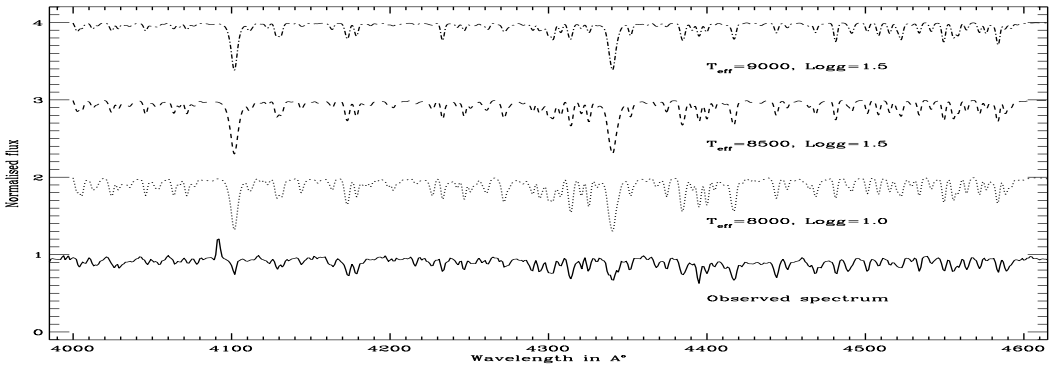

Figure 12: Synthesis spectra for different models are compared with the observed spectrum. The observed spectrum is of 2.5Å resolution taken at VBO Kavalur. Observed spectrum matches well for T_{eff}=8500K, log g=1.5, V_{turb}=13km s^{-1} and [Fe/H]=0.0.

8000K, 8500K and 9000K. The best fit was found for T_{eff} = 8500K, log g = 1.5, V_T=13km s^{-1} and [Fe/H] = 0.0.

The line at 5876Å was identified as a HeI line by Bakker et al.(1996a) who also state that the lines at 5047Å and 5045Å as due to HeI and NII respectively. However, we find that the 5047 and 5045 lines are in fact due to FeII. Except HeI 5876Å, we have not found any other helium lines in the spectrum and nor have we found any NII or OII lines. In fact, Hibbert et al. (1991) indicate the presence of a CI line at 5876Å. It is likely that the line at 5876Å may be due to CI instead of HeI.

If we assume that the 5876Å line is due to HeI then for a solar helium abundance and log g = 1.5, T_{eff} = 9000K is found. Since we do not see any other helium lines, it is likely that HeI 5876Å may be formed in the stellar wind or in the chromosphere of the star. On the basis of the presence of this helium line Bakker et al. (1996a) suggested that HD 101584 is a B9II star with T_{eff} = 12000K. On the basis of the analysis of our spectra we have not found any evidence for such a high temperature. We have also analysed the equivalent widths of absorption lines in the spectrum of HD 101584 given by Bakker et al.(1996a). The final abundances of some of the elements are listed in Table 2. The abundances listed in Table 2 show that the star is overabundant in carbon and nitrogen. It appears that the material processed by the triple alpha, C-N and O-N cycle has reached the surface. Olofsson and Nyman (1999) also see and enhancement in the $^{13}C/^{12}$C. This also gives a clear evidence of the third dredge-up and carbon rich.

3.7 Discussion and Conclusions

The optical spectrum of the post-AGB star HD 101584 is rather complex. We find several emission lines and P-Cygni profiles indicating an ongoing mass-loss and the

Table 2: Chemical composition of HD101584.

Element	[element/H]		Lines
	T_{eff}=8500K log g=1.5	T_{eff}=9000K log g=1.5	
C	1.0±0.1	0.3±0.1	C II 6578,6582
N	0.5±0.1	0.6±0.1	N I 7423,7442,8703, 8711,8718,8728
O	0.1	0.18	O I 6158
Mg[1]	0.2	0.02	Mg II 4481.13
Ti[1]	0.0±0.4	0.4±0.4	Ti II 15 lines
Fe[1]	-0.1±0.1	0.5±0.1	Fe I 3 lines
	0.2±0.4	0.3±0.4	Fe II 6lines

[1] The equivalent widths were taken from Bakker (1996a)

presence of a circumstellar gaseous envelope. From the analysis of the absorption lines we find the atmospheric parameters to be T_{eff}=8500K , log g=1.5, V_t=13km s^{-1} and [Fe/H]=0.0.

Carbon and nitrogen are found to be overabundant indicating that material processed by triple alpha, C-N and O-N cycles has reached the surface. Since our blue spectra are of relatively low resolution and because of the presence of emission and shell components it is difficult to estimate reliable abundances of s-process elements. The OI line at 6156Å is blended with a weak FeI emission line. The OI triplet at 7777Å is very strong and affected by NLTE. In any case it appears that the oxygen abundance is nearly solar. A NLTE analysis of the high resolution OI 7777Å triplet may yield a more reliable oxygen abundance.

The nitrogen abundance is based on 6 lines in the 7440Å and 8710Å region. We have not used the strong nitrogen lines. Nitrogen seems to be clearly overabundant. The carbon abundance is based on two CII lines at 6578Å and 6582Å. There is a clear

indication that carbon is overabundant. The abundance of Mg, Ti, and Fe are nearly solar. The Ti abundance is based on 15 lines and the Fe abundance is based on 6 lines. Many of the other atomic lines are affected by emission and shell components. In our opinion, the line at 5876Å might be due to CI (Hibbert et al. 1991) and not to HeI, as previously suggested by Bakker et al. (1996a). We have not found any other HeI, NII or OII lines. Our analysis shows that the T_{eff} is 8500±500K.

Bakker et al. (1996b) found small amplitude light and velocity variations and suggested that HD 101584 is a binary with an orbital period of 218 days. The radial velocity variations may be due to pulsation, macroturbulence motions or shock waves in the outer layers of the stellar atmosphere. Many post-AGB supergiants show small amplitude light and velocity variations (Hirvnak 1997). These variations may not be interpreted as due to the presence of a binary companion. Long term monitoring of the radial velocities is needed in order to understand the causes for these variations.

The spectrum and the brightness of HD 101584 appears to remain the same during last two or three decades. There is no evidence for significant variations in brightness similar to those observed in Luminous Blue Variables (LBVs). The chemical composition and all the available multiwavelength observational data collected during the last two decades by various observers indicates that HD 101584 is most likely a post-AGB star.

The presence of several P-Cygni lines with significant outflow velocities, the OH maser and CO emission profiles (Te Lintel Hekkert et al. 1992, Trams et al. 1990) and the IRAS infrared fluxes and colours (Parthasarathy and Pottasch 1986) indicates the possibility that HD 101584 is a post-AGB star with a bipolar outflow with a dusty disk. The CO observations of Olofsson and Nyman (1999) also gives a similar picture. Since HD 101584 shows a strong Hα emission line, high resolution imaging with the Hubble Space Telescope (HST) may reveal the bipolar nebula and the presence of a dusty disk similar to that observed in other post-AGB stars like IRAS 17150-3224 (Kwok et al. 1998) or IRAS 17441-2411 (Su et al. 1998).

Table 1: List of emission lines detected in the high resolution spectrum of HD 101584

λ obs (Å)	λ lab (Å)	Ident.	χ (eV)	log gf	F_λ* (mÅ)	$\Delta\lambda$ (Å)	V_{Helio} km/s
5360.022	5360.115	TiII	2.60-4.92	-4.040		-0.093	10.60
5360.517	5360.755	FeII	10.52-12.83	-3.082	118.4	-0.237	2.51
5362.698	5362.864	FeII(48)	3.20-5.52	-2.739	47.36	-0.165	6.56
5365.597		unid					
5367.167	5367.205	NiII	14.61-16.93	-2.571	79.71	-0.038	13.69
5367.731	5367.912	TiII	1.57-3.88	-4.480		-0.181	5.69
5369.928	5369.928	unid					
5371.07	5371.275	FeII	10.56-12.87	-0.705	45.52	-0.20	4.36
5371.704	5371.934	CaI	5.4-7.71	-3.163		-0.220	2.97
5372.76	5372.807	CaII	9.03-11.35	-1.337	21.64	-0.04	13.17
5376.27	5376.477	MnI	2.93-5.23	-4.091	45.13	-0.20	4.26
5378.	5378.247	CoI	4.03-6.34	-0.425	32.41	-0.24	2.03
5379.305	5379.581	FeI(928)	3.70-6.01	-1.521	33.83	-0.275	0.43
5380.048	5380.322	CI(11)	7.70-10.00	-1.840	32.67	-0.273	0.54
5381.379	5381.599	CaI	5.46-7.77	-4.960	49.97	-0.220	3.54
5381.874	5382.046	CoI	4.51-6.82	-3.234	15.82	-0.171	6.24
5383.763	5383.927	CrI	4.54-6.85	-2.606	22.12	-0.163	6.70
5386.093	5386.093	unid					
5388.659	5388.659	unid					
5393.491	5393.762	FeII	11.19-13.49	-2.154	17.12	-0.270	0.74
5394.247	5394.496	NiII	12.64-14.94	-1.029	14.61	-0.249	1.97
5395.886	5396.051	NiII	14.63-16.93	-2.851	10.14	-0.164	6.67
5396.532	5396.701	NiII	14.63-16.93	-2.561	54.78	-0.168	6.42

*Flux above the normalised local continuum

Table 1(continued): List of emission lines detected in the high resolution spectrum of HD 101584

λ obs (Å)	λ lab (Å)	ID	χ (eV)	log gf	F_λ * (mÅ)	$\Delta\lambda$ (Å)	V_{Helio} km/s
5397.4	5397.640	FeII	10.73-13.03	-2.883	51.29	-0.240	2.46
6133.723	7132.985	FeI(1002)	4.08-5.82	-0.851	36.31	0.738	46.96
6135.76	6135.370	VI(34)	1.05-3.08	-0.750	23.13	0.389	35.22
6137.179	6136.624	FeI(169)	2.45-4.48	-1.307	30.29	0.555	43.31
6138.25	6137.702	FeI(207)	2.59-4.62	-1.177	70.63	0.547	42.95
6140.167	6139.65	FeI(208)	2.59-4.62	-4.609	38.79	0.517	41.43
6142.214	6141.727	FeI(816)	3.70-5.63	-1.540	61.82	0.486	39.95
6154.659	6154.094	NiII	14.88-16.91	-2.268	5.54	0.564	43.71
6144.813	6144.294	CrI	4.10-6.13	-3.624	80.21	0.519	41.51
6145.448	6144.936	TiI	1.89-3.91	-2.520	16.08	0.512	41.17
6146.688	6146.27	TiI(153)	3.18-5.20	-2.541	15.79	0.417	36.57
6148.146	6147.742	FeII(74)	3.89-5.92	-2.721	20.85	0.403	35.87
6149.804	6149.249	FeII(74)	3.89-5.92	-2.724	122.7	0.555	43.25
6150.747	6150.10	FeII(40)	3.22-5.24	-4.754	73.71	0.646	47.73
6152.178	6151.624	FeI(62)	2.18-4.20	-3.582	17.06	0.554	43.20
6152.655	6152.098	CrI	4.10-6.12	-1.986	33.16	0.556	43.31
6155.679	6155.102	NiII	13.14-15.16	-0.682	7.19	0.577	44.30
6161.957	6161.295	CaI(20)	2.53-4.54	-1.293	27.97	0.662	48.41
6162.99	6162.180	CaI(3)	1.90-3.92	-0.167	49.42	0.810	55.61
6165.354	6164.716	CaI	6.05-8.07	-2.261	73.94	0.638	47.22
6166.282	6165.893	NiII	9.75-11.77	-2.297	9.67	0.389	35.10
6166.907	6166.187	CrII	13.06-15.07	-3.490	18.24	0.720	51.21
6167.456	6167.456	unid			10.3		
6170.189	6169.559	CaI(20)	2.53-4.54	-0.527	13.17	0.629	46.80

*Flux above the normalised local continuum

Table 1 (continued): List of emission lines detected in the high resolution spectrum of HD 101584

λ obs (Å)	λ lab (Å)	ID	χ (eV)	log gf	F_λ* (mÅ)	$\Delta\lambda$ (Å)	V_{Helio} km/s
6170.733	6170.340	VI(20)	4.80-6.81	-0.654	23.53	0.216	26.71
6174.685	6174.685	unid			39.17		
6181.032	6180.625	TiI	3.18-5.19	-3.632	43.54	0.407	35.93
6277.13	6277.470	TiI(144)	1.73-3.71	-3.794	112.2	-0.205	6.20
6279.541	6279.740	ScII(28)	1.5-3.48	-1.265	41.49	-0.287	2.29
6280.406	6280.622	FeI(13)	0.86-2.83	-3.720	44.44	-0.216	5.67
6282.404	6282.638	CoI(37)	1.74-3.72	-2.021	13.03	-0.234	4.81
6283.225	6283.353	ScII	7.45-9.43	-0.441	40.34	-0.127	9.90
6295.826	6295.949	TiI(144)					
6297.524	6297.799	FeI(62)	2.23-4.20	-2.871	39.23	-0.274	2.91
6300.083	6300.311	[OI]			163	-0.228	5.15
6301.27	6301.508	FeI(816)	3.66-5.63	-0.745	23.32	-0.237	4.68
6302.042	6302.499	FeI(816)	3.69-5.66	-1.203	62.88	-0.457	-5.75
6302.807	6303.461	FeI(1140)	4.32-6.30	-3.434	20.01	-0.653	-15.11
6305.09	6305.314	FeII(200)	6.23-8.20	-2.039	27.17	-0.224	5.34
6307.214	6307.529	FeII	2.83-4.80	-5.685	57.4	-0.314	1.02
6309.636	6309.886	ScII(28)	1.5-3.47	-1.630	55.71	-0.250	4.12
6311.379	6311.504	FeI(342)	2.83-4.80	-3.392	103.2	-0.125	10.06
6313.52							
6314.529	6314.668	NiI(67)	4.16-6.13	-0.921	163.5	-0.139	9.39
6316.52	6315.814	FeI(1014)	4.08-6.05	-0.683	44.72	0.706	49.54
6317.802	6318.027	FeI(168)	2.46-4.42	-2.338	98.8	-0.181	7.40

*Flux above the normalised local continuum

Table 1 (continued): List of emission lines detected in the high resolution spectrum of HD 101584

λ obs (Å)	λ lab (Å)	ID	χ (eV)	log gf	F_λ* (mÅ)	$\Delta\lambda$ (Å)	V_{Helio} km/s
6318.545	6318.717	MgI(23)	5.12-7.08	-1.730	60.1	-0.171	7.84
6351.598	6351.448	CoI(200)					
6354.852	6355.027	FeI(342)	2.85-4.80	-2.346	7.6	-0.174	7.62
6358.596	6358.687	FeI(13)	0.86-2.81	-4.546	47.9	-0.0908	11.59
6363.68	6363.79	[OI]			28.9	-0.109	10.69
6364.625	6364.706	FeI(1229)	4.59-6.54	-1.469	74.78	-0.081	12.05
6369.4	6369.464	FeII(40)	2.89-4.84	-4.253	186.8	-0.063	12.86
6380.058	6383.715	FeII	5.56-7.50	-2.271	1512	-3.656	-155.97
6381.582	6381.416	TiI(196)					
6539.783	6539.72	FeI(405)					
6546.217	6546.245	FeI(268)	2.76-4.66	-1.634	127.2	-0.0283	14.97
6554.056	6554.226	TiI(102)	1.44-3.34	-1.201	32.48	-0.169	8.49
6561.179	6561.179	Hα			3681		
6563.326	6563.403	CoI(80)					
6568.959	6569.231	FeI(1253)					
6572.512	6572.779	CaI(1)	0.00-1.89	-4.104	124.5	-0.266	4.10
6574.009	6574.238	FeI(13)	0.99-2.88	-4.688	65.55	-0.229	5.82
6574.831	6575.022	FeI(207)					
6580.992	6581.220	FeI(34)					
6586.144	6586.343	MnI(51)					
6587.438	6587.75	CI(22)					
7092.793	7091.942	FeI(1277)	4.96-6.71	-1.509	120.4	0.886	53.22

*Flux above the normalised local continuum

Table 1 (continued): List of emission lines detected in the high resolution spectrum of HD 101584

λ obs (Å)	λ lab (Å)	ID	χ (eV)	log gf	F_λ* (mÅ)	$\Delta\lambda$ (Å)	V_{Helio} km/s
7095.905	7095.425	FeI(1105)	4.21-5.96	-2.221	337.4	0.479	36.21
7098.1	7097.655	TiI	3.30-5.30	-3.423	16.88	0.445	34.74
7102.397	7101.932	NiI	4.54-6.29	-1.941	53.25	0.464	35.55
7103.904	7103.15	FeI(167)	2.43-4.18	-4.488	18.39		
7108.084	7107.468	FeI(1005)	4.19-5.94	-1.317	11.32	0.449	34.87
7109.397	7109.397	unid			8.62		
7111.541	7110.905	NiI(64)	1.93-3.68	-3.042	70.85	0.648	43.29
7117.991	7117.991	unid			23.54		
7122.867	7122.191	NiI(126)	3.54-5.29	-0.169	55.08	0.676	44.40
7125.038	7124.47	CoI(53)			14.34		
7125.752	7125.283	FeI(1220)	4.60-6.34	-1.465	32.71	0.468	35.65
7125.752	7125.283	FeI(1220)	4.60-6.34	-1.465	32.71	0.468	35.65
7126.566	7126.19	CaI	6.02-7.77	-0.647	60.47	0.375	31.74
7419.082	7418.668	FeI(1001)	4.12-5.79	-1.17	107.8	0.414	32.62
7420.15	7419.31	NiI(287)	5.50-7.17	-0.695		0.839	49.84
7422.671	7422.30	NiI(139)	3.69-5.28	+0.06	57.36	0.371	30.88
7430.991	7430.5	FeI(204)	2.58-4.24	-3.81	21.02	0.491	35.71
7432.698	7431.97	TiI(142)	1.74-3.41	-2.283	15.53	0.728	45.27
7435.814	7435.3	unid			47.41		
7437.521	7437.16	CoI(53)	1.95-3.61	-3.64	45.96	0.360	30.43
7440.984	7440.6	TiI(225)	2.25-3.90	-1.19	38.7	0.383	31.35
7446.188	7445.70	FeI(1077)	4.24-5.90	-0.31	61.72	0.487	35.53

*Flux above the normalised local continuum

Table 1 (continued): List of emission lines detected in the high resolution spectrum of HD 101584

λ obs (Å)	λ lab (Å)	ID	χ (eV)	log gf	F_λ* (mÅ)	$\Delta\lambda$ (Å)	V_{Helio} km/s
7449.784	7449.34	FeII(73)	3.87-5.53	-3.60	316.5	0.444	33.77
7450.505	7450.33	YII(?)				0.174	22.92
7452.982	7452.50	FeII(14F)			54.88		
7462.061	7461.527	FeI(204)	2.55-4.20	-3.48		0.534	37.36
7462.889	7462.38	FeII(73)	3.87-5.53	-2.98	540.5	0.509	36.35
8327.273	8327.061	FeI(60)	2.20-3.69	-1.298	307.8	0.212	23.79
8330.807	8330.587	unid			55.59		
8332.142	8331.926	FeI(1153)	4.39-5.88	-1.020	36.98	0.215	23.89
8335.342	8335.150	CI(10)	7.70-9.19	-0.420	69.24	0.191	23.01
8339.584	8339.398	Fe(1153)	4.44-5.93	-1.421	51.58	0.185	22.80
8349.31	8349.02	FeI(12)	0.91-2.40	-5.605	106.4	0.290	26.54
8364.508	8364.243	TiI(33)	0.83-2.32	-1.652	28.96	0.264	25.61
8365.885	8365.642	FeI(623)	3.25-4.74	-2.040	110.0	0.243	24.84
8675.626	8674.751	FeI(339)	2.82-2.42	-1.89	100.7	0.875	46.10
8676.22	8675.38	TiI(68)	1.06-2.50	-1.357	43.2	0.839	44.88
8689.396	8688.632	FeI(60)	2.17-3.59	-1.41	393.9	0.764	42.24
8693.139	8692.34	TiI(68)	1.04-2.46	-1.92	27.48	0.798	43.41
8727.923	8727.4	[CI]			302.5	0.522	33.80
8735.521	8734.70	TiI(68)	1.05-2.48	-2.087		0.821	44.05

*Flux above the normalised local continuum

Chapter 4

Spectroscopy of a F-supergiant HD 331319 (IRAS 19475+3119)

4.1 Abstract

HD 331319 is a F-type supergiant with a detached cold circumstellar dust shell with far-IR colours similar to planetary nebulae. In this chapter an analysis of high resolution spectrum of HD 331319 is presented. We have derived the atmospheric parameters and the chemical composition of HD 331319. We estimated T_{eff} = 6000K , log g = 0.0 from the Hβ line profile. From excitation equilbrium of FeI and FeII we obtain two different temperatures, 7500K and 7750K respectively. This kind of differences are seen in many post-AGB supergiants. So we derived the chemical composition for these three temperatures. We find that the nitrogen is enhanced. Also the carbon and oxygen abundances are high compared to iron. The enhancement in the carbon and nitrogen abundance indicate that the surface composition has been altered by the nucleosynthesis and mixing. The total C,N,O abundances with respect to iron indicate that third dredge up also has been taken place. For a temperature

of 6500K and log g=0.5, the metallicity is [Fe/H] = -1.0 and the α process elements are enhanced. The s-process elements show [s/Fe] =0.0. The Yittrium and barium abundances are very low compared to iron, that is [Ba/Fe]=-0.8, [Y/Fe]=-0.5.

4.2 Introduction

Bidelman (1981) has classified the star as F3 Ia. HD 331319 (F3 Ib) is having IRAS fluxes similar to that of a PPN (Proto Planetary Nebula) (Preite-Martinez, 1988). He derives a dust temperature of 136K. The near IR fluxes also suggests that it is a PPN (Garcio et al. 1997). CO emission has been detected in HD 331319 in the CO survey of very cold IRAS objects (Likkel et al. 1987,1991), in order to detect new post-AGB candidates. In their survey, HD 331319 is one of the coldest object besides IRAS 09371+1212. The CO emission profile has symmetrical wings extending from -20Km s^{-1} to +20Km s^{-1} from the line center. There is no OH maser emission from this object(Likkel et al. 1991). The reason could be that the environment is carbon rich. Another posssibility is that a decreased mass loss rate has reduced the OH column density below that required to sustain an OH maser. From the color temperature and IRAS variability and from the CO observations Likkel et al. (1991) conclude that it is a post-AGB supergiant. The CO expansion velocity from CO 1-0 and 2-1 lines are typical of a post-AGB star. The near-infrared spectroscopy of HD 331319 (Hrivnak et al. 1994) show no 21μm feature and 3.3μ feature, which indicates that the circumstellar gas may be carbon rich.

4.3 Observations and Analysis

The observations were made on 3rd August 1993 using the 2.5m Issac Newton Telescope (INT) at La Palma with a 1800 grooves/mm grating (H1800V) and a GEC CCD as detector. The resolution is about 0.3 Å at 5000Å. The spectra covers wave-

length regions 4350-5200Å, 5240-5550Å and 7000-7230Å. The spectrum was reduced using IRAF spectral reduction software. The equivalent widths of the absorption lines were obtained by fitting gaussians using the SPLOT package inside IRAF. The continuum normalization is also done using IRAF. The reduced spectra are compared with the theoritically calculated spectra. We have used KURUCZ (1993) LTE stellar model atmospheres. For doing the radiative transfer calculation and fitting the theoritical spectrum. We used the computer code MOOG by Sneden (1973) and recently modified (C. Sneden 1997, private communication). We have used the Atomic line database at Vienna (VALD-2 Ryabchikova et al. 1999).

4.4 Atmospheric parameters

The first estimate of atmospheric parameter was got from the spectral class given in the MK spectral classification. T_{eff} of 7300K and log g=0.5 corresponding to F3Ib was used as a initial estimate. We tried to fit the Hβ profile using this stellar model (Fig. 1). We found that Hβ profile fits best for a T_{eff}=6000K and log g=0.0. We have tried to get the atmospheric parameters from the line analysis. But the spectrum of HD 331319 shows many strong lines. And many of the lines are blended. We did a spectrum synthesis using T_{eff}=6000K and log g=0.0 and microturbulence ξ_t=7km s^{-1}. We found that HD 331319 is metal poor with [M/H]=-1.0. But we saw that the abundance from the neutral and single ionized lines seem to give a large differences, it is nearly 1.0dex. We tried the model T_{eff}=7500K and log g=0.5 and found that the difference in the abundances between neutral and ionized lines have decreased. But still it was nearly 0.3dex. The model T_{eff}=7700K and log g=1.0 for a microturbulence velocity of ξ_t = 7km s^{-1} seem to give same abundance for both neutral and ionized lines (Fig. 2). For this model we found that the metallicity [Fe/H] =0.0. One explanation for Hβ line profile giving different result compared to the values derived from the excitation and ionization equilibrium of metallic lines

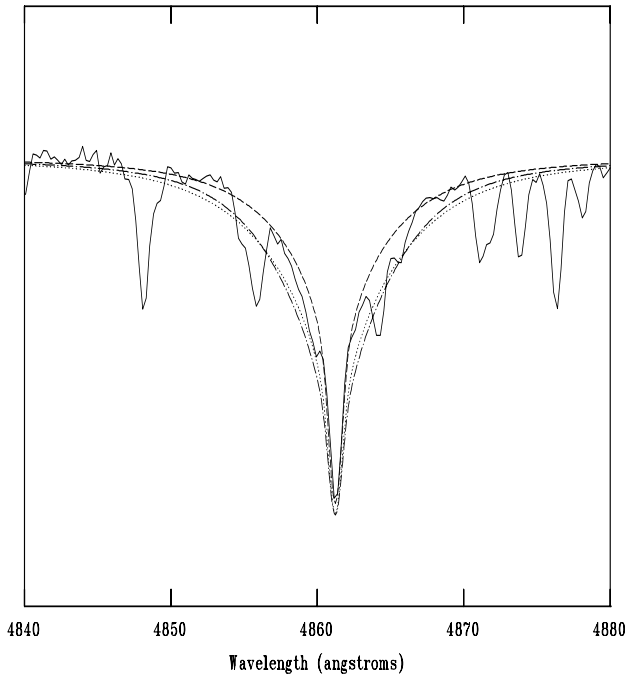

Figure 1: The Hβ line profile is compared with the theorically calculated line profile for different stellar atmospheric models. The dashed line which matches well with the observations corresponds to T_{eff}=6000 K and log g=0.0, the dotted line corresponds to T_{eff} =6500K and log g=0.5 and the dashed dotted line corresponds to T_{eff} =7000K and log g=0.5

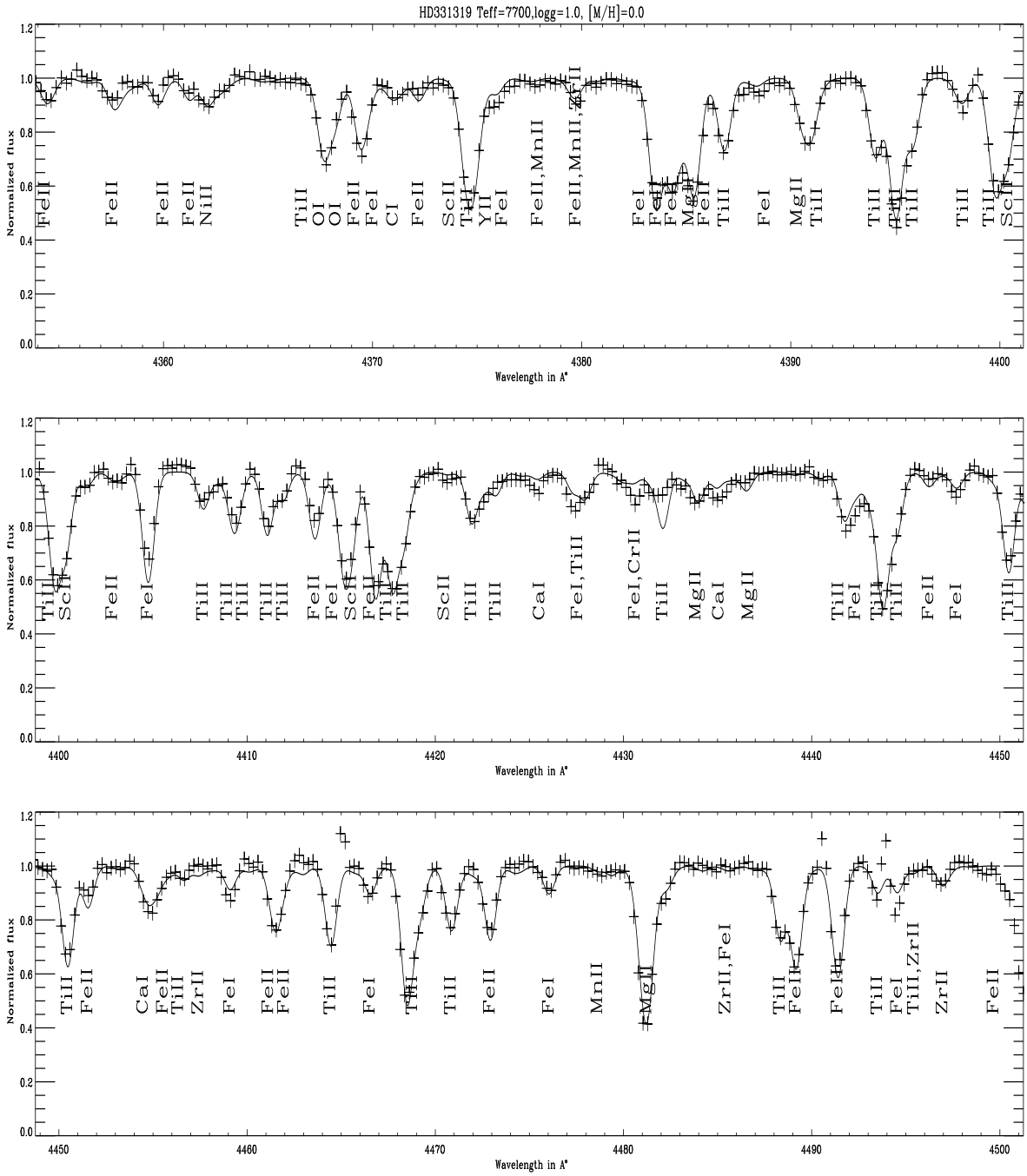

Figure 2: The observed spectrum with a resolution of 0.3Å is compared with the theoritically synthesised spectra for a model with T_{eff}=7700K, log g=1.0, ξ_t=7 km s^{-1} and [M/H]=0.0

could be that the Hβ line could have been modified due to a extended envelop or a circumstellar shell. The metallic lines and also the Hβ line have same radial velocity. In many late supergiants it is found that the log g and T_{eff} values derived using ionization balance and excitation equilibrium does not seem to represent the actual values. The log g derived from ionization equilibrium and fitting the wings of the metallic lines seem to give different results. But the deviation is less than 0.1 dex. The microturbulence is estimated by forcing the strong and weak lines of the same species to give same abundance. We obtained a value of 7Kms^{-1}. Macroturbulence velocity is found to be 30kms^{-1}. Since supergiants have very low rotional velocity, just by changing the macroturbulence velocity, we matched the line profiles and estimated the macroturbulence velocity. This value of macroturbulence velocity seem to be rather high for a post-AGB star. It is found that the ionized lines are more close to LTE than the neutral lines. This due to the UV flux in the inner layers changing the ionization equilbrium. This is more pronounced in the case of metal-poor stars were the UV radiation is not absorbed much.

4.5 Chemical composition

For Teff=6500K and log g=0.5, the chemical composition shows that nitrogen is enhanced and also carbon and oxygen are more abundant than iron. The C,N,O abundances show that there was a mixing due to the third dredge-up. But the s-process elements are not found to be enhanced. Yittrium and barium seem to be quite low. Magnesium and silicon seems to be high compared to iron, indicating α captured products mixing on the surface. The s-process abundances are similar to iron. But Barium and yittrium abundances seems to be very low. We found [Ba/Fe]==0.8, [Y/Fe]=-0.5, [Sc/Fe]=-0.2 and [Ca/Fe]=-0.2.

For the value T_{eff}=7700, log g=1.0 and microturbulence ξ_t=7km s^{-1} we derived the elemental abundances. We found that the metallicity is solar. The C,N,O abun-

dances look as if the surface composition has been altered by the third dredge up products.

4.6 Discussions and Conclusions

The IRAS colors and the variability indicates that AGB phase phase of evolution of HD 331319 was terminated quite recently . The expansion velocities obtained from the CO observations which is 15-20Kms^{-1} is similar to that of the post-AGB stars. The near-IR imaging and photometry (Kastner et al. 1995) does not show any extended nebula, So it is more probable that HD 331319 is a post-AGB supergiant than a massive popI supergiant.

The enrichment in the nitrogen abundance shows that the CNO cycle hydrogen burning products have come to the surface. We also see enrichment in carbon. This indicates that the helium burning products are mixed on to the surface through the third dredge-up. We donot see enrichment in s-process elements. According to the theoritical predictions, the third dredge-up is associated with the enrichment in carbon and s-process elements. Probably in this case there would not have been enough neutron flux for s-process to happen.

The abscence of OH maser emission indicates that the envelope could be carbon rich. But Hirvnak et al. (1994) in their near infrared spectrum do not see the 21μm feature, which is associated with carbon rich environment. They also donot see 3.3μm PAH emission also. The spectrum rapidly raises in the flux near 15μm. The near IR and far IR IRAS fluxes and variabilities are quite consistent with post-AGB nature of the object. The CO observations and the expansion velocities are also similar to a post-AGB star. Our chemical composition analysis indicates that surface is contaminated by hydrogen burning product and also helium burning product through

Table 2: Chemical composition of HD 331319.

Element	[element/H]		
	T_{eff}=6500K log g=0.5	T_{eff}=7500K log g=0.5	T_{eff}=7750K log g=1.0
C	-0.5	0.2	0.3
N	1.2	1.2	1.2
O	0.1	0.1	0.2
Mg	-0.55	-0.5	-0.5
Si	0.0	-0.3	-0.3
Ca	-1.2	-0.3	0.0
Sc	-1.2	-0.5	-0.3
Ti	-1.0	-0.5	-0.3
V	-1.0	-0.5	0.0
Cr	-1.0	-0.5	0.0
Mn	-1.0	-0.5	0.0
FeI	-1.4	-0.4	-0.1
FeII	-0.8	-0.1	-0.1
Co	-1.0	-0.5	0.0
Ni	-1.0	-0.5	0.0
Y	-1.5	-1.0	-0.1
Zr	-1.0	-0.3	0.0
Ba	-1.8	-0.3	0.0

third dredge-up. In many post-AGB stars the atmospheres are far from LTE. So the excitation and ionization equilibrium do not work well. So we feel that the T_{eff}=6500K and log g=0.5 for which enrichment of α process elements and C,N,O elements are consistent, which indicate that the star has gone through the third dredge-up.

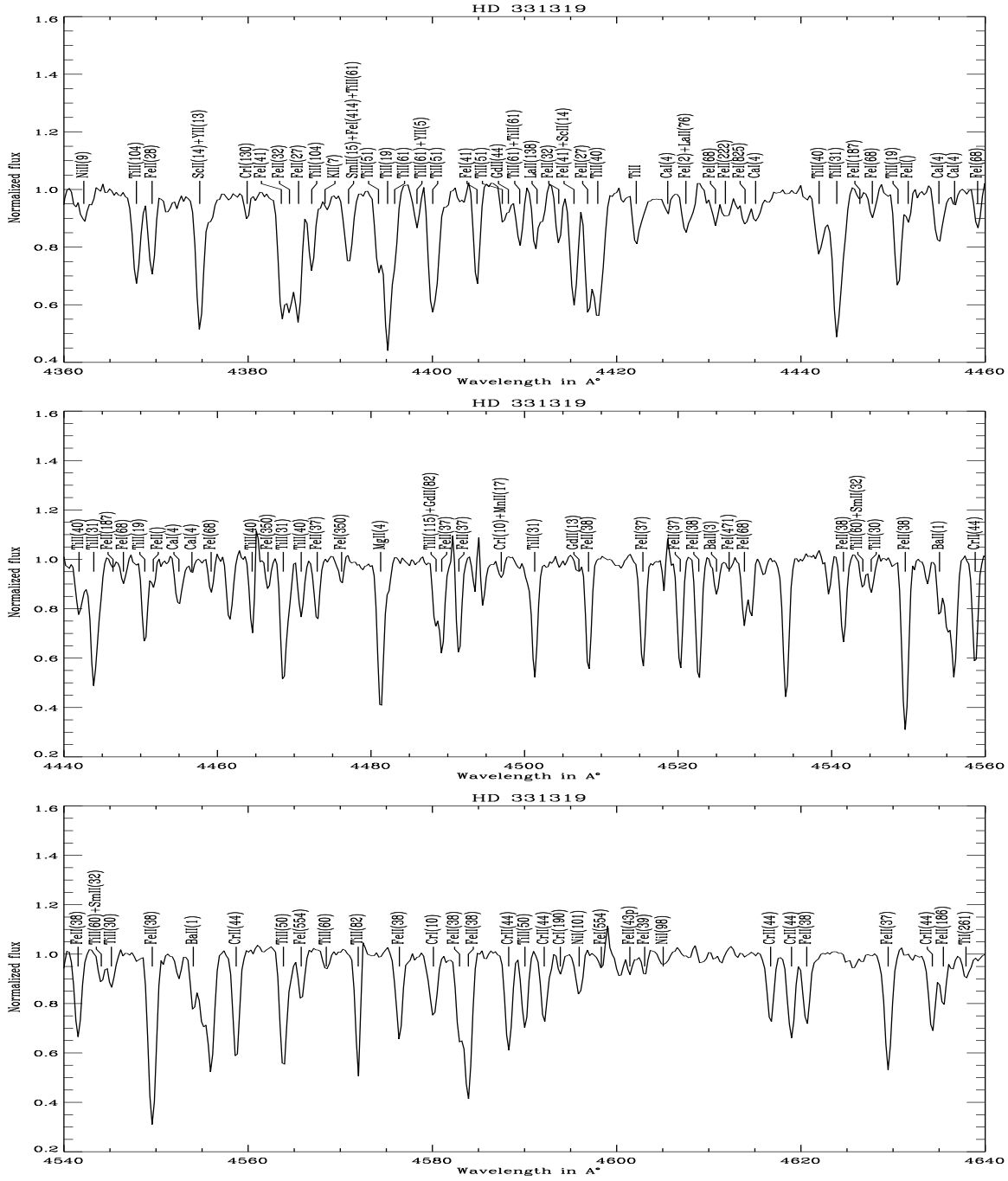

Figure 3(continued): High resolution spectra of HD 331319 from 2.3m, INT, at La Palma

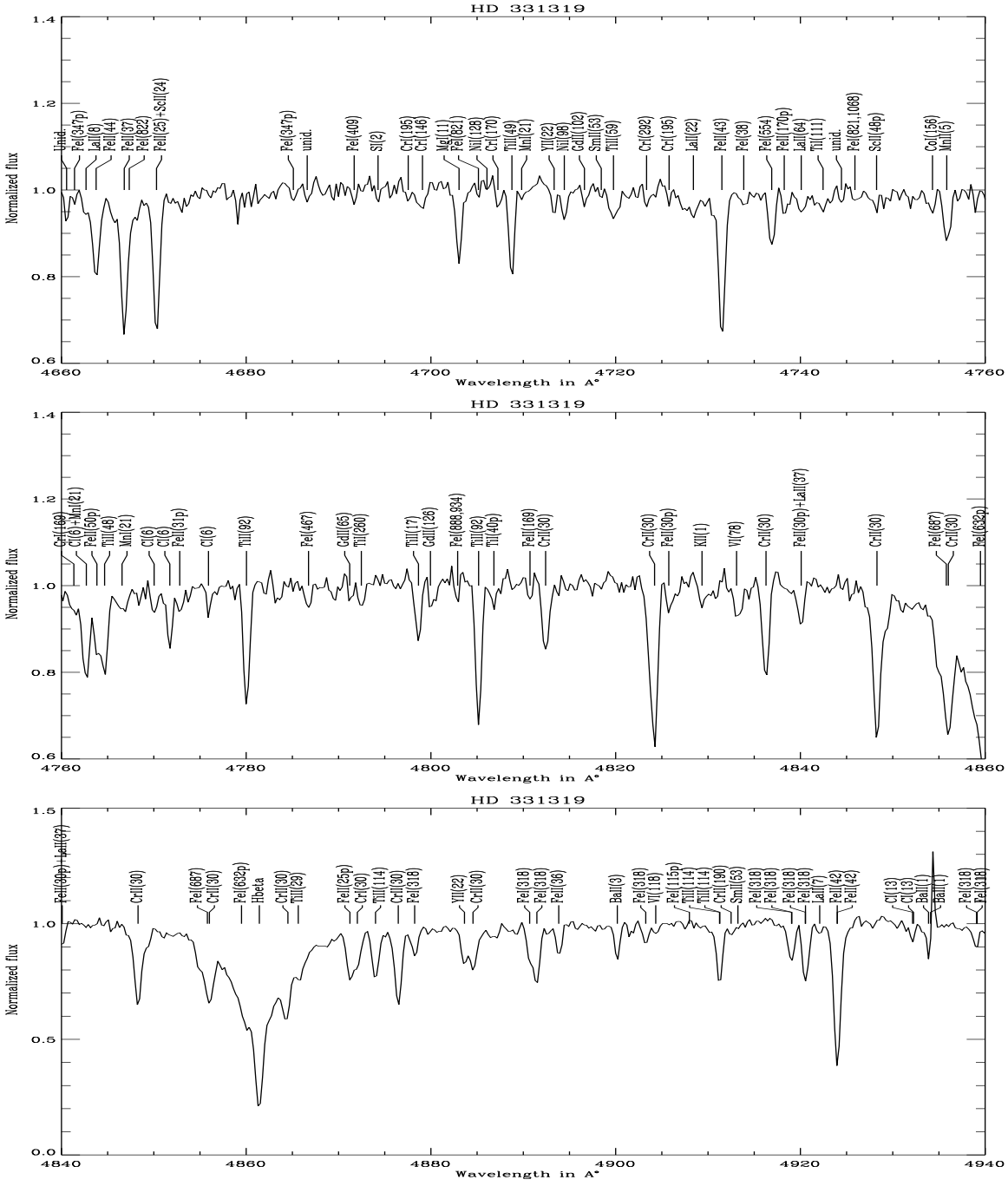

Figure 4(continued): High resolution spectra of HD 331319 from 2.3m, INT, at La Palma

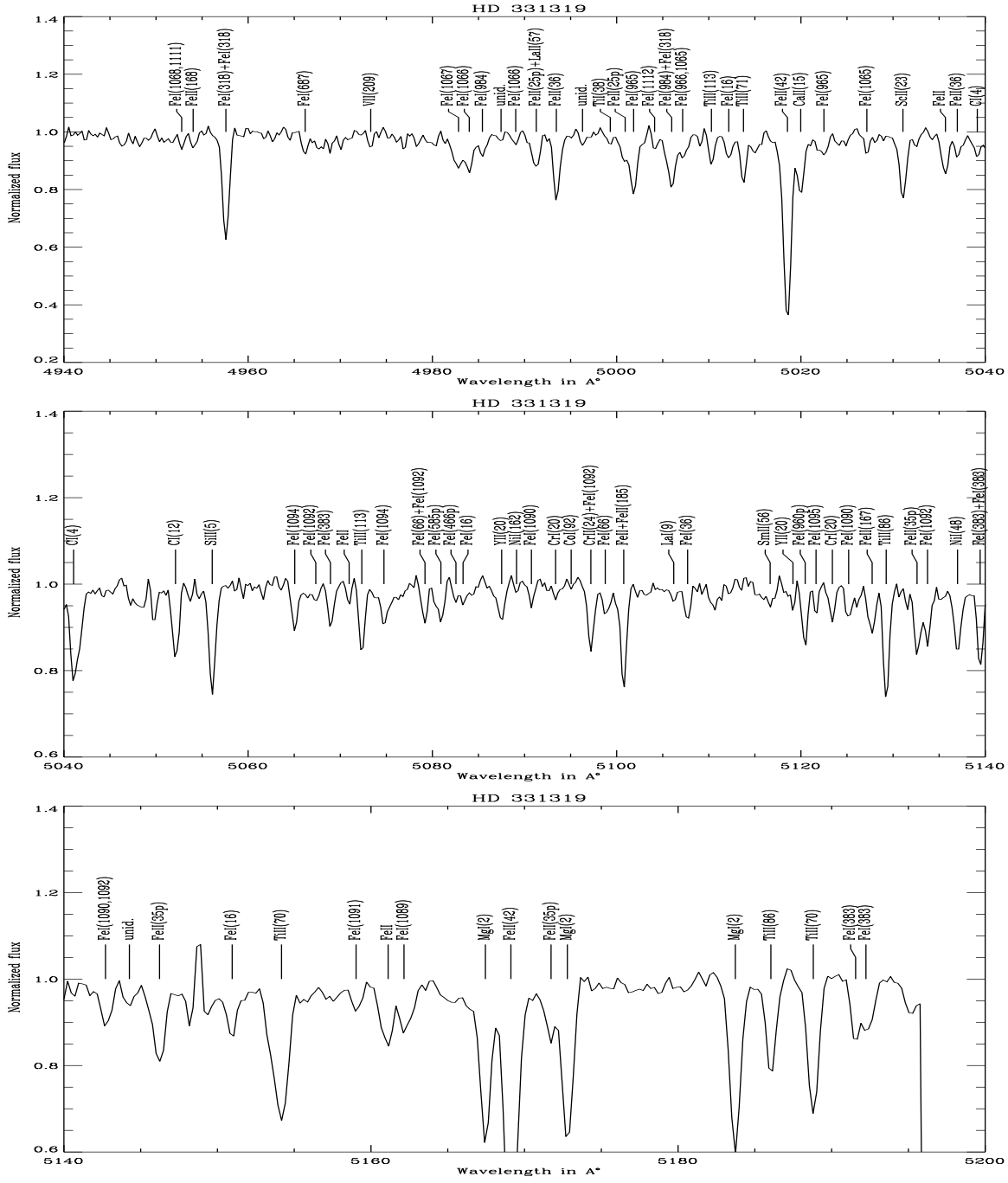

Figure 5(continued): High resolution spectra of HD 331319 from 2.3m, INT, at La Palma

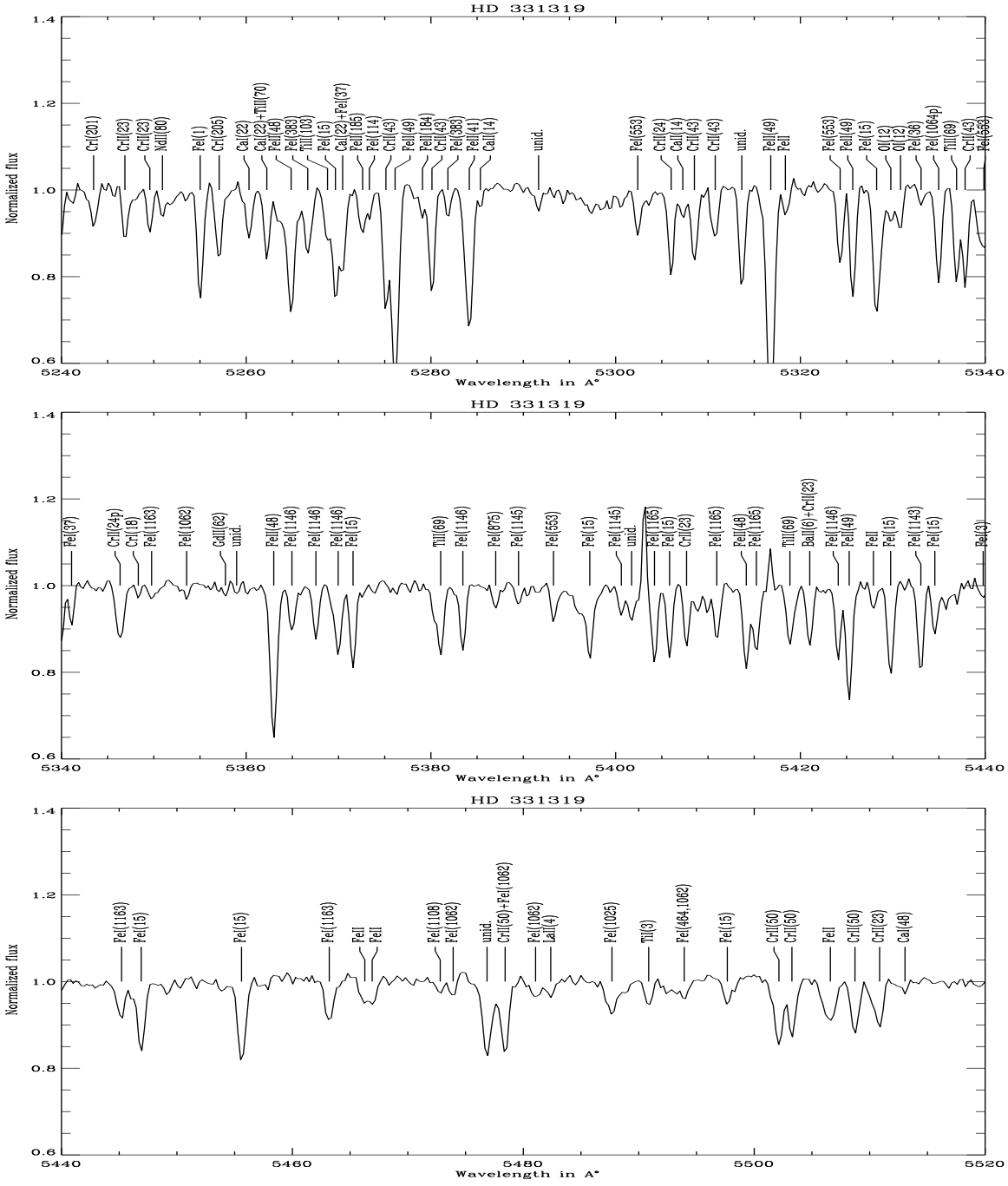

Figure 6(continued): High resolution spectra of HD 331319 from 2.3m, INT, at La Palma

Table 3: Absorption lines in spectrum of HD 331319

L.Obs	eqw	L.Lamb	Ident.	Comments
4357.665	0.1011	4357.514	CrI(198)	
4359.785	0.05426	4359.623	CrI(22)	
4362.162	0.1401	4362.099	NiII(9)	
4367.871	0.3	4367.657	TiII(104)	
4369.57	0.2569	4369.404	FeII(28)	
4374.745	0.4653	4374.455	ScII(14)	Blended with YII(13)
4379.89	0.07038	4379.771	CrI(130)	
4383.599	0.3239	4383.557	FeI(41)	
4384.486	0.4014	4384.33	FeII(32)	
4385.473	0.369	4385.381	FeII(27)	
4386.902	0.2257	4386.858	TiII(104)	
4388.344	0.05055	4388.16	KII(7)	
4390.901	0.3237	4390.858	SmII(15)	+.954FeI(414)+.977 TiII(61)
4394.15	0.2546	4394.057	TiII(51)	
4395.135	0.4495	4395.031	TiII(19)	
4395.902	0.18	4395.848	TiII(61)	
4398.323	0.141	4398.314	TiII(61)	+.03 YII(5)
4400.035	0.6913	4399.767	TiII(51)	
4404.838	0.2941	4404.761	FeI(41)	
4407.586	0.06062	4407.678	TiII(51)	
4408.248	0.08135	4408.248	GdII(44)	v.w check solarspec
4409.474	0.1765	4409.22	TiII(61)	+.519TiII(61)
4411.356	0.2428	4411.21	LaII(138)	
4413.711	0.1498	4413.60	FeII(32)	
4415.367	0.4142	4415.125	FeI(41)	+.559ScII(14)

Table 1: Absorption lines in spectrum of HD 331319

L.Obs	eqw	L.Lamb	Ident.	Comments
4416.847	0.2742	4416.817	FeII(27)	
4417.948	0.6419	4417.718	TiII(40)	
4422.126	0.3642	4421.949	TiII (93)	
4425.542	0.04818	4425.441	CaI(4)	
4427.514	0.1947	4427.312	FeI(2)	+.52LaII(76)
4430.725	0.1732	4430.618	FeI(68)	
4431.801	0.1427	4431.626	FeII(222)	
4433.939	0.1281	4433.793	FeI(825)	
4435.081	0.1647	4434.960	CaI(4)	
4441.975	0.2665	4441.73	TiII(40)	
4443.894	0.7546	4443.802	TiII(31)	
4446.396	0.04178	4446.248	FeII(187)	
4447.75	0.1066	4447.722	FeI(68)	
4450.538	0.3071	4450.487	TiII(19)	
4451.642	0.09118	4451.545	FeII()	
4454.98	0.2474	4454.781	CaI(4)	
4456.677	0.06774	4456.612	CaI(4)	
4459.18	0.1473	4459.121	FeI(68)	
4461.584	0.302	4461.43	FeII(10F)	
4464.525	0.2582	4464.458	TiII(40)	
4466.59	0.09955	4466.554	FeI(350)	
4468.58	0.4676	4468.493	TiII(31)	
4470.91	0.2082	4470.864	TiII(40)	
4472.994	0.213	4472.921	FeII(37)	
4476.174	0.08046	4476.021	FeI(350)	

Table 1: Absorption lines in spectrum of HD 331319

L.Obs	eqw	L.Lamb	Ident.	Comments
4481.262	0.6344	4481.327	MgII(4)	
4488.478	0.2893	4488.319	TiII(115)	+.401 GdII(82)
4489.213	0.3545	4489.185	FeII(37)	
4491.451	0.3344	4491.401	FeII(37)	
4493.499	0.09592			
4494.583	0.1617			
4496.967	0.08376	4496.862	CrI(10)	+.989 MnII(17)
4501.324	0.4731	4501.270	TiII(31)	
4507.078	0.08712	4506.931	GdII(13)	
4508.337	0.4516	4508.283	FeII(38)	
4515.419	0.4043	4515.337	FeII(37)	
4520.279	0.3813	4520.225	FeII(37)	
4522.693	0.4469	4522.634	FeII(38)	
4525.006	0.1259	4524.928	BaII(3)	
4526.647	0.07146	4526.563	FeI(471)	
4528.64	0.225	4528.619	FeI(68)	
4541.539	0.3192	4541.523	FeII(38)	
4544.06	0.1206	4544.009	TiII(60)	+.948 SmII(32)
4545.154	0.1368	4545.144	TiII(30)	
4549.59	0.7427	4549.467	FeII(38)	
4554.047	0.1712	4554.033	BaII(1)	
4558.7	0.3729	4558.659	CrII(44)	
4563.831	0.4568	4563.761	TiII(50)	
4565.758	0.183	4565.684	FeI(554)	

Table 1(continued) : Absorption lines in spectrum of HD 331319

L.Obs	eqw	L.Lamb	Ident.	Comments
4568.481	0.08375	4568.312	TiII(60)	
4571.943	0.3592	4571.971	TiII(82)	
4576.416	0.3003	4576.331	FeII(38)	
4580.108	0.291	4580.056	CrI(10)	
4582.947	0.3031	4583.829	FeII(38)	
4583.901	0.5222	4583.829	FeII(38)	
4585.758	0.02065			
4588.277	0.3696	4588.217	CrII(44)	
4590.043	0.2631	4589.961	TiII(50)	
4592.135	0.236	4592.09	CrII(44)	
4593.884	0.07246	4593.84	CrI(190)	
4595.926	0.1685	4595.951	NiI(101)	
4598.333	0.04633	4598.122	FeI(554)	
4600.344	0.09508			
4601.43	0.07324	4601.34	FeII(43p)	
4603.043	0.05728	4602.944	FeI(39)	
4605.051	0.07671	4604.994	NiI(98)	
4545.154	0.1368	4545.144	TiII(30)	
4549.59	0.7427	4549.467	FeII(38)	
4554.047	0.1712	4554.033	BaII(1)	
4558.7	0.3729	4558.659	CrII(44)	
4563.831	0.4568	4563.761	TiII(50)	
4616.713	0.2664	4616.64	CrII(44)	
4618.978	0.3491	4618.83	CrII(44)	
4620.632	0.2629	4620.513	FeII(38)	

Table 1(continued) : Absorption lines in spectrum of HD 331319

L.Obs	eqw	L.Lamb	Ident.	Comments
4629.466	0.4289	4629.336	FeII(37)	
4634.263	0.3106	4634.11	CrII(44)	
4635.458	0.1662	4635.328	FeII(186)	
4637.917	0.08487	4637.887	TiI(261)	
4654.491	0.07025	4654.286	CeII(154)	
4655.744	0.05272	4655.661	NiI(115)	
4657.085	0.3152	4656.974	FeII(43)	
4660.555	0.043	Unid		
4661.412	0.01656	4661.33	FeI(347p)	
4662.661	0.06515	4662.51	LaII(8)	
4663.756	0.2304	4663.700	FeII(44)	
4666.801	0.2574	4666.750	FeII(37)	
4667.34	0.1896	4667.459	FeI(822)	
4670.293	0.2968	4670.170	FeII(25)	+.404 ScII(24)
4685.104	0.04302	4685.03	FeI(347p)	
4686.606	0.05844	unid		
4691.689	0.03502	4691.414	FeI(409)	
4694.276	0.03061	4694.13	S I(2)	
4697.542	0.06263	4697.395	CrI(195)	
4699.085	0.1049	4698.947	CrI(146)	
4703.044	0.1511	4702.9758	MgI(11)	
4705.146	0.02046	4704.958	FeI(821)	
4706.065	0.01514	4705.93	NiI(128)	
4707.253	0.04292	4706.102	CrI(170)	
4708.767	0.1669	4708.663	TiII(49)	

Table 1(continued) : Absorption lines in spectrum of HD 331319

L.Obs	eqw	L.Lamb	Ident.	Comments
4709.821	0.03782	4709.715	MnI(21)	
4713.337	0.046	4713.26	Y II(22)	
4714.441	0.05923	4714.421	NiI(98)	
4716.618	0.04489	4716.576	GdII(102)	
4718.444	0.01965	4718.329	SmII(53)	
4719.766	0.1156	4719.515	TiII(59)	
4723.348	0.03502	4723.18	CrI(292)	
4725.786	0.02504	4725.67	CrI(195)	
4728.417	0.08162	4728.41	LaII(22)	
4731.5	0.3024	4731.439	FeII(43)	
4733.866	0.04665	4733.596	FeI(38)	
4736.896	0.1163	4736.780	FeI(554)	
4738.25	0.04026	4738.52	FeII(170p)	
4740.091	0.06171	4739.80	LaII(64)	
4742.455	0.06048	4742.32	TiI(111)	
4744.444	0.02474	unid		
4745.906	0.02726	4745.806	FeI(821,1068)	
4748.249	0.03226	4748.12	ScII(48p)	
4754.301	0.03691	4754.358	CoI(156)	
4755.846	0.1139	4755.728	MnII(5)	
4761.343	0.1315	4761.242	CrI(169)	
4762.692	0.2188	4762.41	CI(6)	+.376MnI(21)
4763.838	0.124	4763.79	FeII(50p)	
4764.672	0.1881	4764.535	TiII(48)	
4766.559	0.1409	4766.430	MnI(21)	

Table 1(continued) : Absorption lines in spectrum of HD 331319

L.Obs	eqw	L.Lamb	Ident.	Comments
4770.031	0.04775	4770.00	C I(6)	
4771.733	0.1171	4771.72	C I(6)	
4772.803	0.07319	4772.77	FeII(31p)	
4775.917	0.03367	4775.87	C I(6)	
4780.029	0.2508	4779.986	TiII(92)	
4786.75	0.06189	4786.810	FeI(467)	
4791.208	0.02836	4791.150	GdII(65)	
4792.469	0.06581	4792.482	TiI(260)	
4798.654	0.1031	4798.535	TiII(17)	
4799.946	0.04765	4799.859	GdII(126)	
4802.893	0.06933	4802.883	FeI(888,934)	
4805.161	0.293	4805.105	TiII(92)	
4806.822	0.09883	4806.75	TiI(40p)	
4810.726	0.03588	4810.760	FeII(169)	
4812.415	0.179	4812.35	CrII(30)	
4824.215	0.4983	4824.13	CrII(30)	
4825.753	0.1056	4825.71	FeII(30p)	
4829.348	0.07075	4829.23	K II(1)	
4833.09	0.1088	4833.027	V I(78)	
4836.276	0.2127	4836.22	CrII(30)	
4840.083	0.08564	4840.00	FeII(30p)	+.02 LaII(37)
4848.292	0.3969	4848.24	CrII(30)	
4855.797	0.2952	4855.683	FeI(687)	
4856.016	0.6378	4856.19	CrII(30)	
4859.492	0.4824	4859.31	FeI(632p)	

Table 1(continued) : Absorption lines in spectrum of HD 331319

L.Obs	eqw	L.Lamb	Ident.	Comments
4861.423	1.098	4861.332	Hbeta	
4864.517	0.8522	4864.32	CrII(30)	
4865.639	0.429	4865.620	TiII(29)	
4871.228	0.1616	4871.27	FeII(25p)	
4872.034	0.1291	4872.02	CrI(30)	
4874.004	0.1832	4874.025	TiII(114)	
4876.462	0.3038	4876.41	CrII(30)	
4878.238	0.09681	4878.218	FeI(318)	
4884.556	0.21	4884.57	CrII(30)	
4883.635	0.1429	4883.69	Y II(22)	
4890.688	0.1298	4890.762	FeI(318)	
4891.47	0.2018	4891.496	FeI(318)	
4893.839	0.1302	4893.780	FeII(36)	
4900.18	0.1148	4899.934	BaII(3)	
4903.256	0.07249	4903.317	FeI(318)	
4904.34	0.0395	4904.350	V I(118)	
4911.243	0.2422	4911.205	TiII(114)	
4912.5	0.1492	4912.49	CrII(190)	
4919.046	0.1577	4918.999	FeI(318)	
4920.538	0.2308	4920.509	FeI(318)	
4922.091	0.05248	4921.80	LaII(7)	
4923.989	0.6018	4923.921	FeII(42)	
4932.144	0.103	4932.00	C I(13)	
4933.872	0.089	4934.086	BaII(1)	corrupted by cosmic ray
4939.074	0.1235	4938.820	FeI(318)	

Table 1(continued) : Absorption lines in spectrum of HD 331319

L.Obs	eqw	L.Lamb	Ident.	Comments
4907.985	0.05455	4907.743	FeI(115p)	
4911.275	0.2362	4911.205	TiII(114)	
4913.236	0.1996	4913.248	SmII(53)	
4919.069	0.1838	4918.999	FeI(318)	
4920.55	0.2501	4920.509	FeI(318)	
4923.995	0.6605	4923.921	FeII(42)	
4932.251	0.09574	4932.00	C I(13)	
4934.101	0.2055	4934.086	BaII(1)	
4939.137	0.1389	4938.820	FeI(318)	
4952.788	0.05657	4952.646	FeI(1068,1111)	
4954.027	0.07109	4953.979	FeII(168)	
4957.583	0.3452	4957.302	FeI(318)	4957.603FeI(318)
4966.187	0.07267	4966.096	FeI(687)	
4973.307	0.03443	4973.16	V II(209)	
4982.831	0.2049	4982.507	FeI(1067)	
4984.002	0.1871	4983.855	FeI(1066)	
4985.427	0.118	4985.261	FeI(984)	
4987.45	0.03907	unid		
4989.042	0.04032	4988.963	FeI(1066)	
4991.271	0.1827	4991.11	FeII(25p)	+4991.27LaII(57)
4993.454	0.2095	4993.355	FeII(36)	
4996.295	0.05527	unid		
4999.309	0.0781	4999.504	TiI(38)	
5000.922	0.1706	5000.73	FeII(25p)	
5001.839	0.2292	5001.871	FeI(965)	

Table 1(continued) : Absorption lines in spectrum of HD 331319

L.Obs	eqw	L.Lamb	Ident.	Comments
5004.117	0.06209	5004.034	FeI(1112)	
5005.974	0.296	5005.720	FeI(984)	+5006.126FeI(318)
5007.16	0.1482	5007.289	FeI(966,1065)	
5010.283	0.08566	5010.202	TiII(113)	
5012.167	0.08084	5012.071	FeI(16)	
5013.763	0.1454	5013.712	TiII(71)	
5018.537	0.7107	5018.434	FeII(42)	
5019.979	0.1899	5019.979	CaII(15)	
5022.494	0.1048	5022.244	FeI(965)	
5022.476	0.15			
5024.124	0.03722			
5027.154	0.04547	5027.136	FeI(1065)	
5031.072	0.1981	5031.019	ScII(23)	
5032.493	0.04381			
5035.686	0.1649	5035.773	FeII	
5036.977	0.1749	5036.92	FeII(36)	
5039.144	0.1194	5039.05	C I(4)	
5041.057	0.426	5041.66	C I(4)	
5049.759	0.05457			
5052.115	0.1879	5052.122	C I(12)	
5056.102	0.2311	5056.020	SiII(5)	
5065.058	0.1077	5065.020	FeI(1094)	
5067.343	0.05364	5067.162	FeI(1092)	
5068.933	0.1059	5068.774	FeI(383)	
5070.961	0.03097	5070.957	FeII	

Table 1(continued) : Absorption lines in spectrum of HD 331319

L.Obs	eqw	L.Lamb	Ident.	Comments
5072.334	0.139	5072.30	TiII(113)	
5074.742	0.1121	5074.757	FeI(1094)	
5079.192	0.106	5079.226	FeI(66)	+5079.002FeI(1092)
5080.92	0.101	5080.95	FeI(585p)	
5082.555	0.04758	5082.68	FeI(466p)	
5083.325	0.07111	5083.342	FeI(16)	
5087.518	0.1022	5087.42	Y II(20)	
5089.132	0.02571	5088.956	NiI(162)	
5090.743	0.04492	5090.787	FeI(1090)	
5093.372	0.09229	5093.41	CrI(20)	
5095.064	0.03379	5094.955	CoI(92)	
5097.201	0.138	5097.29	CrII(24)	+5096.998FeI(1092)
5098.762	0.1465	5098.703	FeI(66)	
5100.767	0.2042	5100.704	FeII	+5100.840FeII(185)
5106.193	0.01987	5106.23	LaI(9)	
5107.702	0.05833	5107.645	FeI(36)	
5116.659	0.1042	5116.700	SmII(56)	
5119.136	0.0496	5119.12	Y II(20)	
5120.463	0.1425	5119.90	FeI(960p)	
5121.64	0.04879	5121.646	FeI(1095)	
5123.415	0.08335	5123.465	CrI(20)	
5125.179	0.08576	5125.130	FeI(1090)	
5127.729	0.1646	5127.866	FeII(167)	
5129.255	0.2223	5129.143	TiII(86)	
5132.604	0.1433	5132.67	FeII(35p)	

Table 1(continued) : Absorption lines in spectrum of HD 331319

L.Obs	eqw	L.Lamb	Ident.	Comments
5133.742	0.1152	5133.692	FeI(1092)	
5137.	0.1396	5137.075	NiI(48)	
5139.453	0.1533	5139.260	FeI(383)	+5139.468FeI(383)
5142.709	0.09989	5142.541	FeI(1090,1092)	
5144.267	0.06413	unid		
5146.23	0.1867	5146.12	FeII(35p)	
5150.96	0.07671	5150.843	FeI(16)	
5154.175	0.3322	5154.061	TiII(70)	
5159.028	0.04872	5159.066	FeI(1091)	
5161.116	0.1812	5159.93	FeII	
5162.15	0.1726	5162.288	FeI(1089)	
5167.452	0.3394	5167.3216	MgI(2)	
5169.111	0.702	5169.030	FeII(42)	
5171.727	0.1703	5171.62	FeII(35p)	
5172.79	0.3704	5172.6843	MgI(2)	
5183.728	0.3715	5183.6042	MgI(2)	
5186.043	0.2072	5185.90	TiII(86)	
5188.806	0.297	5188.700	TiII(70)	
5191.563	0.1213	5191.460	FeI(383)	
5192.235	0.2132	5192.350	FeI(383)	
5237.446	0.2813	5237.34	CrII(43)	
5239.875	0.1155	5239.823	ScII(26)	
5243.479	0.1097	5243.395	CrI(201)	
5246.869	0.08578	5246.75	CrII(23)	
5249.565	0.0902	5249.40	CrII(23)	

Table 1(continued) : Absorption lines in spectrum of HD 331319

L.Obs	eqw	L.Lamb	Ident.	Comments
5255.02	0.2187	5254.956	FeI(1)	
5257.074	0.1357	5257.07	CrI(205)	
5260.305	0.1351	5260.375	CaI(22)	
5262.234	0.1406	5262.244	CaI(22)	+5262.104 TiII(70)
5264.866	0.2746	5264.801	FeII(48)	
5266.663	0.1917	5266.562	FeI(383)	
5268.803	0.09866	5268.62	TiII(103)	
5269.663	0.1667	5269.541	FeI(15)	
5270.444	0.1516	5270.270	CaI(22)	+5270.360 FeI(37)
5272.608	0.1185	5272.413	FeII(185)	
5273.335	0.05985	5273.379	FeI(114)	
5275.125	0.242	5274.99	CrII(43)	
5276.118	0.453	5275.994	FeII(49)	
5279.087	0.06755	5278.955	FeII(184)	
5280.11	0.1926	5280.08	CrII(43)	
5281.841	0.05752	5281.796	FeI(383)	
5284.156	0.3791	5284.092	FeII(41)	
5285.358	0.03425	5285.34	CaII(14)	
5291.653	0.04949	unid		
5302.392	0.1016	5302.307	FeI(553)	
5306.005	0.1402	5305.85	CrII(24)	
5307.275	0.0453	5307.30	CaII(14)	
5308.527	0.1287	5308.44	CrII(43)	
5310.778	0.1018	5310.70	CrII(43)	
5313.656	0.2141	unid		

Table 1(continued) : Absorption lines in spectrum of HD 331319

L.Obs	eqw	L.Lamb	Ident.	Comments
5316.793	0.5387	5316.609	FeII(49)	
5318.372	0.08046	5318.267	FeII	
5324.303	0.1527	5324.185	FeI(553)	
5325.667	0.2092	5325.559	FeII(49)	
5328.253	0.2679	5328.042	FeI(15)	
5329.791	0.1335	5329.59	O I(12)	
5330.842	0.04403	5330.66	O I(12)	
5333.064	0.03344	5332.903	FeI(36)	
5334.97	0.1805	5334.32	FeI(1064p)	
5336.908	0.1712	5336.809	TiII(69)	
5337.833	0.1578	5337.79	CrII(43)	
5339.867	0.2432	5339.935	FeI(553)	
5341.094	0.06249	5341.026	FeI(37)	
5346.345	0.1504	5346.12	CrII(24p)	
5348.318	0.02427	5348.319	CrI(18)	
5349.76	0.06719	5349.742	FeI(1163)	
5353.554	0.03618	5353.386	FeI(1062)	
5357.753	0.02226	5357.790	GdII(62)	
5358.967	0.02245	unid		
5362.982	0.3392	5362.864	FeII(48)	
5364.951	0.1008	5364.874	FeI(1146)	
5367.548	0.1049	5367.470	FeI(1146)	
5369.957	0.1495	5369.965	FeI(1146)	
5371.568	0.1439	5371.493	FeI(15)	
5381.055	0.1356	5381.020	TiII(69)	

Table 1(continued) : Absorption lines in spectrum of HD 331319

L.Obs	eqw	L.Lamb	Ident.	Comments
5383.458	0.1159	5383.374	FeI(1146)	
5387.012	0.04849	5386.958	FeI(875)	
5389.483	0.04608	5389.461	FeI(1145)	
5393.269	0.07773	5393.174	FeI(553)	
5397.198	0.1568	5397.131	FeI(15)	
5400.611	0.05562	5400.509	FeI(1145)	
5401.727	0.08086	unid		
5404.204	0.13	5404.144	FeI(1165)	
5405.839	0.1174	5405.778	FeI(15)	
5407.677	0.1038	5407.62	CrII(23)	
5410.948	0.09538	5410.913	FeI(1165)	
5414.14	0.1558	5414.089	FeII(48)	
5415.236	0.1264	5415.201	FeI(1165)	
5418.867	0.1176	5418.802	TiII(69)	
5421.011	0.1214	5421.05	BaII(6)	+5420.90 CrII(23)
5424.094	0.1157	5424.072	FeI(1146)	
5425.283	0.2083	5425.269	FeII(49)	
5427.906	0.04197	5427.832	FeII	
5429.775	0.1742	5429.699	FeI(15)	
5433.038	0.1783	5432.950	FeI(1143)	
5434.555	0.09522	5434.527	FeI(15)	
5439.789	0.03958	5439.72	FeI(3)	
5445.208	0.08687	5445.045	FeI(1163)	
5446.907	0.1242	5446.920	FeI(15)	
5455.595	0.1768	5455.613	FeI(15)	

Table 1(continued) : Absorption lines in spectrum of HD 331319

L.Obs	eqw	L.Lamb	Ident.	Comments
5463.195	0.1006	5463.282	FeI(1163)	
5466.275	0.0725	5466.021	FeII	
5466.911	0.05809	5466.94	FeII	
5472.804	0.03962	5472.72	FeI(1108)	
5473.927	0.029	5473.908	FeI(1062)	
5476.862	0.1567	unid		
5478.428	0.1381	5478.35	CrII(50)	+5478.48 FeI(1062)
5490.862	0.0663	5490.840	TiI(3)	
5497.669	0.05822	5497.519	FeI(15)	
5482.376	0.04229	5482.27	LaII(4)	
5503.265	0.1152	5503.18	CrII(50)	
5506.594	0.1398	5506.268	FeII	
5508.727	0.1207	5508.60	CrII(50)	
5510.861	0.08763	5510.68	CrII(23)	
5513.06	0.0186	5512.979	CaI(48)	

Chapter 5

Chemical composition of the post-AGB F-supergiant HD 187885

5.1 Abstract

We have analysed high resolution spectrum of the post-AGB F-supergiant HD 187885. We have derived T_{eff} from different methods. We discuss here the chemical composition of HD 187885 and the atmospheric parameters. We find that HD 187885 is a metal poor [Fe/H] $\sim$ -1.0, and overabundant in carbon and s-process elements. It appears to have experienced third dredge up and has gone through the carbon phase on AGB.

5.2 Introduction

HD187885 is a high galactic latitude F-supergiant which shows a strong far-IR excess (Parthasarathy and Pottasch 1986; Hrivnak etal 1989). In a later paper Parthasarathy et al. (1988) discuss IUE observations and conclude that, although their low resolution

optical spectrum is consistent with a spectral classification of a F2-3I supergiant, the UV flux indicates a much hotter source. The presence of 5876Å He I line (Van Winckel et al. 1996), indicates a higher temperature. HD 187885 is detected in both ^{12}CO and ^{13}CO J=1-0 and J=2-1 lines (Likkel et al., 1987; Bujarrabal et al. 1992). From the CO observations an expansion velocity of 13kms^{-1} is deduced (van der Veen et al. 1993).

The circumstellar material is found to be carbon rich as indicated by the strength of the HCN line compared to CO lines and from the possible dectection of 11μm feature in the IRAS LRS together with the absence of OH and H_2O maser emission (Bujarrabal et al. 1992). In the ^{12}CO line profile there is evidence for two components with the main component having an expansion velocity of 13kms^{-1}, and a higher velocity component with an outflow velocity of 40kms^{-1}.

Van winckel et al.(1996) found that HD 187885 has low iron abundance, and clear enrichment of carbon and s-process abundance, showing the third dredge-up. theoritical predictions.

5.3 Observations and analysis

A high resolution and high signal to noise ratio spectra of HD 187885 were obtained with the European Southern Observatory (ESO) Coude Auxiliary Telescope (CAT) equipped with the Coude Echelle Spectrograph (CES) and a CCD as detector. The spectra cover the wavelength regions 4190 - 4600Å, 5010 -5050Å, 5360 - 5400 Å, 6140-6180Å, 6540 - 6590Å, 7085 - 7140Å, 7410 - 7470Å and 8650 - 8775Å. The spectral resolution ranged from 0.165Å at 6150Å to 0.210Å at 8700Å. The observations were made on 6th June 1991. The data reduction has been carried using IRAF software.

5.4 Atmospheric parameters and chemical composition

For the initial estimate of the atmospheric parameters we used the Hγ line profile fitting (Fig. 1). We found the model with T_{eff}=7500K and log g=0.5 matches better than the other models.

We have selected unblended lines of FeI and FeII and used the line analysis program MOOG by Sneden (1999). We found that both FeI and FeII are giving different microturbulence velocities. The ξ_t for FeI was found to be 6kms^{-1} and for FeII lines it is 7.5kms^{-1}. We used both the microturbulence velocities and derived the abundances. There was a difference of 0.1dex in the derived abundances, for these two microturbulance velocities, in case of neutral lines. For ionized lines the difference is around 0.2dex. We have used T_{eff} = 6500, 7000 and 7500K, log g=0.5 and [M/H]=-1.0 models and derived the abundances. For the cases of 6500,7000K the FeI and FeII gives a different abundances, the difference is around 0.8dex to 0.5dex. As we increase the microturbulence velocity the difference in the abundances derived from both FeI and FeII reduces. This could be probably that one needs a much lower gravity models than the one used here. We found that as we increase the T_{eff} this difference between the derived abundances of FeI and FeII decreases and at T_{eff}= 7500K and log g=0.5, both FeI and FeII gives same abundance. The presence of HeI line at 5876Å (Van Winckel et al. 1996) demands a higher temperatures. In our spectrum we did not find any HeI lines at 4437,5015, and 5047Å. Since HD 187885 is carbon rich post-AGB star the 5876Å line could be a carbon line (Hibbert et al. 1991). In the post-AGB F supergiant HD 101584 (Sivarani et al.1999) also the line at 5876Å is seen but the other HeI lines are not present. So the 5876Å line in HD 187885 could be a carbon line or HeI line forming in the wind or in the chromosphere. We list the abundances of HD 187885 for all the three models in Table. 1. The trend in all the models are the same. The result is HD 187885 is metal poor star and the C,N,O

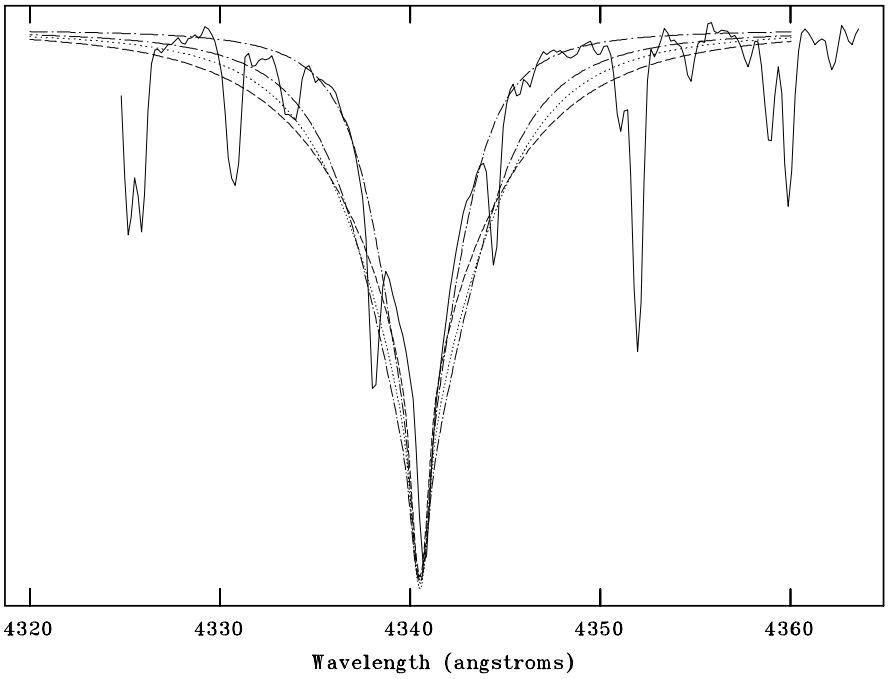

Figure 1: The observed and computed Hγ profiles for T_{eff}=6500, 7000, 7500K and log g=0.5, T_{eff}=7700K and log g=1.0. The one which fits well which is a dot-dash curve, corresponds to T_{eff} =7000K and log g=0.5

abundances are high with respect to iron. The s-process elements are also enhanced. We have used the Kurucz LTE lineblanketed model atmopheres (1993) and MOOG LTE line analysis code (Sneden 1993) for calculating the abundances. The linelist used for the spectrum synthesis is taken from Vienna Atomic Line Databse (VALD, Ryabchikova et al. 1999 and the references therein)

5.5 Discussions and conclusion

From the abundance calculations derived using model atmospheres with different parameters show that HD 187885 is metal poor, CNO elements are enhanced and abundances of s-process elements are enriched. The line analysis shows that the mi-

Table 1: Chemical composition of HD 187885.

Element	[element/H]					
	T_{eff} 6500K		T_{eff} 7000K		T_{eff} 7500K	
	log g 0.5	σ	log g 0.5	σ	log g 0.5	σ
Fe I	-2.0	0.04	-1.56	0.08	-0.87	0.07
Fe II	-1.5	0.13	-1.06	0.1	-0.94	0.13
Ti II	-1.4	0.18	-0.99	0.2	-0.77	0.16
C I	-0.4	0.14	-0.25	0.13	0.18	0.12
N I	0.29	0.22	0.07	0.19	0.02	0.17
O I	0.0	0.04	-0.17	0.03	-0.22	0.03
S I	-0.93		-0.7		-0.18	
Ca I	-1.69	0.4	-1.18	0.48	-0.30	0.49
Sc II	-1.67	0.1	-1.34	0.05	-0.81	0.02
Y II	0.27	0.3	0.12	0.68	0.78	0.68
Zr II	0.64	0.3	-0.32	0.22	0.16	0.18
Ba II	0.65	0.3	-0.06	0.60	0.82	0.63
Ce II	1.13	0.3	-0.67	0.06	0.09	0.05
Sm II	-0.6	0.3	0.86	0.62	1.69	0.61

croturbulence velocities are different for both neutral and ionized iron. We obtain T_{eff} = 7000K from the excitation equilibrium. But FeI and FeII gives a large deviations in the derived abundances. In HD 179821 (Reddy and Hirvnak 1999), similar discrepancies between FeI and FeII is found. In many of the late type post-AGB stars it found that the log g and T_{eff} derived from the ionization and excitaion equilibrium does not seem to represent the actual temperatures (Prieto et al 1999, Edvardsson (1988) and Fuhrmann (1998a)). The gravities derived from strong-line profile fitting and ionization equilibrium gives differnt values. Recently (Thévenin and Idiart 1999) investigated the NLTE effects in iron abundances of late-type stars. They found that most FeI lines in metal-poor stars are formed in conditions far from LTE. But FeII is found not to be affected by significant NLTE effects. The main NLTE effects invoked in the case of Fe I is overionization by UV, thus the classical ionization equilibrium is not satisfied. So the derived abundances are not very accurate.

HD187885 is one of three stars which show very clear evidence of third dredge-up and matches with the theoritical predictions, that is the enhancement in the carbon abundance along with the s-process elements. Within the errors, the abundances are [Fe/H]=-1.5 to -1.0, [C/Fe]=1.2, [N/Fe]=1.0, [O/H]=0.8, [S/Fe]=0.8, [Ca/Fe]=1.3, [Y/Fe]=1.8, [Zr/Fe]=1.1, [Ba/Fe]=1.8, [Ce/Fe]=1.1, [Sm/Fe]=2.6$\pm$0.6. The abundance pattern is quite similar to HD 56126 (Parthasarathy et al. 1992 and Klochkova 1995).

In the globular cluster ω Centauri, however there are 3 UV-bright stars that also display s-process enhancement, together with significant CNO overabundances (Gonzalez and Wallerstein, 1994). They occur several magnitudes above the horizontal branch of the cluster, and it is generally assmumed that the stars are evolving off the AGB towards the planetary nebula stage. HD 187885 and HD 56126 could be field analog of these objects.

Chapter 6

Spectroscopy of the post-AGB star IRAS 10215-5916

6.1 Abstract

IRAS 10215-5916 is a double-lined spectroscopic binary. In our high resolution spectra we found molecular features from a cool companion of T_{eff}=3750K. We also see the spectral signature of a relatively hotter star of T_{eff}=7250K. We found that both the components of the binary system are metal poor. We have derived the carbon and oxygen abundances. They are also depleted compare to the solar value. The α process elements are also depleted with respect to the solar value. Since we see the volatile elements also depleted, the binary system correspond to a older population.

6.2 Introduction

In their final stages of evolution, both massive (M $>8M_{\odot}$) and intermediate-mass (1-8$M_{\odot}$) stars are enshrouded with dust as a result of intense mass loss. For the

massive stars, this heavy mass loss occurs during the red supergiant phase. For intermediate-mass stars this happens during the AGB evolution. After the mass loss, the central star starts contracting and increases its temperature. The UV radiation starts ionizing the dusty circumstellar envelope (CSE), producing eitheir a Planetary Nebula (PN) or a post-RSG nebula surrounding a Wolf-Rayet star. This short-lasting transition period is very less understood.

IRAS10215-5916 is one such object. The evolutionary status is not clear whether it is in post-AGB or post-RGB phase. Garćia-Lario et al. (1994) discovered nebular emission from this IR object. From their high resolution spectra they found an expansion velocity of 17kms^{-1}, which is similar to values that are observed in PPN. The imaging in near-IR shows IRAS10215-5916 is extended and asymmetric. The nebular lines and the extended morphology was explained by incorporating an unseen hot binary which ionizes the nebula and forms a disk. IRAS10215-5916 was thought to be G type star in the transition between AGB and PN stage (Parthasarathy 1989).

The expansion velocities were also measured from the CO(J=1-0) rotational line (Josselin et al. 1998). They found a value of 40 kms^{-1}, which is high for a low-mass AGB star.

Recently Molester etal.(1999) had done a detailed modelling of the flux distribution from optical to infrared (from IRAS and ISO). They found that IRAS10215-5916 is binary system with a cool component of T_{eff} 3750K and a hot component of T_{eff} 7250K. The hot component was found to be 1.8 times more luminous than the cooler one. They observed emission features of amorphous and crystalline silicates in the ISO spectrum in the range 5-195μm. They found that the different dust components have different temperatures implying that they are thermally coupled.

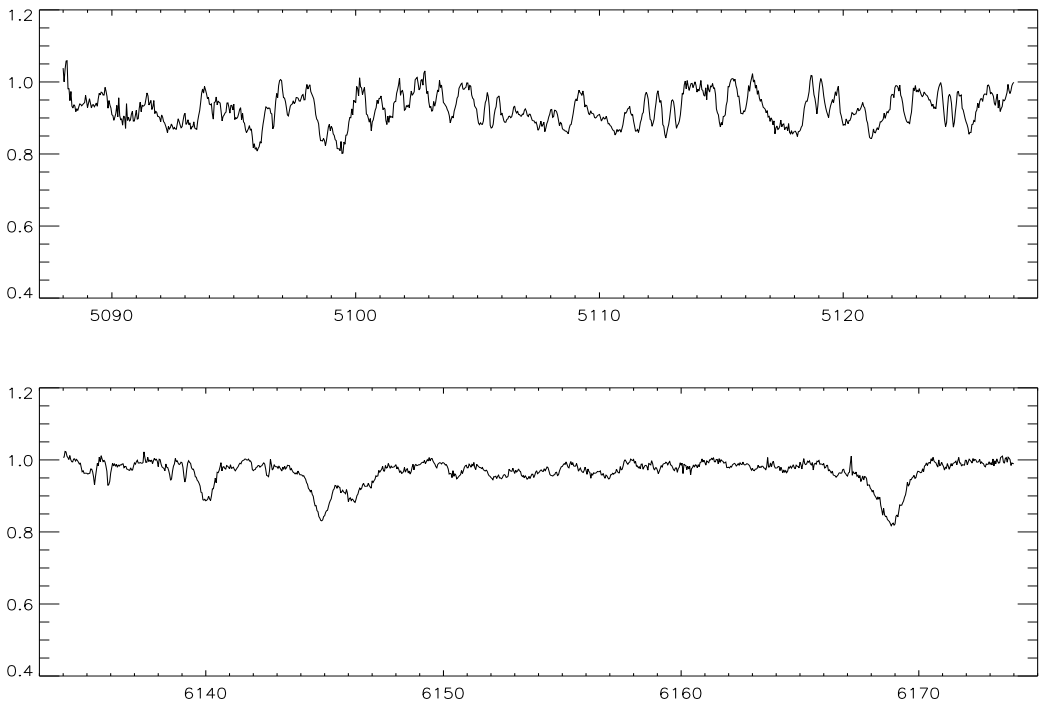

Figure 1:

6.3 Observations and analysis

The high resolution spectra were obtained from 1.4m CAT-CES, with a resolving power of R=50000. The spectra covers (Fig. 1) wavelength regions 5090-5130Å, 6135-6180Å, 6340-6380Å, 6535-6590Å, 7995-8060Å and 8396-8456Å. The spectra were wavelength calibrated and normalised using IRAF.

We have assumed the values given by Molster et al. (1999) for the temperatures of two components of the binary system and the luminosity ratio. For these values, that is T_{eff}=7250K and 3750K and a luminosity ratio L_{warm}/L_{cool}=1.8, we calculated the theoritical spectrum. We used the Kurucz stellar atmospheric models (Kurucz 1993). For the calculating the theoritical spectrum for T_{eff}=7250K we used the *synspec* code by Hubeny (1986). For the cool star we used *spectrum* code by R. O. Gray (1998). We added the flux calibrated spectrum of the cool and hot star. One of the component of the binary system is multiplied by the relative surface area and added to the other.

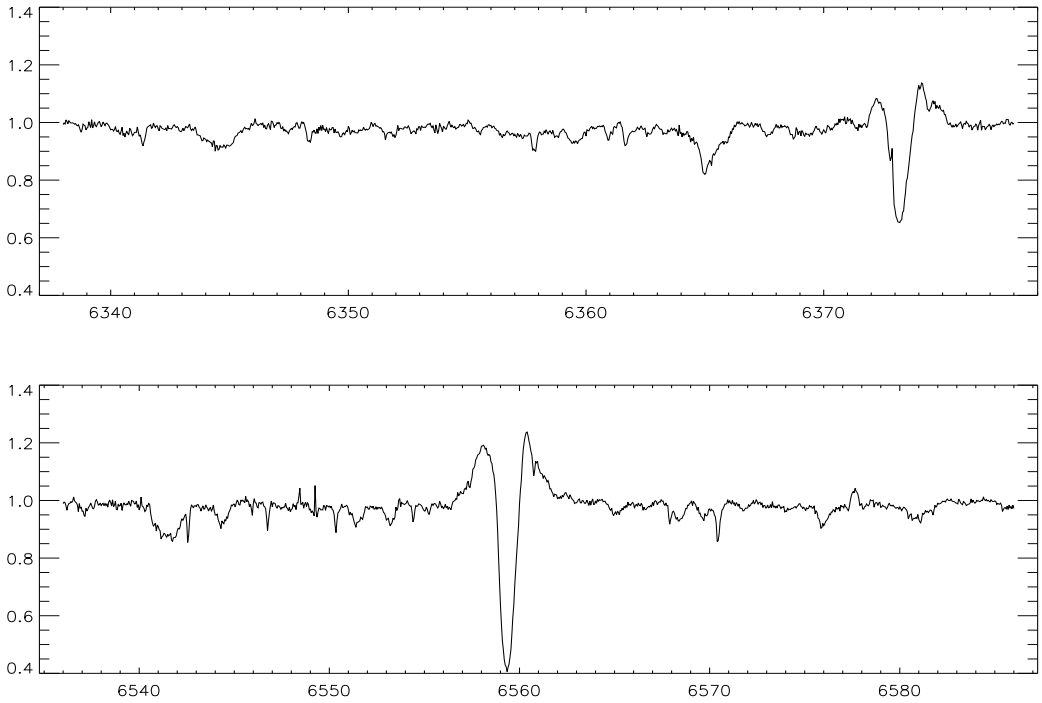

Figure 1:

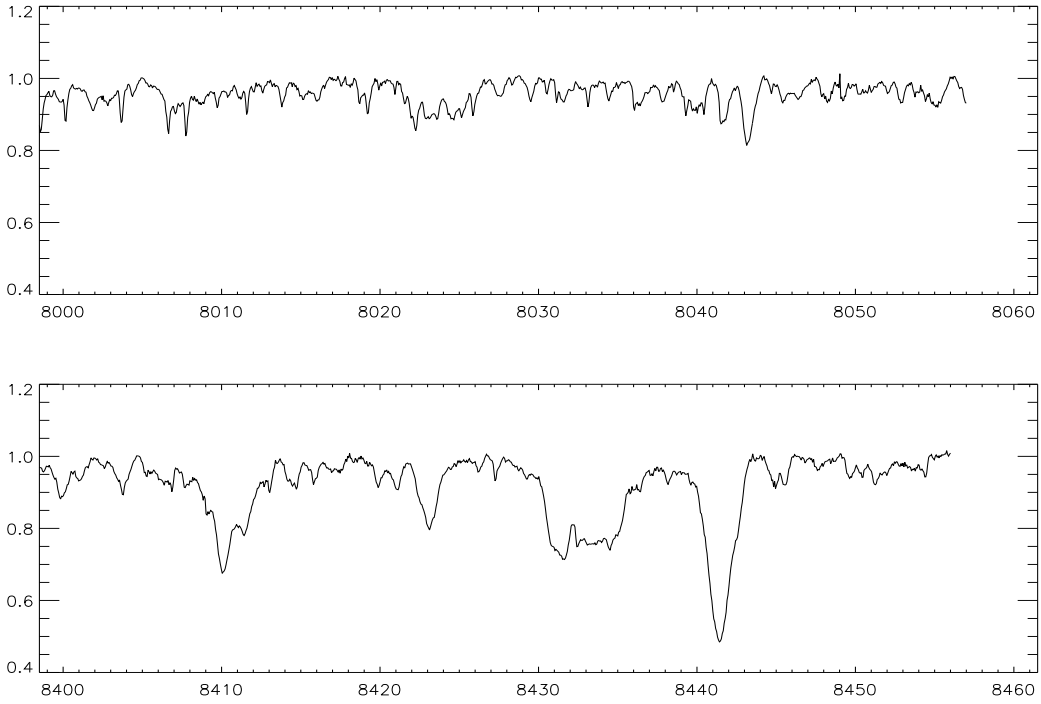

Figure 1:

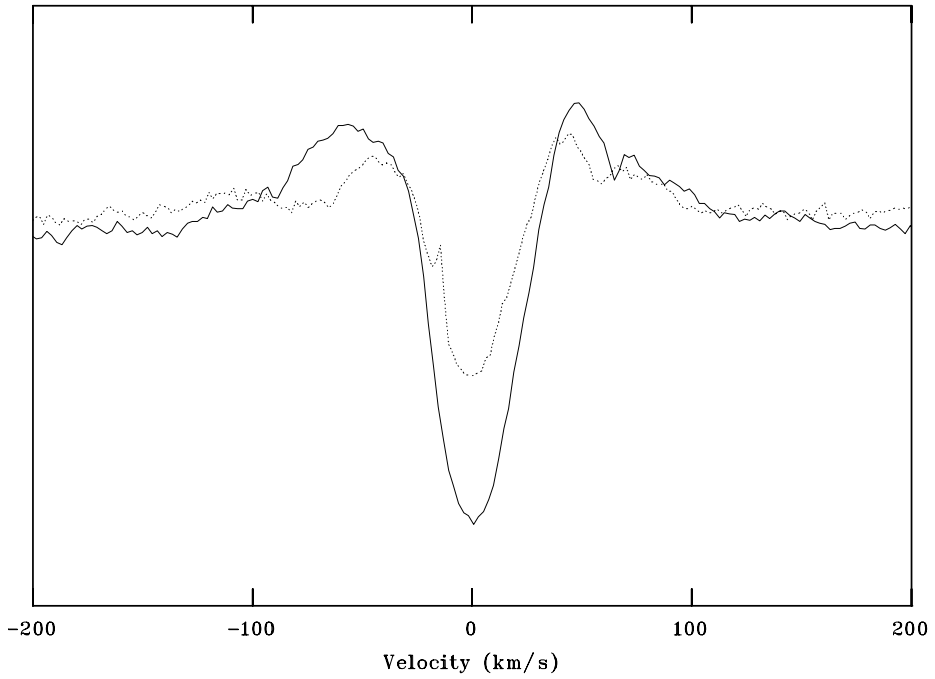

Figure 1:

The resultant spectra was normalized and compared with the observed spectra. We used EB-V)=1.2 given by Molster et al. 1999).

6.4 Results

IRAS 10215-5916 shows a composite spectrum of a M type and F type star. In the red region there are very few strong lines from the cool star. In the blue region around 5100Å we see absorption lines due to molecules of CN, C_2 and CH. The metallic lines of hot F star is weak.The SiII lines at 6347Å and 6372Å are unusually broad. Even the oxygen IR triplet lines are very broad. The broad absorption lines of SiII 6347, 6372Å and the OI IR triplet lines cannot be explained due to rotation. Because both the binary components are low gravity supergiants. Also they are in the binary system. So these broad lines of SiII and OI are combination of photospheric and

circumstellar lines. It can be due to macroturbulence. There are many absorption features due to the diffuse interstellar bands. There are nebular lines of [NII]. The Hα and FeII 6383Å shows a double peak emission. The velocites of the double peak emission is of the order of 50kms^{-1}, which is close to the value obtained from the CO observations. The difference in the expansion velocities from the nebular lines and CO lines could be that these high velocity features are forming from a bipolar outflow region. So it is still consistent with the picture of a post-AGB binary. We found the E(B-V) values derived from the DIBs are different for lines at different wavelengths. We also found a slight correlation between the E(B-V) and the wavelengths of the lines. The E(B-V) value is high at longer wavelengths(Fig. 2). This could be due to addition of some flux after the formation of the DIBs, may be flux from the binary companion. This says that the DIBs are formed in the circumstellar environment of the hot star.

We found that IRAS 10215-5916 is quite similar to HD 101584 (Sivarani et al. 1999). The similarity in the line profile of Hα and FeII 6383Å is seen in HD 101584 also.We found that even the DIBs in both the stars are the same and they have same equivalent widths. And HD 101584 is carbon rich with bipolar OH and CO emission.

The theoritical spectrum of the binary system shows that the hot star in the binary is metal poor (Fig. 3). The carbon and oxygen also show depletion with respect to solar. The chemical composition of the hot component is listed in table 1. The hot star shows more depletion of metals than the cool component. The flux from the hotter star dominate the spectrum and which is added to the cool star. So any change in the equivalent width for a change in abundance is also scaled, which makes hard to estimate abundances correctly.

If the metal poor charateristics is due to fractionation then the cool star should show more metal depletion than the hotter one. More depletion of metals in hot component can be explained by assuming a circumstellar dust around the hot star apart from the circumbinary dust. The theorical spectrum synthesis of the binary

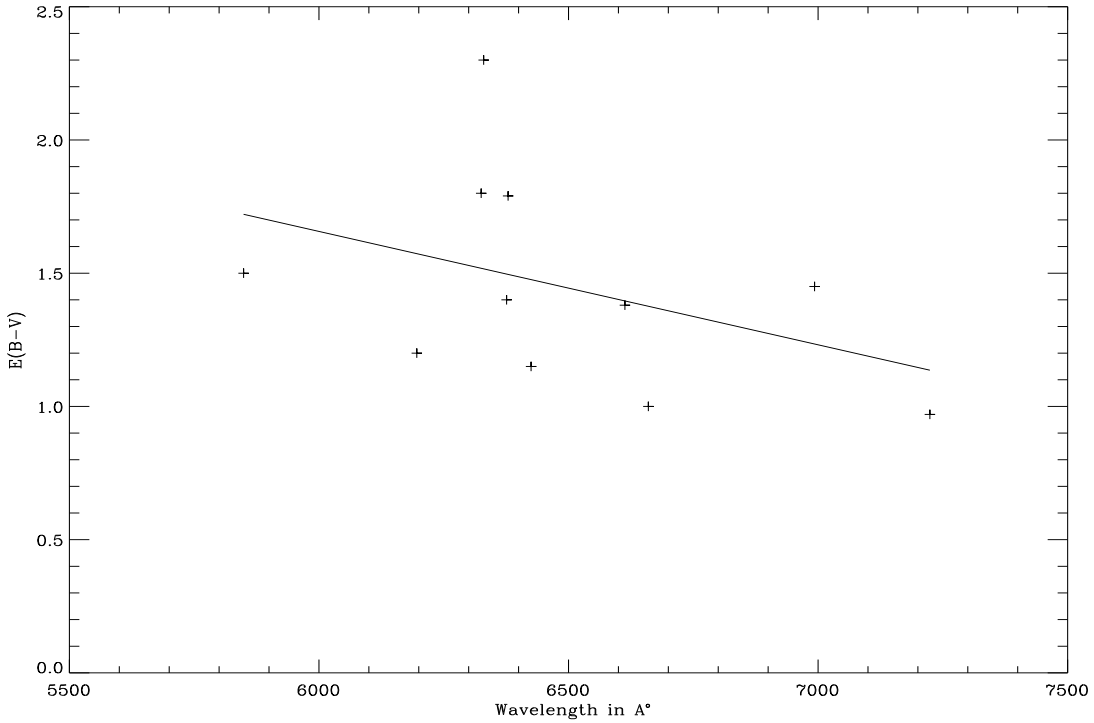

Figure 2: The E(B-V) derived from DIBs at different wavelengths seems to show a correlation. Some these values are taken from Molster et al. (1999)

Table 2: Chemical composition of hot component of the binary. For T_{eff}=7250K and logg=0.5 for the hot component and T_{eff}= 3750K and logg=0.0

Element	C	O	Mg	Si	Fe-peak	Y	Sr	Zr	Ba
[element/H]	-0.2	-1.0	-1.0	-1.0	-2.0	-1.0	-1.0	-1.0	-1.0

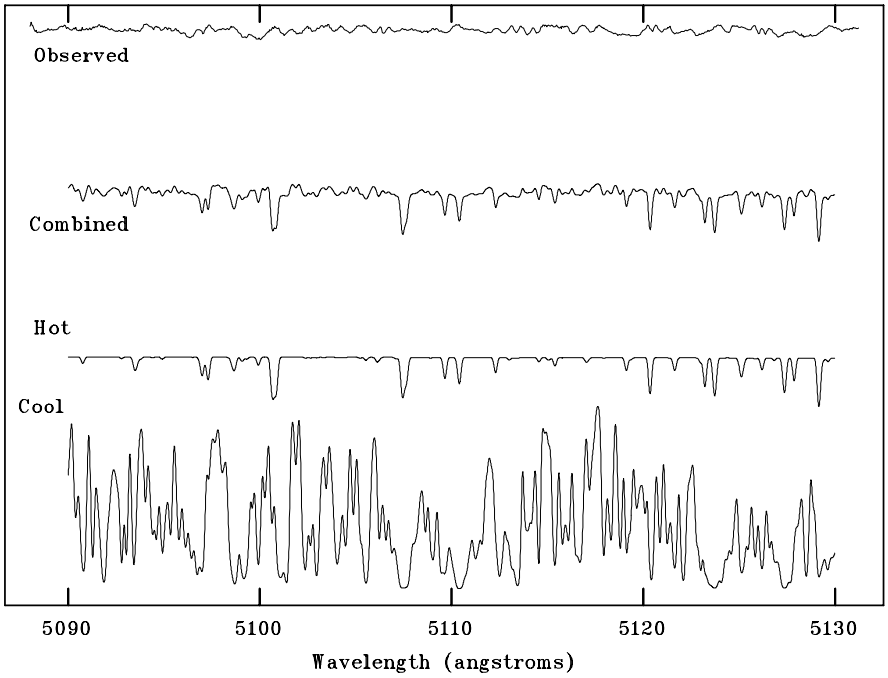

Figure 3: The theoritical spectrum is for temperatures and logg corresponding to 7250K,0.5 and 3750K, 0.0 of the binary components. We scaled the fluxes with respect their relative luminosities before addition. For a solar composition all the metallic lines from the hot star is strong

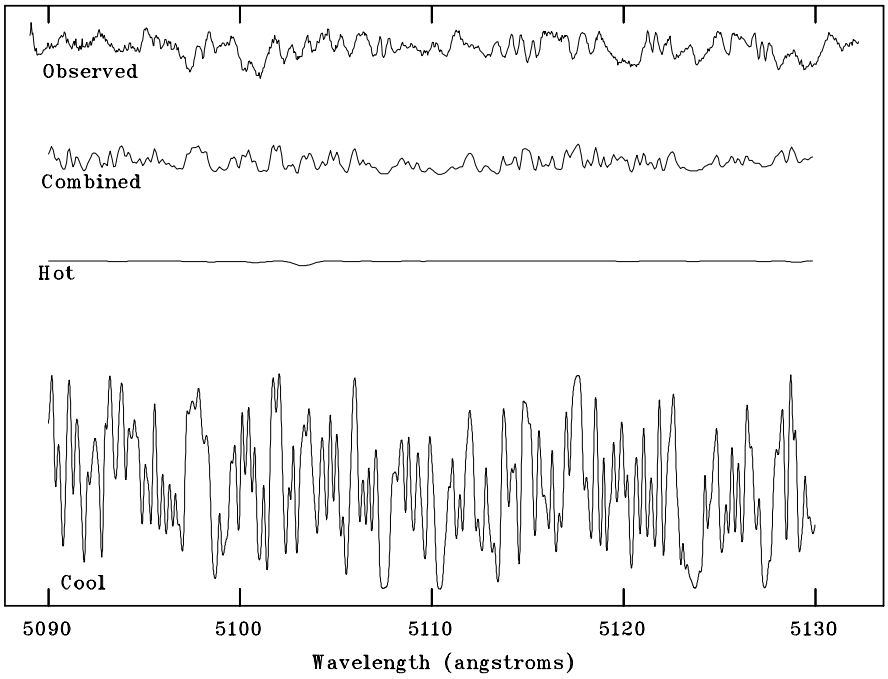

Figure 4: Spectrum synthesis of the binary spectra. We used T_{eff}=7250K, log g=0.5 for the hot star and T_{eff}=3750K,logg=0.0 for the cool star in the binary system with a relative ratio L_{warm}/L_{cool}=1.8.

system matches for slightly different values extinction for both cool and the hot component. We found that the hot star has more extinction than the cooler one. The abundances of the hot star shows enhancement of carbor with respect to oxygen, implying IRAS 10215-5916 to be a carbon star. The presence of the DIBs also support carbon enrichment. Barium is found to be not depleted. But there is contamination due to molecular lines and DIBs close by. The other lighter and heavier α process elements enhanced compared to iron.

We found difference of 7kms^{-1} in their radial velocity. This implies a highly eccentric orbit and hence a large orbit for the binary system.

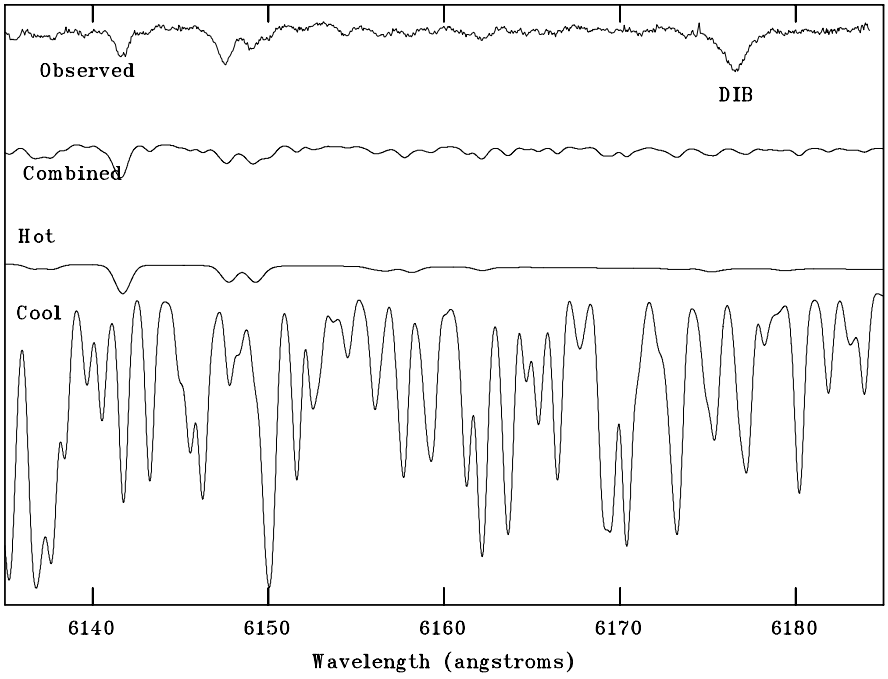

Figure 5: Spectrum synthesis of the binary spectra. We used T_{eff}=7250K, log g=0.5 for the hot star and T_{eff}=3750K,logg=0.0 for the cool star in the binary system with a relative ratio L_{warm}/L_{cool}=1.8.

Figure 6:

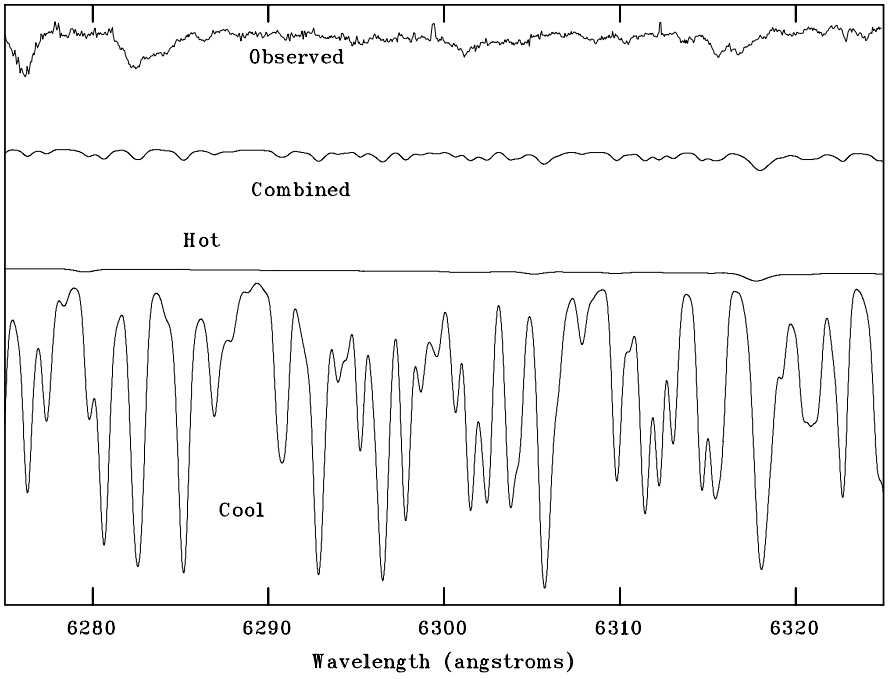

Figure 7: Spectrum synthesis of the binary spectra. We used T_{eff}=7250K, log g=0.5 for the hot star and T_{eff}=3750K,logg=0.0 for the cool star in the binary system with a relative ratio L_{warm}/L_{cool}=1.8.

Figure 8:

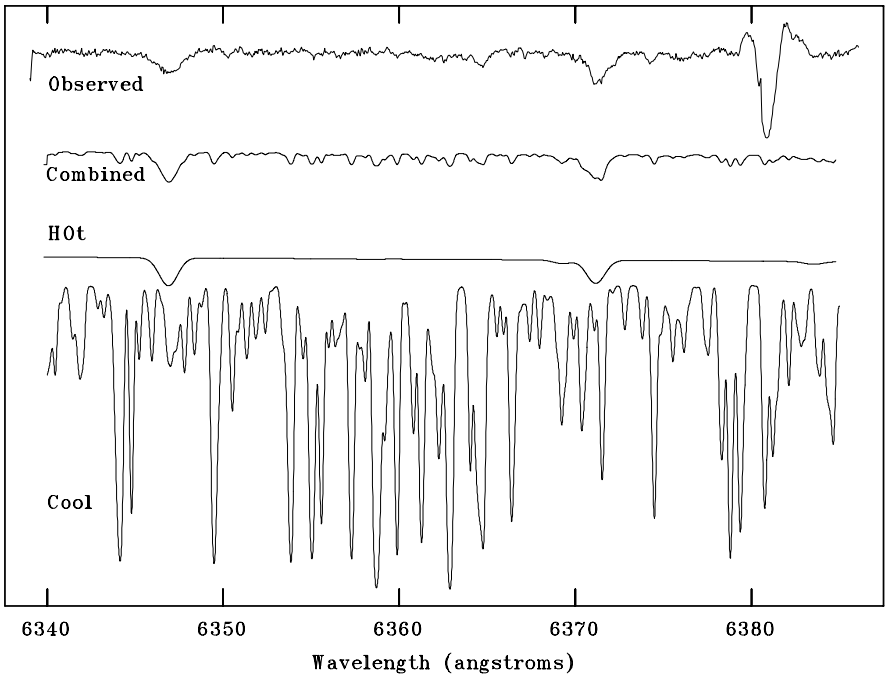

Figure 9:

Figure 10: Spectrum synthesis of the binary spectra. We used T_{eff}=7250K, log g=0.5 for the hot star and T_{eff}=3750K,logg=0.0 for the cool star in the binary system with a relative ratio L_{warm}/L_{cool}=1.8.

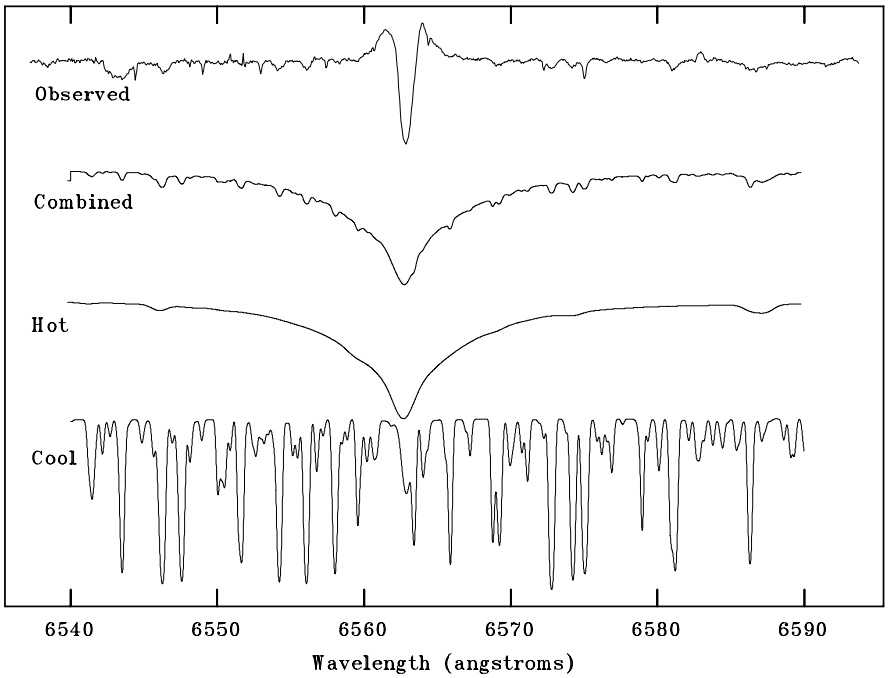

Figure 11:

Figure 12: Spectrum synthesis of the binary spectra. We used T_{eff}=7250K, log g=0.5 for the hot star and T_{eff}=3750K,logg=0.0 for the cool star in the binary system with a relative ratio L_{warm}/L_{cool}=1.8. The weak and sharp lines in the observed spectra are telluric lines.

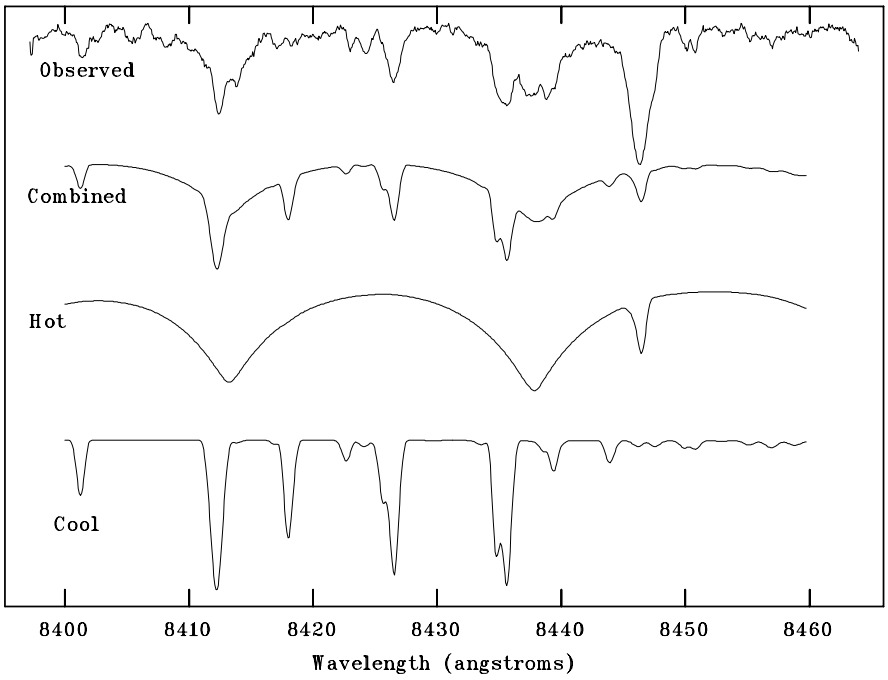

Figure 13:

Figure 14: Spectrum synthesis of the binary spectra. We used T_{eff}=7250K, log g=0.5 for the hot star and T_{eff}=3750K,logg=0.0 for the cool star in the binary system with a relative ratio L_{warm}/L_{cool}=1.8. In this calculation we have not included the molecules in the linelist, So many of the faint features of the cool star is not seen in the calculated spectrum

6.5 Conclusions

The double peak emission of Hα and FeII 6383Å could be from a bipolar emission which is collimated due to the circumbinary disk. The hot star in the binary system is found to be metal poor and this cannot be attributed to depletion due to dust, because we find carbon and oxygen also to be depleted. So IRAS 10215-5916 belong to a older population. The CO emission could be from bipolar and hence it is not insistent with post-AGB nature of the hot star. We found carbon is enhanced. So IRAS 10215-5916 is carbon rich post-AGB in the binary system.

Chapter 7

Spectroscopy of HD 168625

7.1 Abstract

In this chapter we have analysed the high resolution optical spectra of HD 168625 and derived the atmospheric parameters and the chemical composition. We obtained T_{eff}=15000K, log g=2.5 and [M/H]=0.0, and estimated the chemical composition. HD 168625 has large nitrogen abundance and very large neon abundance. The oxygen abundance is solar. Carbon is depleted. Magnesium, silicon and sulfur also has low abundance. The large neon abundance could be due to NLTE effect.

7.2 Introduction

HD 168625 (also V4030 Sgr) is classified as B9-A0 supergiant by Morgan el al. (1955). It is an IRAS source with far-IR colors similar to planetary nebulae and post-AGB stars. Its evolutionary status is not clear. The circumstellar dust shell indicates that it has experienced mass loss in the recent past. High resolution spectroscopy may enable us to understand the evolutionary status of this star. It is known to be in the

close proximity to HR Car in the HR diagram, and at the low luminosity end of the luminous blue variable (LBV) region. LBVs are extreme supergiant stars. They are grenerally thought to represent a short-lived intermediate stage in the evolution of massive stars from O to WolfRoyet (WR)stars (c.f. reviews by Humphreys 1989; Hiller 1992; Wolf 1992). About ten LBVs are known in our Galaxy. LBVs are characterized by the high variability in their temperature, radii and in the mass loss properties. They also display irregular photometric variations over timescales of decades. They appear to move (at const. bolometric luminosity) from hot, visual minimum phase (T_{eff} =20000-30000K) across the upper luminosity boundary to a cooler (T_{eff} < 10000K) visual maximum phase, where they develop false photospheres and typically resemble very luminous A-type supergiants. No major spectrophotometric variations has been observed recently for HD 168625 to classify it to be a LBV. But there are also LBVs which have long periods of quiescence like PCygni and η Carinae.

Assuming the membership of M17 complex in Sgr OB1 association, HD168625 is placed at a distance of 2.2kpc. From this the coressponding E(B-V) =1.46, M_{bol}=-8.6 are found. This places it close to HR Car and at the low-luminosity end of LBV region.

In this work we have investicated the evolutionary status of HD 168625 from the high resolution optical spectrum and on the basis of the chemical composition.

7.3 Observations and analysis

High resolution spectrum was obtained using the 2.5m Issac Newton Telescope (INT) located at La Palma, which is equipped with a Intermediate Dispersion Spectrograph (IDS). The observations were made on 24th May 1991. The spectra covers wavelength regions 5325-5450Å, 6125-6225Å, 6300-6400Å, 6525-6625Å, 7060-7175Å, 7400-7500Å and 8680-8780Å. It has a resolution of 0.3Å at 6000Å. The data is reduced using the IRAF software. The wavelength calibrated normalized spectra is compared with

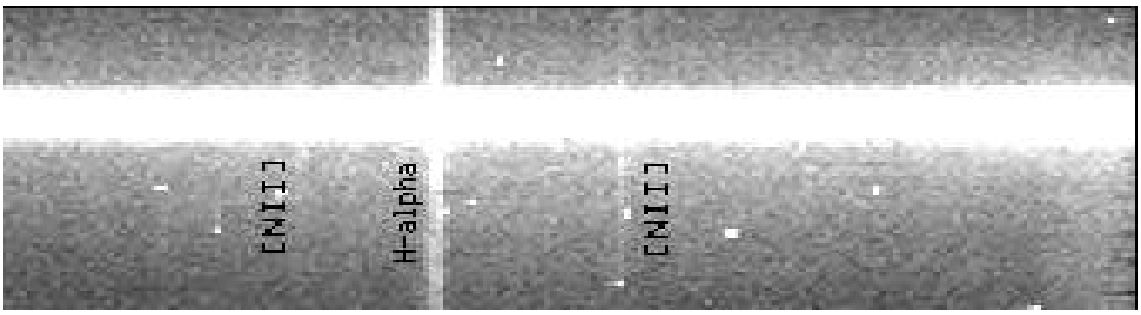

Figure 1:

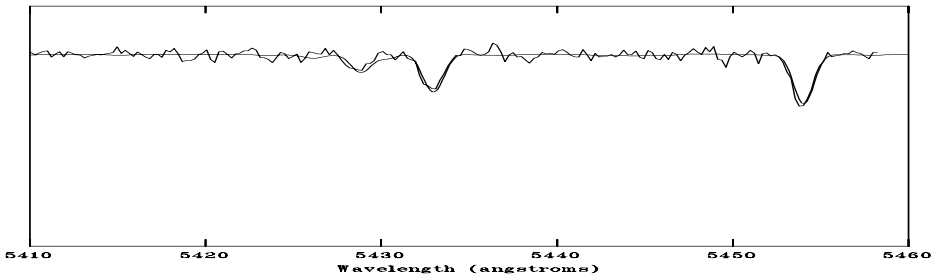

Figure 2:

theoritical spectrum. The theoritical spectrum is calculated using the SYNSPEC code by Hubeny (1986). We had used the Kurucz (1993) model atmospheres. The linelist for the spectrum synthesis is taken from the Kurucz lineslist (1993).

7.4 Results

The high resolution optical spectrum of HD 168625 show absorption lines of CII, NII, OII, MgII, SII, SiII NeII and HeI. From the SII lines we estimated a temperature of 15000K and log g=2.5. The long slit spectra shows an extended emission in Hα and also in [NII] 6548, 6583Å lines (Fig. 1). This indicates an extened nebula around the star. The spectra also shows lot of strong diffuse interstellar bands (DIBs). The estimated chemical composition is listed in Table.1

From the spectrum synthesis (Fig. 2), we found that the nitrogen abundance is enhanced and the neon abundance is quite high. The oxygen abundance is solar. The

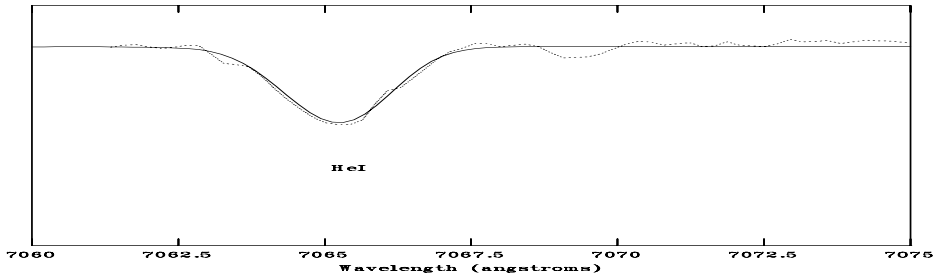

Figure 2:

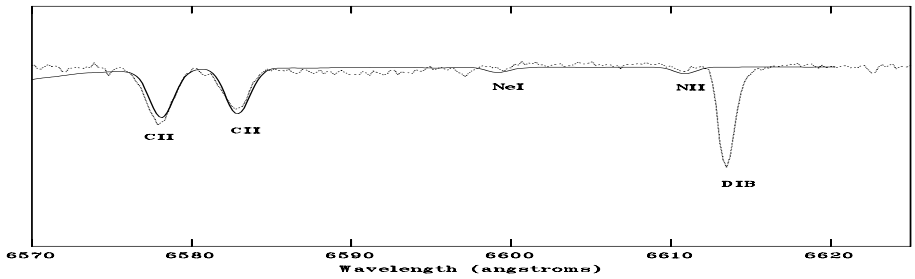

Figure 2:

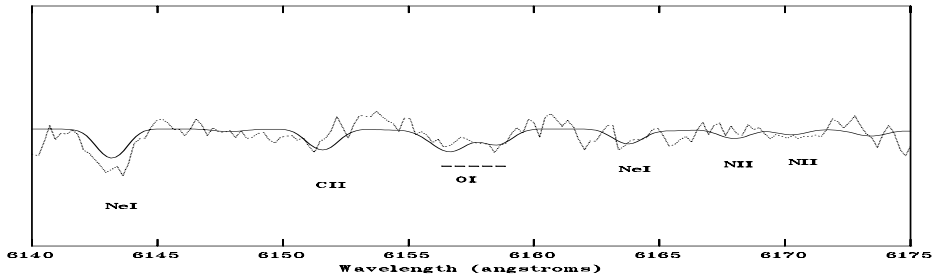

Figure 2:

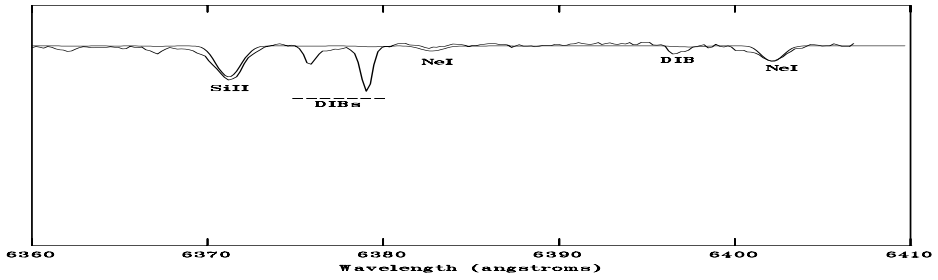

Figure 1:

Table 1: Chemical composition of HD 168625.

[element/H]	[C/H]	[N/H]	[O/H]	[Mg/H]	[S/H]	[Si/H]	[Ne/H]
T_{eff}=15000K log g=3.0	-0.34	0.52	0.0	-0.3	-0.46	-0.57	0.8

sulfur and silicon abundances are low. We have obtained the IUE NEWSIPS data from Vilspa. From the UV spectrum we derived E(B-V)=1.4. From the Hipparcos parallax (2.49 mas) for HD 168625, and (B-V)=1.227, V=8.96 we derived, a distance of 401.6 pc and estimated M_v=-4.1, $(B-V)_o$=-0.173. This places the star to be B5II.

7.5 Discussions

The spectral type of HD168625 seem to vary between B2 (Popper & Seyfert 1940) to A0 (Morgan et al. 1955) and B5.6 (Chentsov & Lund 1989). The equivalent widths of the lines are also seem to vary. So the derived abundance assuming a static atmosphere should be taken with a caution. The enhancement in the nitrogen abundance seen in HD168625 is consistent with the nitrogen rich nebula. This also gives an evidence that the nebula has formed from the material ejected from the CNO processed stellar surface.

The distances derived from the Hipparcos parallax seem to be inconsistent with the previous results. The distance 0.4kpc from the Hipparcos measurement is very less than the distance of 2.2kpc, assuming that HD 168625 belongs to the Omega nebula. The reddening derived from the nebular lines show E(B-V)=0.75, which is less than 1.4 which is derived for the star. This indicates that HD 168625 is further away from the Omega nebula. Futher evidence came from the velocity shifts of NaI D lines, which show higher positive shift compared to HD 168607 which is a nearby LBV in the Omega nebula.

There is still a possibility that the excess reddening of the star light compared to

the nebula is probably due to large dust grains around the star. The near IR imaging gives evidence for such a possibility of having larger grains. It appears, HD 168625 is a relatively be a star with a cool dusty disk.

From the Hα line emission a gas mass of $0.1 M_{\odot}$ is derived assuming a distance of 2.2 kpc. This is found to be less if HD 168625 has to be a LBV. But if one assumes a distance of 0.4 kpc then the mass will be around $0.01 M_{\odot}$. Also the morphology of the nebula around HD168625 is peculiar. The [NII] linesindicate the presence of a low excitation nebula. This is typical of planetary nebulae. The enrichment of nitrogen in the nebula as well as in the star shows that it is an evolved star. But we also see very high enrichment of neon in the star. But the surrounding nebula does not seem to show any nebular lines of neon.

There are lot of unidentified IR lines and also DIBs seen in the spectra. Generally the origin of these lines are thought to be the Poly Aromatic Hydrocarbons (PAHs). These are strong in the cases where the C/O high. But we see enriched nitrogen. So more detailed study is needed to know about the origin of these features.

The evolutionary status of HD168625 is not clear. It may be a LBV or a post-AGB star with a core mass of the order 1.0 $M_{\odot}$. The overabundance of nitrogen is similar to that observed in type I planetary nebulae. Accurate distance is needed to estimate the absolute luminosity of HD 168625. The LBV star HR Car also shows over abundance of nitrogen. The right underabundance of sulphur in HD168625 indicates that it may be slightly metal poor. The variations in the spectrum and overabundance of nitrogen, low galactic latitude are more consistence with the interpretation that HD168625 is a LBV.

Chapter 8

Line profile variations in pre-mainsequence star IRAS 04555+2949

8.1 Abstract

In our selected samples based on the IR colours similar to post-AGB and PN, some of them were found to be pre-mainsequence stars. These pre-mainsequence stars show variations in their emission line profiles, which is common in many the pre-mainsequence Herbig Ae/Be stars. Here we found that variations in line profiles observed in HD 31648 to be periodic. So we attribute these variations to be due to changes in the optical depth of the rotating disk around the star. Mostly an planet like body coming in between in the observer and the lineforming region. The amplitude of the changes seem to be less. From a high signal to noise spectra we were able to see this. Here we only present the preliminary results. We also present the spectrum of HD 36112, which again a Herbig Ae/Be star, which so very similar spectrum.

8.2 Introduction

Many pre-mainsequence stars with IR excess were found to be probable candidates for proto planetary system. HD 31648 (IRAS 04555+2949) is a pre-mainsequence star, which has a spectral type A2e. It is located in the Tarus-Auriga star formating region at a distance of 140 pc. HD 31648 is found to have a rotating disk of gas and dust (Manning et al 1997). It is thought to be a young counterpart of β Pic. β pic is one of the best known example of a mainsequence star with a disk (Backman and Paresce, 1993). From the CO (2-1) spectral line mapping and modelling the variability, Manning et al (1997) found that HD 31648 has a rotating disk which is gravitationally bound to the central star.

Study of HD 31648 will enable us to understand more about the origin of the debris disks and the early stages of the formation of planetary system. We present here the variability of lines profiles, which show periodicity close to the rotational period of the rotating disk. The variations of emission line profile indicates the variations in the optical depth of the emitting region.

8.3 Observations

All the spectra were obtained using 2.3m telescpoe at Vainu Bappu Observatory, Kavalur, which is equipped with a OMR spectrograph. We used 1200l/mm grating. The spectral resolution is 2.0 at 5000Å. Except for 6 continuous nights of observations, all the other observations are done on random dates.

8.4 Results and discussions

We see periodic variations in the line profiles of HeI 5876Å, HeI 6678Å and the NaI D emission lines of HD31648. We also see variations in Hα line profile. It changes

from P-Cygni to single peak emission. The calcium triplet lines and OI 7777Å triplet lines show emission and they show variability in the line profiles. The presence of sodium and calcium lines in emission in the spectra shows the presence of warm gas probably close to the star. The equivalent widths of SiII 6347Åand 6372Åalso show variations. From the spatial direction of the spectra, we found that the emission at Hα is extended. The variation in the line profile of the He I 5876Åshows 6-7days period. The He I 6678Å line also varies the similar way. The gaseous disks, which are seen in many of the pre-mainsequence stars are potential sites for studying planets in their formation. Observing the variations of emission lines originating from these gaseous disks will give information on the structure of the disk. Any structural changes in the disk will give rise to variations in the optical depth and this inturn gives variations in the intensity as well as in the profiles of the emission lines. We observed variations in the emission line profiles of HD31648 which originates from the disk. We found that the line profiles seem to repeat. So the disk might be rotationally supported one. In the case of HD36112 we see sharp decline in the intensity of HeI 6678$\AA$ line in one of the epoch. Here we show that these variations can due to planetsimals moving in the disk crossing the line of sight. We have found the disk extension in Hα is more than 100AU, which is typical size of β Pic type proto-planetary disk.

8.5 conclusion

We found the changes in the profiles to be periodic so it can not be due to some sporodic events which are seen in pre-mainsequence stars. The magnitude of the variability is also quite less. So the variations could be either due to emission from a object or a spot which is rotating or due to dense clump coming in the observers line-of-sight, and which is rotating in a disk around the star. This can be confirmed by looking for radial velocity changes in these emission lines. Our data was of poor resolution for that. From a high resolution and high signal to noise spectrum one

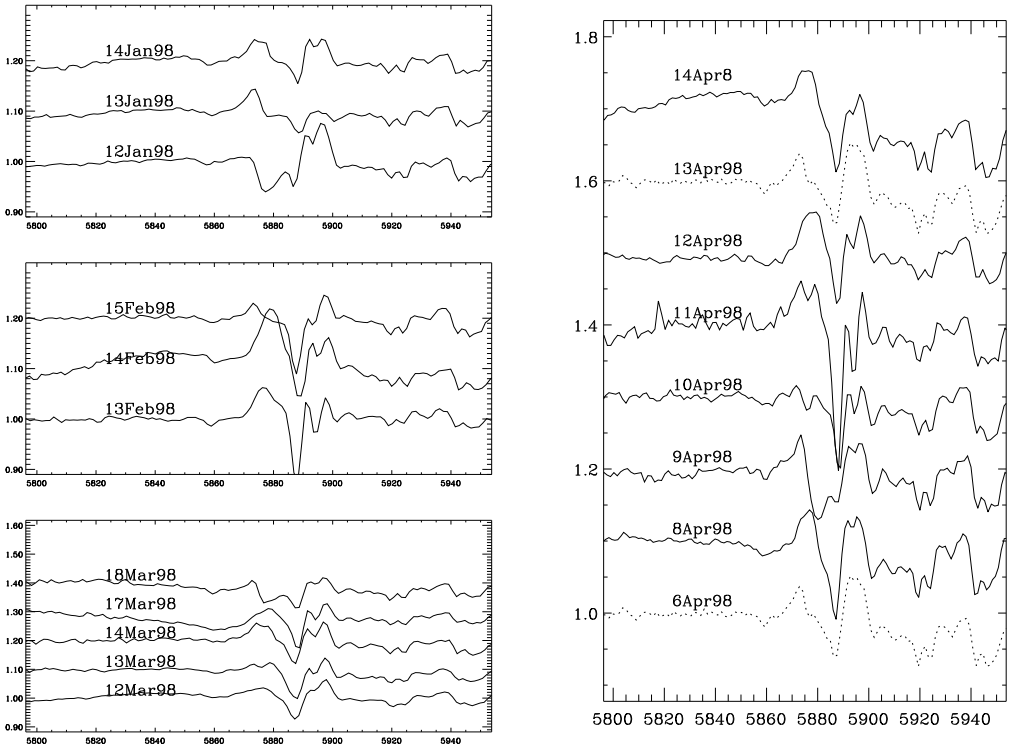

Figure 1(a): The HeI 5876 and the NaI D lines seem to show varitions in the timescale of days. The plot with the dotted lines is show that the line profiles looks alike on those days.

might be able to resolve it. From multiwavelenght imaging and spectroscopy can model and understand these proto planetary disks.

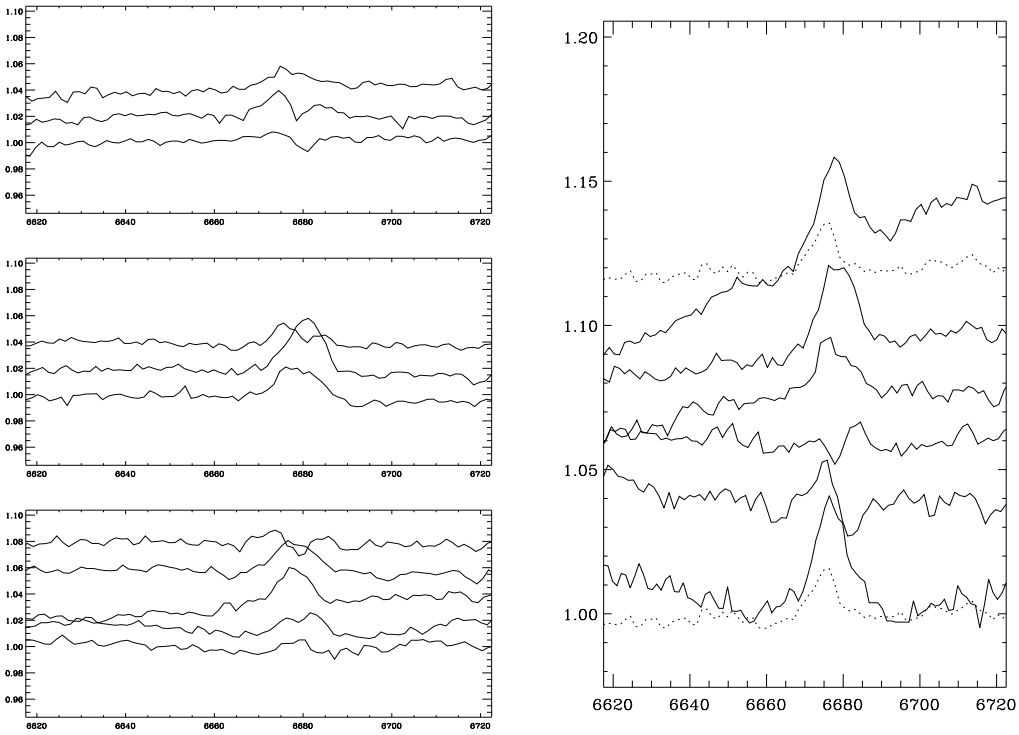

Figure 1(b): The spectra in this figure is part of the same spectrum shown in Fig. 1a so it corresponds to the same dates. The plot in the dotted line shows again that the profiles are similar for those epoch of observations.

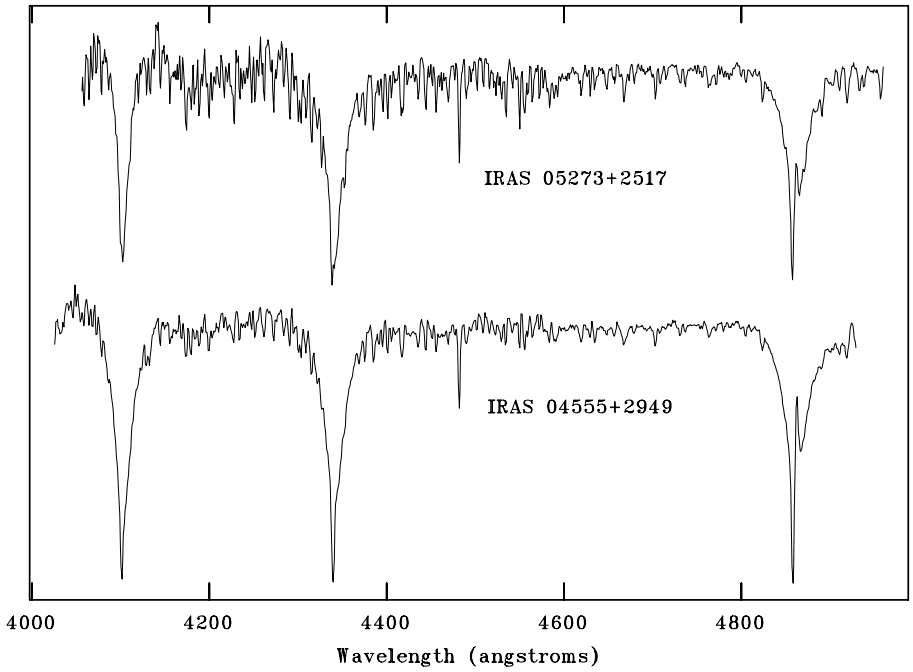

Figure 2: Low resolution spectrum of HD 31648 and HD 36112

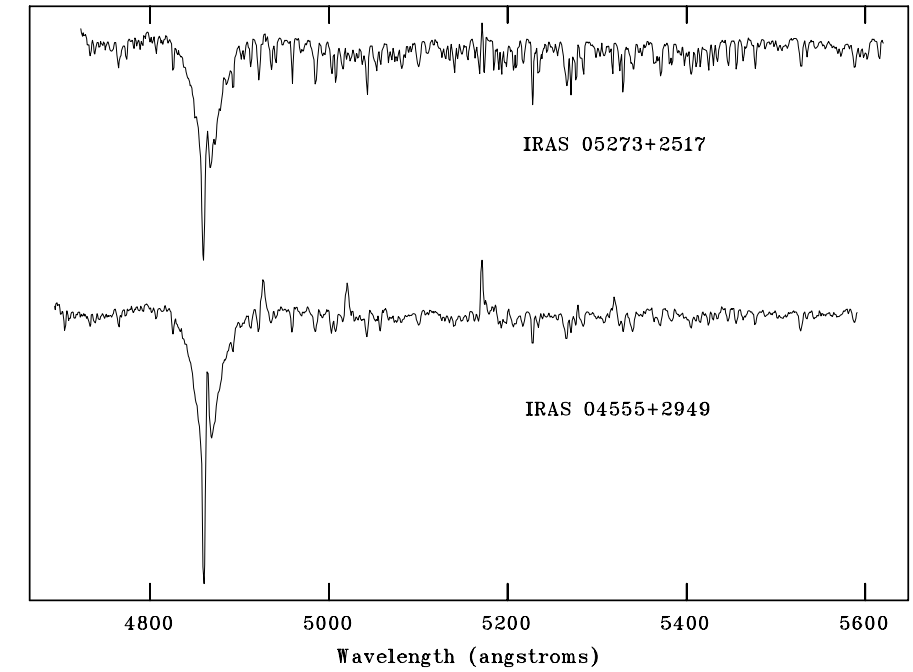

Figure 2(continued): Low resolution spectrum of HD 31648 and HD 36112.

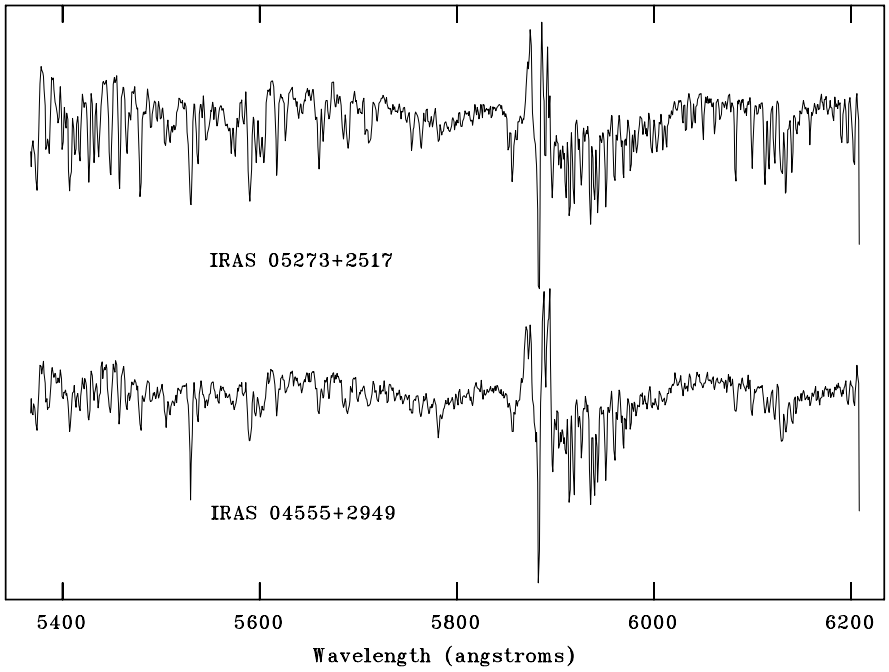

Figure 3(continued): Low resolution spectrum of HD 31648 and HD 36112.

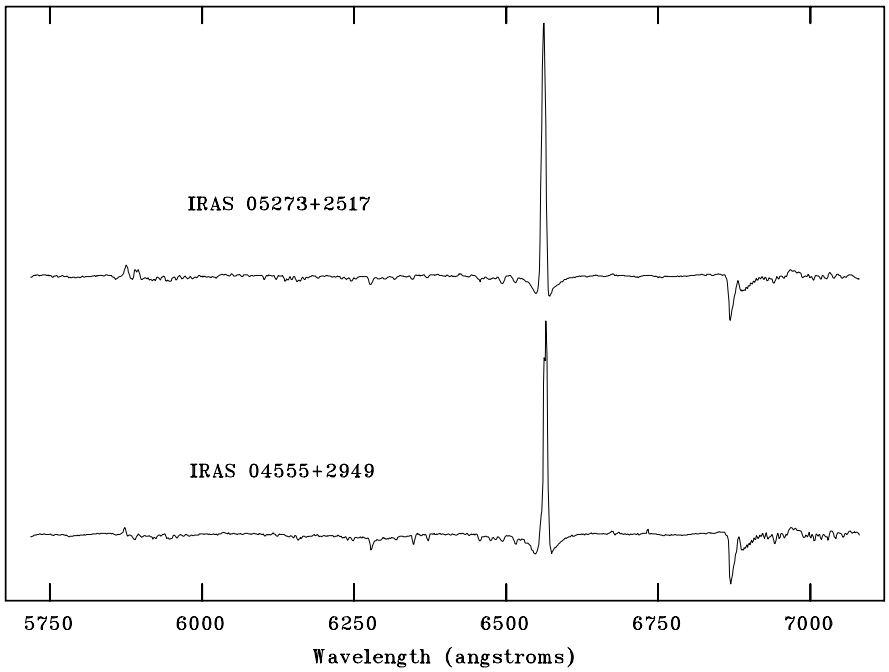

Figure 4(continued): Low resolution spectrum of HD 31648 and HD 36112.

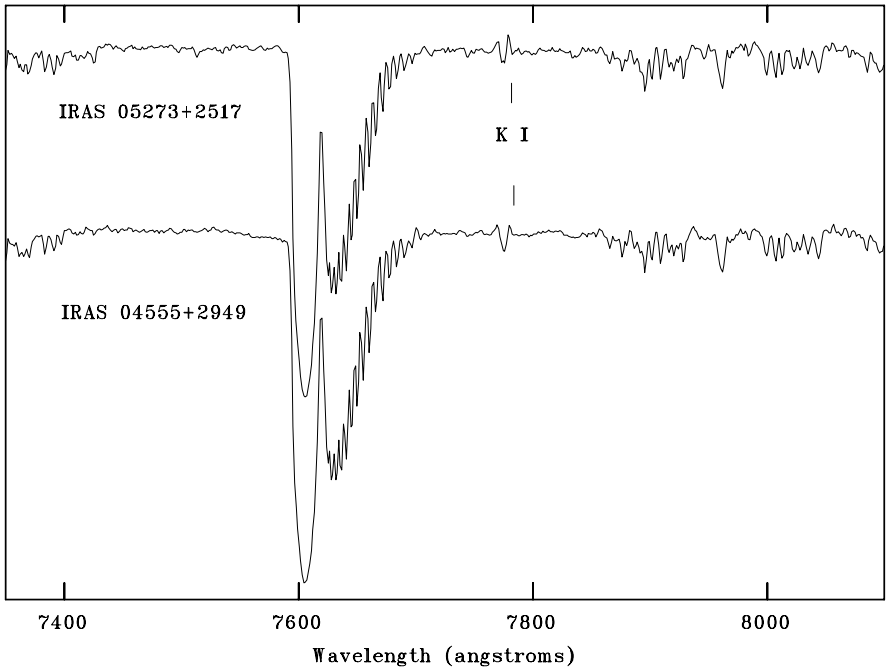

Figure 5(continued): Low resolution spectrum of HD 31648 and HD 36112.

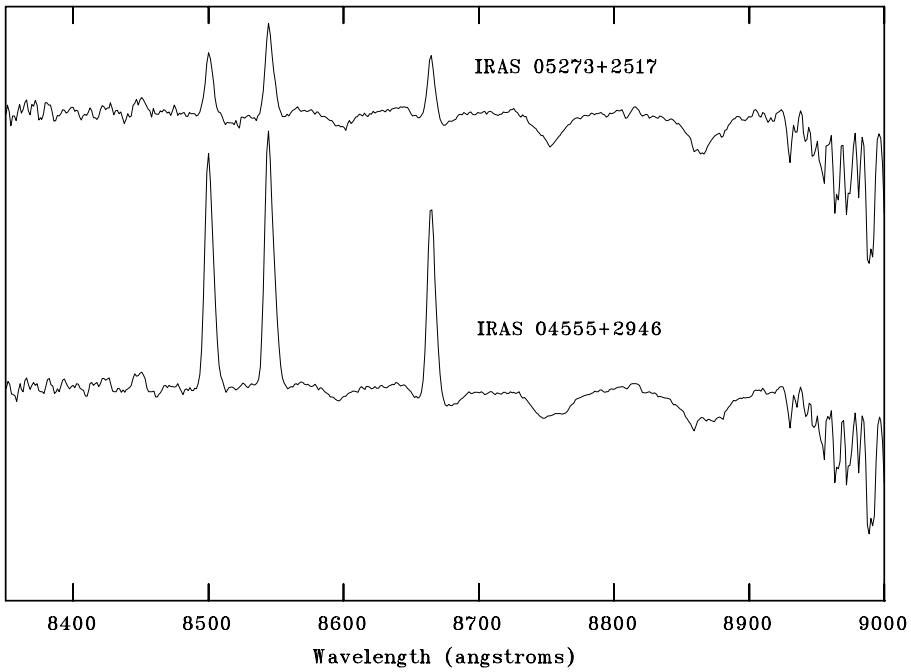

Figure 6(continued): Low resolution spectrum of HD 31648 and HD 36112.

Chapter 9

Conclusions

In this work we have studied the optical spectrum of A-F stars with circumstellar dust, which includes pre-mainsequence Herbig Ae/Be stars, Vega-like stars and post-AGB stars. From the far IR colours we have shown objects which have detached shells and A-F supergiant spectrum as the criteria for post-AGB stars. We did low and high resolution spectroscopy of some of the interesting objects. The circumstellar dust shells around these low mass A and F supergiants are a result of severe mass loss suffered during their AGB phase of evolution. The major part of the thesis work concerns on the chemical composition of these selected objects with IRAS colours similar to post-AGB and PN. Both low and intermediate mass stars go through the post-AGB stage. Depending on the core mass, envelope mass, mass-loss rate, mixing and binarity, the post-AGB stars seem to show a variety of elemental abundance patterns.

In chapter 3 we have studied the high resolution spectrum of HD 101584 which was thought to be post-AGB star in the transition towards PN. From our high resolution spectrum we derived the atmospheric parameters and the chemical composition. We conclude that HD 101584 is a A-type carbon rich post-AGB star. Recently the ^{12}CO and ^{13}CO observations seems to show enhancement in ^{13}C. This also supports the fact

that the star is carbon rich and has gone through the third dredge-up. The presence of several emission lines, the profile of Hα, the IRAS data and CO profiles show that HD 101584 is having a dusty disk with bipolar outflow.

In chapter 4 we have studied the chemical composition of a F-type supergiant HD 331319 which is having a cold detached circumstellar dust shell with far-IR colours similar to PN. The C,N,O abundances were found to be high, relative to iron. We found that the atmospheric parameters derived were affected by the NLTE effect. There is a large difference seen in the abundances derived from FeI and FeII lines. In many other post-AGB stars also show similar differences . The differences are due to the extended atmosphere and NLTE. We see a clear enhancement of C,N,O, indicating mixing due to third dredge-up. So HD 331319 is clearly a post-AGB F supergiant.

In chapter 5 we have studied the chemical composition of the high galactic latitude F-supergiant HD 187885 with far-IR colours similar to post-AGB stars. This one of the three stars which clearly shows mixing due to third dredge-up as predicted by the theoretical models. Carbon is enhanced and it is associated with the enhancement of s-process elements as predicted by the theory. The overabundance of carbon and s-process elements shows that HD 187885 has gone through the carbon star phase evolution and now it is a post-AGB F supergiant.

In chapter 6 we have studied the spectrum of IRAS 10215-5916, which is double-lined spectroscopic binary star with a cool M-type supergiant as one of the component in the binary system. The hot star in the binary system is an early F-supergiant. We see double peak broad emission from the Hα and FeII line at 6383Å. The line profiles are similar. The double peak structure is due to the bipolar outflow, which is driven by the disk formed due to the binary companion. Our analysis of the spectra shows that the F-type star is of low metallicity, we see the carbon and oxygen also showing low abundances. Because of the presence of lines due to the M-type supergiant companion, we could not do a accurate calculations for the abundances.

At this point we could say that IRAS 10215-5916 is a metal poor F-supergiant with a M-type supergiant companion. Probably the F-star is a post-AGB supergiant. The double peak emission of CO, Hα and FeII 6383Å shows an expansion velocity of 50kms^{-1} due to the bipolar outflow.

In chapter 7 we have studied the chemical composition of HD 168625 which is a IRAS source with far-IR colours similar to post-AGB stars. It was classified as a A-type post-AGB supergiant and also as a Luminous Blue Variable. The spectrum seems to show variations from A_e type to B_e type. We derived a T_{eff}=15000K and logg=2.5. The chemical composition show nitrogen enrichment. There is a spatially resolved nebula seen around the star. It is still unclear that it is post-AGB supergiant or a LBV. The distances from the Hipparcos does not seem to match with the memembership of HD 168625 being in the Sgr OB1 association. The extinctions derived from DIBs, UV and spectroscopy seem to give a large value. The star has a large circumstellar extinction. The mass found in the circumstellar envelope seems to be less for a LBV.

In chapter 8 we have studied the line profile variability seen in a pre-mainsequence star HD 31648. HD 31648 has IR colors similar to that of post-AGB stars. The object show emission lines in NaI D, HeI, balmer lines, CaII triplet and OI 7777Å lines. We have looked for the variability in the line profiles and found that the line profiles seem to repeat. So this could be associated with the rotation of a giant planet in the keplerian disk which comes in the observers line of sight. The period was found to be of the order of 6-7 days. This gives an estimate of the distance of the object from the star to be of the order of 100AU. This is quite consistent with the size of a proto-planetary disk. The variability amplitudes are quite small. Because of the high signal to noise we were able to see the variations clearly. The CO observations by Manning et al (1997) clearly gives an evidence for a gravitationally supported rotating disk around the star.

The post-AGB are optically bright when they are in the spectral range A-F. Some

of the post-AGB stars have bipolar outflows, which is seen from the CO and OH observations. These post-AGB stars are thought to be the progenitors of bipolar PN. The winds and outflows which shapes PNs differently from an spherically symmetric AGB and post-AGB stars are still not understood. For studying wind mechanisms pulsations and shocks which drive the mass loss and shapes the PNs , one needs more high resolution spatially resolved imaging and spectroscopy.

The chemical abundance patterns seen in different post-AGB stars are very different. Some of the post-AGB stars show clear evidence for mixing due to third dredge up. The mixing and the envelop burning in post-AGB stars depends on the core and envelope mass, which depends on the initial mass as well as the mass loss rates.

Detailed spectroscopic analysis of HD 101584, HD 331319 and HD 187885 shows that they are post-AGB A-F supergiants. The over abundance of carbon and s-process elements clearly indicates that it has gone through the third dredge-up and carbon star phase of the AGB.

The detailed spectroscopic study of IRAS 10215-5916 and HD 168625 reveals that those very interesting objects for further study. At present it is difficult to distinguish the evolutionary status of these stars. They could be post-AGB stars or massive stars in mass-loss and rapid evolutionary phase. We need accurate absolute magnitudes and distances of these stars to decide their evolutionary status.

References

Abt H.A., Morrell N.I., 1995, ApJS 99, 135

Andersen J., Nordström B., 1977, A&AS 29, 309

Andrillat Y., Jaschek C., Jaschek C., Jaschek M., 1995, A&A 299 493

Aumann H.H., Gillett F.C., Beichmann C.A., de Jong T., Houch J.R., Low F.J., Neugebauer G., Walker R.G., Wesselius P.R., 1984, ApJ 278, L23

Backman D., Paresce F. in Protostars & Planets III (eds Levy E.H., Lunine J., 1253 (Univ. Arizona Press, Tucson, 1993)

Bakker E.J., 1994, A&AS 103, 189

Bakker E.J.,Lamers H.J.G.L.M., Waters L.B.F.M., Waelkens C., Trams N,R., Van Winckel H., 1996a, A&A 307, 869

Bakker E.J.,Lamers H.J.G.L.M., Waters L.B.F.M., Waelkens C., 1996b, A&A 310, 861

Baschek B., Searle L., 1969, ApJ 155, 537

Baschek B., Heck A., Jaschek C., Jaschek M., Koppen J., Scholz M., Wehrse M., 1984, A&A 131, 378

Baschek B., Slettebak A., 1988, A&A, 207, 112

Bidelman W.P., 1981, AJ, 86. 553

Bohlender D.A., Walker G.A.H, 1994, MNRAS 266, 891

Bohlender D.A., Landstreet J.D., 1990, MNRAS 247, 606

Boothroyd A.I., Sackmann I.-J., 1992, ApJ, 393, L21

Burbidge E.M., Burbidge G.R., 1956 ApJ, 124, 116

Bujarrabal V., Alcolea J., Planeas P., 1992, A&A 257, 701

Buscombe, W. 1984 in " MK spectral Classification Catalogue " North Western Univ.

Buser R., Kurucz R.L.,1987, A&A, 70, 555

Buser R., Kurucz R.L.,1992, A&A, 264, 557

Castelli F., 1991, A&A 251, 106

Crawford D.L., Mander J., 1966, AJ, 71, 114

Edvardsson B., 1988, A&A 190,148

Federman S.R., Sheffer Y., Lambert D.L., Gilliland R.L., 1993, ApJ, 413, L51

Friedjung M., Muratorio G. 1987, A&A, 188, 100

Fuhrmann K., 1998, A&A 338, 161

García-Lario P., Parthasarathy M., de Martino D., Monier R., Manchado A., de Córdoba S.F., Pottasch S.R., 1997, A&A, 326, 1103

García-Lario P., Manchado A., Parthasarathy M., Pottasch S.R., 1994, A&A, 285, 179

García-Lario P., Manchado A., Pych W., Pottasch S.R., 1997, A&AS 126, 479

Gerbaldi M. Faraggiana R., 1993, PASPC 44, 368

Graham J.A., Slettbak A., 1973, AJ 78, 295

Gray R.O., 1988, AJ 95, 220

Gray R.O, Corbally C.J., 1993, AJ, 106, 632

Gray D.F., 1992, The observation and analysis of stellar photospheres, Cambridge University Press, P. 348

R. O. Gray (1998) http://www.phy.appstate.edu/spectrum/spectrum.html

Hauck B., Slettebak A., 1983, A&A 127, 231

Hibbert A., Biémont E., Godefroid M., Vaeck N., 1991, A&AS, 88, 505

Hoffleit D., Saladya M., Wlasuk P., 1983, Supplement to the Bright star Catalogue, Yale University Observatory, USA

Holweger H., Koester D., Allard N.F., 1994, A&A 290, L21

Hrivnak B.J., Kwok S., Volk K.M., 1989, ApJ 346, 265

Hrivnak B., 1997, in Planetary Nebulae, ed. H. J.Habing and H.J.G.M. Lamers, IAU symp. No. 180, 303

Hrivnak B.J., Kwok S., Geballe T.R., 1994, ApJ 420, 783

Hubeny I., Stefl S., Harmanec P., 1985, Bull. Astron. Inst. Czechosl. 36, 214

Humphreys R.M., 1976, ApJ 206, 122

Iben I., Jr., 1983, ARA&A, 21, 271

Johnson H.L., Morgan W.W., 1953, ApJ 117, 313

Johnson H.L., 1958, Lowell Obs. Bull., 90

Jura M., 1986 ApJ 309, 732

Jura M., Turner J., 1998, Nature 395, 144

Kastner J.H., Weintraub D.A., 1995, ApJ 452, 833

Kobi D., North P., 1990, A&AS 85, 999

Kurucz R.L., 1979, ApJS, 40, 1

Kurucz R.L., 1994, Solar Abundance Model Atmospheres, Kurucz CD-ROM No.19, Smithsonian Astrophysical Observatory

Kurucz, R. L., 1993, A New Opacity-Sampling Model Atmosphere Program for Arbitrary Abundances. In: Dworetsky M. M., Castelli F., Faraggiana R. (eds.) Proc. IAU Coll. 138, Peculiar Versus Normal Phenomena in A-type and Related Star. ASP Conf. Ser.44, p.87

Kwok S., Su K.Y.L., Hrivnak B.J., 1998, ApJ, 501, L117

Lamers H.J.G.L.M., Waters L.B.F.M., Garmany C.D., Perez M.R. and Waelkens C., 1986, A&A 154, L20

Lang K.R., 1992, Astrophysical data: Planets and stars, Springer Verlag

Lester J.B., Gray R.O., Kurucz R.L., 1986, ApJS, 61, 509

Likkel L., Morris M., 1986, BAAS, 18, 963

Likkel L., Omont A., Morris M., Forveille T., 1987, A&A 173, L11-L14

Likkel L., Forveille T., Omont A., Morris M., 1991, A&A 246,153

Malagnini M.L., Morossi C., Rossi L., Kurucz R.L., 1986, A&A, 162, 140

Molester F.J., Waters L/B.F.M., Trams N.R., van Winckel H., Decin L., van Loon J. Th., Jäger C., Henning Th., Käufl H.-U., De Koter A., Bouwman J., 1999, A&A 350, 163

Mannings V., Koerner D. W., Sargent A., 1997, Nature, 388, 555

Michuad G., Charland Y., 1986, ApJ 311, 326

Moon T.T., Dworetsky M.M., 1985, MNRAS, 217, 305

Morgan W.W., Keenan P.C., Kellman E., 1943, Atlas of Stellar Spectra, University of Chicago Press, Chicago

Morrison N.D., Zimba J.R., 1989, BAAS 21, 1022

Mowlavi N., 1997, Amer. Inst. of Phys., in Tours Symposium on Nuclear Physics III, Ed, H. Utsunomiya

North P., Hauck B., 1979, in Problems of calibration of multicolor photometric systems, Phillip A.G.D., Dudley Obs. Rept. 14, p.183

North P., Nicolet B., 1990, A&A, 228, 78

Olofsson H., Nyman L.A., 1999, A&A 347,194

Osterbrock D.E., 1989, Astrophysics of Gaseous Nebulae and Active Galactic Nuclei, Oxford University Press, p.117

Parthasarathy M., García-Lario P., Pottasch S.R., 1992, A&A, 264, 159

Parthasarathy M., Pottasch S.R., 1986, A&A, 154, L16

Parthasarathy M. and Pottasch S.R. 1988, A&A 192, 182

Parthasarathy M., García-Lario P., Pottasch S.R., 1992, A&A, 264, 15

Parthasarathy M., García-Lario P., Pottasch S.R., 1992, A&A, 264, 159

Parthasarathy M., Pottasch S.R., 1986, A&A, 154, L16

Parthasarathy M., García-Lario P., Sivarani T., Manchado A., Sanz Fernández de Córdoba L., 2000, A&A in press

Paunzen E., Weiss W.W., Heiter U., North P., 1997, A&AS 123, 93

Peterson D.M., 1969, SAO Sp. Rept., 293

Piskunov N.E., Kupka F., Ryabchikova T.A., Weiss W.W., Jeffery C.S., 1995, A&AS 112, 525

Popper D.M., 1980, Ann. Rev. A&A, 18, 115

Preite-Martinez A., 1988, A&AS 76, 317

Reddy B.E., Parthasarathy M., Sivarani T., 1996, A&A 313, 191

Reddy B.E., Parthasarathy M., Gonzalez G., Bakker E.J., 1997, A&A 328, 331

Relyea L.J., Kurucz R.L., 1978, ApJS, 37, 45

Renson P. Faraggiana R., Böhm C., 1990, Bull. Inform. CDS 38, 137

Rosenzweig P., Reinoso E.G., Naranjo O., 1997, JRASC, 91, 255

Ryabchikova T.A. Piskunov N.E., Stempels H.C., Kupka F., Weiss W.W. Proc. of the 6th International Colloquium on Atomic Spectra and Oscillator Strengths, Victoria BC, Canada, 1998, Physica Scripta T80, (1999), in press. (VALD-2)

Schaller G., Schaerer D., Meyenet G., Maeder A., 1992, A&AS 96, 269

Schönberner D. 1983, ApJ 272, 708

Schönberner D. 1993, IAU Symp. 155 *Planetary Nebulae*, eds. R. Weinberger and A. Acker (Kluwer) p. 415

Sivarani T., Parthasarathy M., García-Lario P., Manchado A., Pottasch S.R. 1999, A&AS 137, 505

Slettebak A., 1952, AJ 115, 575

Slettebak A., 1954, AJ 119, 146

Slettebak A., 1975, AJ 197, 137

Smalley B., Dworetsky M.M., 1994, in IAU XXIInd General Assembly 1994 Posters Abstracts, van Woerden H., Twin Press, 229

Smith K.C., van't Veer C., 1988 in Elemental Abundance Analyses, Adelman S.J., Lanz T., Institut d' Astronomie de l'Universite de Lausanne, p.133

Sneden C., 1973, PhD Dissertation, Univ. of Texas at Austin

Sneden C., 1998, Private communication

Strömgren B., 1963, QJRAS, 4,8

Strömgren B., 1966, Ann. Rev. A&A, 4, 433

Su K.Y.L., Volk K., Kwok S., Hrivnak B.J., 1998, ApJ 508, 744

Takeda Y., 1993, P 491, In: Dworetsky M. M., Castelli F., Faraggiana R. (eds.) Proc. IAU Coll. 138, Peculiar Versus Normal Phenomena in A-type and Related Star. ASP Conf. Ser.44

Te Lintel Hekkert P., Chapman J.M., Zijlstra A.A., 1992, ApJ 390, L23

Thévenin F., 1989, A&AS 77, 137,154

Thévenin F., Idiart T.P., 1999, ApJ

Trams N.R., Van der Veen W.E.C.J., Waelkens C., Waters L.B.F.M., 1990, A&A 233, 153

Trams N.R., Waters L.B.F.M., Lamers H.J.G.L.M., Waelkens C., Geballe T.R. and The P.S., 1991, A&AS, 87, 361

Venn K.A., Lambert D.L., 1990, ApJ 363, 234

Viotti R., 1969, Astrophys. Space Sci. 5, 323

van der Veen W.E.C.J., Habbing H.J., 1988, A&A 194,125

van der Veen W.E.C.J., Trams N.R., Waters L.B.F.M., 1993, A&A 269, 231

van Loon J.Th., Molster F.J., van Winckel H., Waters L.B.F.M., 1999, A&A 350, 120

van Winckel H., Waelkens C., Waters L.B.F.M., 1996, A&A 306, L37

Vassiliadis E., Wood P.R., 1993, ApJ, 413, 641

Walker H.J., Wolstencroft R.D., 1988, PASP 100, 1509

Waters L.B.F.M., Trams N.R., Waelkens C., 1992, A&A 262, L37

Wiese W.L., Smith M.W., Glennon B.M., Atomic Transition Probabilities, Vol. 1, NSRDS-NBS(U.S.) 4, 1966

Wiese W.L., Martin G.A., Wavelength and Transition Probabilities for Atoms and Atomic Ions, NSRDS-NBS(U.S.), 68, 1980

Weiss W.W., Paunzen E., Kuschnig R., Schneider H., 1994, A&A, 281, 797

Yorke H.W., 1979, A&A 80, 308

Zuckerman, B., Dyck, H.M. 1986, ApJ 311, 3450

1. HD 105262: A HIGH LATITUDE METAL-POOR POST-AGB A supergiant with large propermotion; B. E. Reddy, M. Parthasarathy, and **T. Sivarani** Astronomy & Astrophysics **313** (1996) 191-196.

2. SPECTROSCOPY OF AE TYPE PRE-MAIN SEQUENCE STARS IRAS 04555+2946 AND IRAS 05273+2517; **T. Sivarani** and M. Parthasarathy *Poster presentation in the XVIII annual meeting of Astronomical Society of India*, PRL, Ahmedabad, India (1997).

3. HIGH RESOLUTION SPECTROSCOPY OF POST-AGB F SUPERGIANT HD 101584 (IRAS 11385 - 5517); **T. Sivarani**, M. Parthasarathy, P. García-Lario, A. Manchado and S.R. Pottasch *Poster presentation in the XVIII annual meeting of Astronomical Society of India*, PRL, Ahmedabad, India (1997).

4. SPECTROSCOPY OF THE POST-AGB STAR HD 101584 (IRAS 11385 -5517); **T. Sivarani**, M. Parthasarathy, P. García-Lario, A. Manchado, and S. R. Pottasch, Astronmy & Astrophysics Suppl. Ser. **137** (1999) 505-519.

5. HIGH RESOLUTION SPECTROSCOPY OF THE HIGH LATITUDE RAPIDLY EVOLVING POST-AGB STAR SAO 85766 (= IRAS 18062+2410); M. Parthasarathy, P. García-Lario, **T. Sivarani**, A. Manchado L. Sanz Fernández de Córdoba, 2000, A&A in press